1-1-2012

P-T Conditions of Selected Samples Across the Blue Ridge Province

Breana A. Felix
felix5@marshall.edu

P-T CONDITIONS OF SELECTED SAMPLES ACROSS THE BLUE RIDGE PROVINCE

A thesis submitted to
the Graduate College of
Marshall University

In partial fulfillment of
the requirements for the degree of
Master of Science

Physical and Applied Science
by
Breana A. Felix

Approved by
Dr. Aley El-Shazly
Dr. William Niemann

Marshall University
July 2012

ACKNOWLEDGMENTS

I would like to thank Dr. Aley El-Shazly for all the hard work and time he has put into helping me with my thesis. He has been a great mentor and has always looked out for my best interest. Whenever I needed him, he was always there for me and I am really grateful for it. I would also like to acknowledge the rest of the Geology Department for their contribution and funding, along with the students who have supported me and kept me sane. I would like to thank David Neff for all of his help and teachings with the SEM. Without him, none of this could have been accomplished. Last, I would like to thank my parents, Ronald and Tanya Felix, and my boyfriend, Adam Chain, for their support and encouragement. Their patience during this time has been phenomenal and I am truly thankful to have them in my life.

TABLE OF CONTENTS

Abbreviations

A: Al_2O_3 + Fe_2O_3 (- K_2O if projecting from K-spar; and – 3 K_2O if projecting from Musc); Ab: albite; Alm: almandine; Amph: amphibole; An: anorthite; Anth: anthophyllite; Ap: apatite; Bt: biotite; C: CaO; Chl: chlorite; Czo: clinozoisite; Ep: epidote; F: FeO; Ged: gedrite; Gr: grossular; Gt: garnet; Hb: hornblende; Ilm: ilmenite; K-spar: K-feldspar; Ky: Kyanite; L: liquid (melt); M: MgO; Mgt: magnetite; Musc: muscovite; Opx: orthopyroxene; Or: orthoclase; Plag: plagioclase feldspar; Qz: quartz; Rt: rutile; Ser: sericite; Sill: sillimanite; Sps: spessartine; Sph: sphene; St: staurolite; Tc: talc; Ti-Hm: ilmeno-hematite (Titan-hematite); V: vapor; X_y: mole fraction of component y; Xn: xenotime.

ABSTRACT

The Blue Ridge province of the Appalachian Mountains has a complex geologic history characterized by more than one metamorphic and deformational event. Mapping of the Blue Ridge has allowed for the province to be broken into the "sub" provinces western, central, and eastern Blue Ridge. The boundaries for these, however, are not well understood due to the difficulty in determining which orogenies caused each metamorphic event.

Detailed petrographic and microprobe analyses were carried out on 17 and 10 samples respectively. Outcrops from Ducktown and Marble in the western Blue Ridge (WBR), Savannah Church, Sylva, and Little Pine Garnet Mine in the central Blue Ridge (CBR), and Beaucatcher Mountain in the eastern Blue Ridge (EBR) that expose pelitic and psammitic rocks metamorphosed under amphibolite to granulite facies conditions were chosen to be used in these analyses. The Ducktown metapelites contain the assemblage garnet, biotite, staurolite, and plagioclase, whereas Savannah Church metapsammites are characterized by the assemblage garnet, biotite, plagioclase, and hornblende. The Sylva metapsammitic outcrop in the middle of the CBR contains the assemblage garnet, biotite, plagioclase, sillimanite, and hornblende. Beaucatcher Mountain metapsammites contain the same assemblage as Savannah Church.

Samples from the WBR are characterized by almandine rich garnet with considerable amounts of spessartine (X_{alm} = 0.54 - 0.56, X_{grs} = 0.02 - 0.05, X_{prp} = 0.15 - 0.17, X_{spss} = 0.20 - 0.22). All samples from the CBR and EBR are characterized by almandine rich garnets (X_{alm} = 0.50 – 0.75, X_{prp} = 0.07 – 0.2, X_{grs} < 0.1), with the exception of samples

from Sylva which have garnets with X_{prp} = 0.17 – 0.25. All garnets are for the most part unzoned with the exception of garnets from Savannah Church, Sylva, and Beaucatcher Mountain where there is an increase in manganese along the rims. Feldspars from these samples are albite rich plagioclases (X_{ab} = 0.50 - 0.70, X_{an} = 0.21 - 0.50, X_{or} = 0.0 - 0.02).

Using the average P-T routine of Thermocalc 3.26 and conventional garnet-biotite and garnet + biotite + aluminosilicate + plagioclase thermobarometry, peak metamorphic conditions for Marble (WBR) were calculated at 530 °C, 6.5 kbars. P-T conditions calculated for Little Pine Garnet Mine are 450 ˚C - 550 ˚C and 4.5 - 5.5 kbars. Conditions for Savannah Church were calculated at 660 ˚C – 700 °C, 8 - 9 kbars with Sylva having conditions at 700 °C- 750 ˚C and 11 - 13 kbars. On the other hand, P-T conditions for Beaucatcher Mountain are estimated at 750 °C - 800 ˚C and 7.0 - 7.7 kbars. These results show that the P-T conditions across the Blue Ridge are only broadly consistent with the isograds mapped for the terrane. The most striking anomaly is the unusually high pressures calculated for the Sylva outcrop, which are inconsistent with the overall trend of decreasing temperatures and pressures from Winding Stair Gap in the south to outcrops in the north established by Carpenter (1970) and Hatcher et al. (2005; 2010).

The purpose of this study is to give a better understanding of the tectonic history of the Blue Ridge. Based on the results of this study, the western Blue Ridge boundary may in fact extend farther east than was believed, to include Little Pine Garnet Mine. The central Blue Ridge exhibits higher pressures and temperatures than the western and eastern Blue Ridge, possibly from being deeply thrusted and brought back to the surface. The eastern Blue Ridge conditions are lower than the results for the central Blue Ridge, which is consistent with the Tugaloo terrane being thrust on top of Laurentia.

INTRODUCTION

The Appalachian Mountains consist of several physiographic/geologic provinces namely the Cumberland/Appalachian Plateau, Valley and Ridge, Blue Ridge, Piedmont, and the Carolina slate belt (Superterrane; Fig. 1). This complex combination of thrusted and folded rocks constitutes a complete Wilson Cycle, in which several orogenic events are recorded, namely: the Grenvillian (Mesoproterozoic), Taconic (Ordovician), Acadian/Neo - Acadian (Devonian - Mississippian), and Alleghanian (Pennsylvanian - Permian). The cycle began with the formation of the supercontinent Rodinia during the Grenvillian Orogeny (e.g. Hatcher et al., 2010). During the Neoproterozoic, Rodinia went through a stage of rifting and drifting that resulted in the opening of the Iapetus ocean. During the declining stages of the Wilson cycle, several terranes representing former rifted continental fragments and island arcs began to amalgamate giving rise to the Laurentian, Iapetan, peri - Gondwanan, and Gondwanan realms (Hibbard et al., 2010).

The Taconic Orogeny involved the closing of the main tract of Iapetus through the accretion of peri - Laurentian and peri - Gondwanan elements of Iapetus to Laurentia to form a new composite leading edge (Hibbard et al., 2010). During the Acadian Orogeny, the Rheic Ocean closed, marking the docking of the peri - Gondwanan realm into the Laurentian margin. Completing the Wilson Cycle was the collision of Gondwana with Laurentia during the Alleghanian, marking the assembly of Pangea (e.g. Hatcher et al., 2005). According to Hibbard et al. (2007 and 2010), Carolinia docked into the Laurentian margin by the end of the Taconic, whereas Hatcher et al. (2005) believe that its collision with Laurentia took place during the Acadian Orogeny. Each of these orogenic events was accompanied by metamorphism and igneous activity and because

some parts of the margin were repeatedly affected by collisions, it is not always easy to link metamorphic mineral assemblages to specific tectonic events. In addition to these controversies and difficulties, the bulk of evidence of later tectonic events in the evolution of the Appalachians is hidden by coastal on - laps and beneath the waters of the Atlantic Ocean. There is also some lack of data and direct observations of the locus of plate interactions for each of these orogenic events.

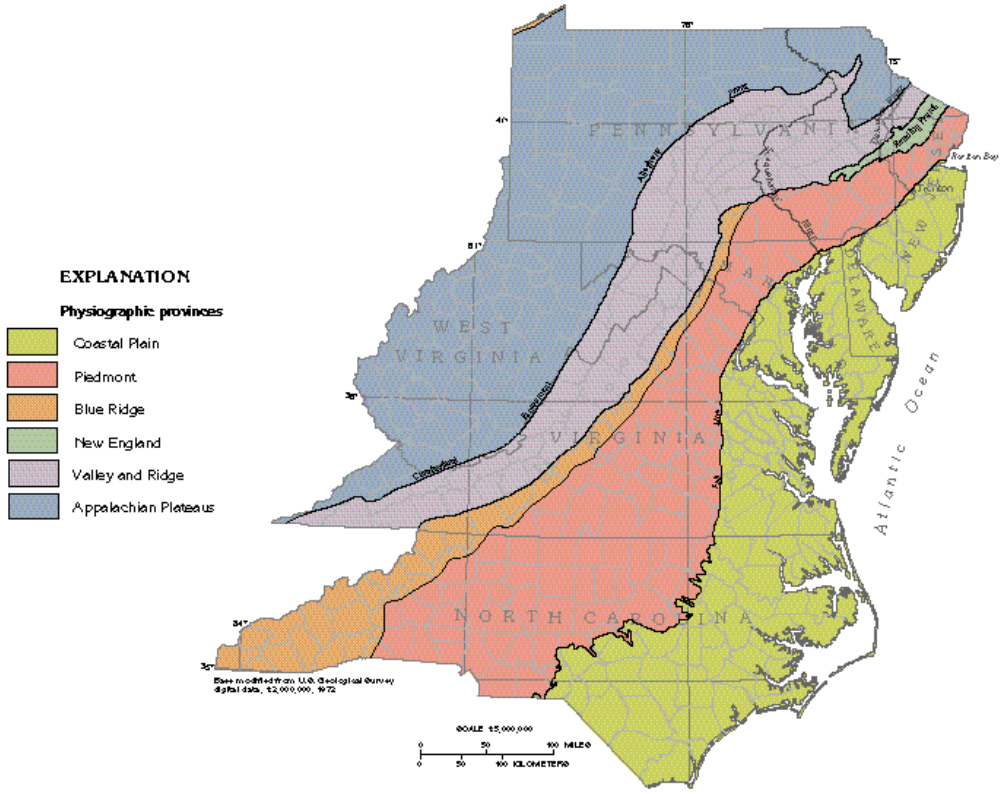

Figure 1. Map of the Appalachians showing the different provinces.

The focus of this project is the Blue Ridge Province, which has a profound and complex history. This province is important because of its structural and metamorphic complexity due to the amalgamation of several terranes during the Taconic and Acadian Orogenies, and the fact that it exposes some of the highest grade metamorphic rocks in

the southern Appalachians. Detailed geologic mapping of the Blue Ridge has allowed for the tectonostratigraphic terranes to be grouped into three provinces; the western, central, and eastern Blue Ridge (Hatcher et al., 2005). The nature of many of the boundaries between these terranes is not well understood or agreed upon because it is difficult to link metamorphism and specific deformational phenomena to specific orogenic events. Figure 2 is an oversimplification of the relationship between metamorphic isograds and terrane boundaries on one hand, and timing of metamorphism on another, inferred from a compilation of radiometric ages (Merschat, 2009).

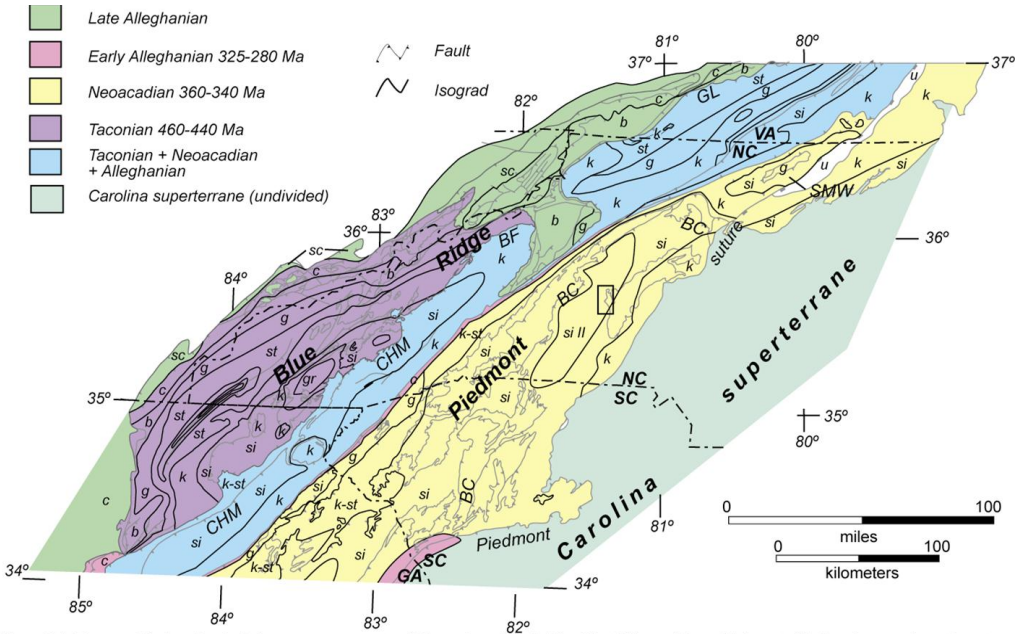

Figure 2. Metamorphic components of Blue Ridge and Inner Piedmont showing inferred ages of each terrane (Merschat, 2009) relative to metamorphic isograds. Abbreviations: g - garnet, k - kyanite, st - staurolite, c - chlorite, si - sillimanite, b - biotite.

According to Hatcher et al. (2005), the western Blue Ridge, represents the Laurentian margin and consists of mostly early to middle Proterozoic basement rocks and sediments deposited along the rifted margin. It is separated from the central Blue Ridge by the Great Smoky - Holston Mountain - Hayesville Fault (Fig. 3a). The Hayesville

Fault in particular identifies an abrupt appearance of abundant mafic and ultramafic rocks to the east, versus a few or no such rocks to the west (Hatcher et al., 1978; 2005). The central Blue Ridge is predominated by quartz - biotite - plagioclase schists and gneisses, whereas rocks of the western Blue Ridge are characterized by the abundance of two-mica, two-feldspar metasandstones (Hatcher et al., 2005). Detrital zircons in schists and gneisses from the central Blue Ridge yield ages as old as Grenvillian, leading Hatcher et al. (2005) to suggest that the protoliths of these rocks most likely represent a distal Laurentian margin sequence.

The central Blue Ridge consists of the Cowrock terrane, Cartoogechaye terrane, and the Dahlonega gold belt (Fig. 3a). The Cowrock terrane contains metasandstones, schists, and some mafic/ultramafic rocks (Hartley, 1973). The eastern boundary of the Cowrock terrane is the Soque River fault, which forms the western boundary of the Dahlonega gold belt and eastern boundary of the Cartoogechaye terrane (Hatcher, 2010). The Cartoogechaye terrane consists of metasandstones, schists, some mafic/ultramafic rocks, and some Grenville basement (Hatcher et al., 2004). This terrane lies to the northeast and atop the Cowrock terrane (Hatcher, 2010). The occurrence of mafic/ultramafic rocks with metasandstone and pelitic schist suggests that they possibly represent former oceanic crust and mantle overlain by ocean floor sediments and/or part of an accretionary wedge (Hatcher, 2010).

The Dahlonega gold belt (DGB) is a linear rock exposure between the Cowrock and Cartoogechaye terranes to the west and the Tugaloo terrane to the east. It is bounded by the Soque River fault to the west and the Chattahoochee fault to the east (Hatcher, 2010). It is comprised of mostly metasandstones and schists with several mafic units

(German, 1985; Hopson et al., 1989). Hibbard et al. (2006) characterize this belt as a metamorphosed magmatic arc, whereas, according to Hatcher (2010), metavolcanic rocks only make up 10% of the DGB. The relationship between the DGB, the Cowrock terrane, Cartoogechaye terrane, and the Laurentian margin is still debated and perplexing.

The eastern Blue Ridge is predominantly made of the western part of the Tugaloo terrane. The Tugaloo terrane lies to the east of the Chattahoochee fault and contains metasandstones, schists, and amphibolites overlain by aluminous schists which are in turn overlain by metasandstones and pelitic schists with small amounts of mafic amphibolites (Hatcher, 1971, 1973), small amounts of Grenville basement rock, and several granitic plutons that intruded during the middle - late Paleozoic (Miller et al., 2000). These plutons are mostly granodiorite with some tonalite (Miller et al., 1998; McDowell et al., 2002; Stahr et al., 2005).

The relationship between metamorphism and tectonics in the BR is still poorly understood; it is difficult to assign mineral assemblages to specific orogenic events. A detailed petrological study of the pelitic rocks from the Blue Ridge has not been carried out, nor has there been any systematic study of thermobarometric conditions or P-T time paths of individual terranes. The metamorphic isograd map (Fig. 4) compiled from various studies (Eckert et al., 1989; Epenshade et al., 1975; Butler, 1991; Goldsmith et al., 1988; Hadley and Goldsmith, 1963; Hadley and Nelson, 1971; Hatcher and Goldberg, 1991; Hatcher and Merschat, 2006; Hatcher et al., 2007; Higgins et al., 2003; Hopson et al., 1989; Merschat, 2003; Merschat and Wiener, 1988; Nelson et al., 1998; Quinn and Wright, 1993; Rankin et al., 1972; Settles, 2002; and Tull and Holm, 2005) can only be considered preliminary since the isograds were based mostly on fieldwork from a limited

number of outcrops rather than detailed petrologic studies. A few careful petrographic studies of samples from several localities that supposedly belonged to a certain metamorphic zone revealed that they contained index minerals belonging to a completely different metamorphic zone (Nesbitt et al., 1982; Carpenter, 1970; Merschat et al., 2010).

Moreover, it is unclear as to whether metamorphic events precede or post - date movement along the terrane boundaries, or if some of the terranes were over or underthrust by others (Fig. 3a & b). There is also the question of when the Tugaloo terrane was emplaced. Hibbard et al. (2007, 2010) suggest that it was emplaced during the Taconic orogeny, whereas Hatcher et al. (2005) believe that it was emplaced during the Acadian. Therefore, a detailed petrological study of some areas in the Blue Ridge is needed, and can also provide a basis for future age dating work that would answer many of these questions. This study presents a petrological analysis of rocks from selected outcrops along with chemical data and thermobarometric estimates that will contribute to providing some answers to these questions.

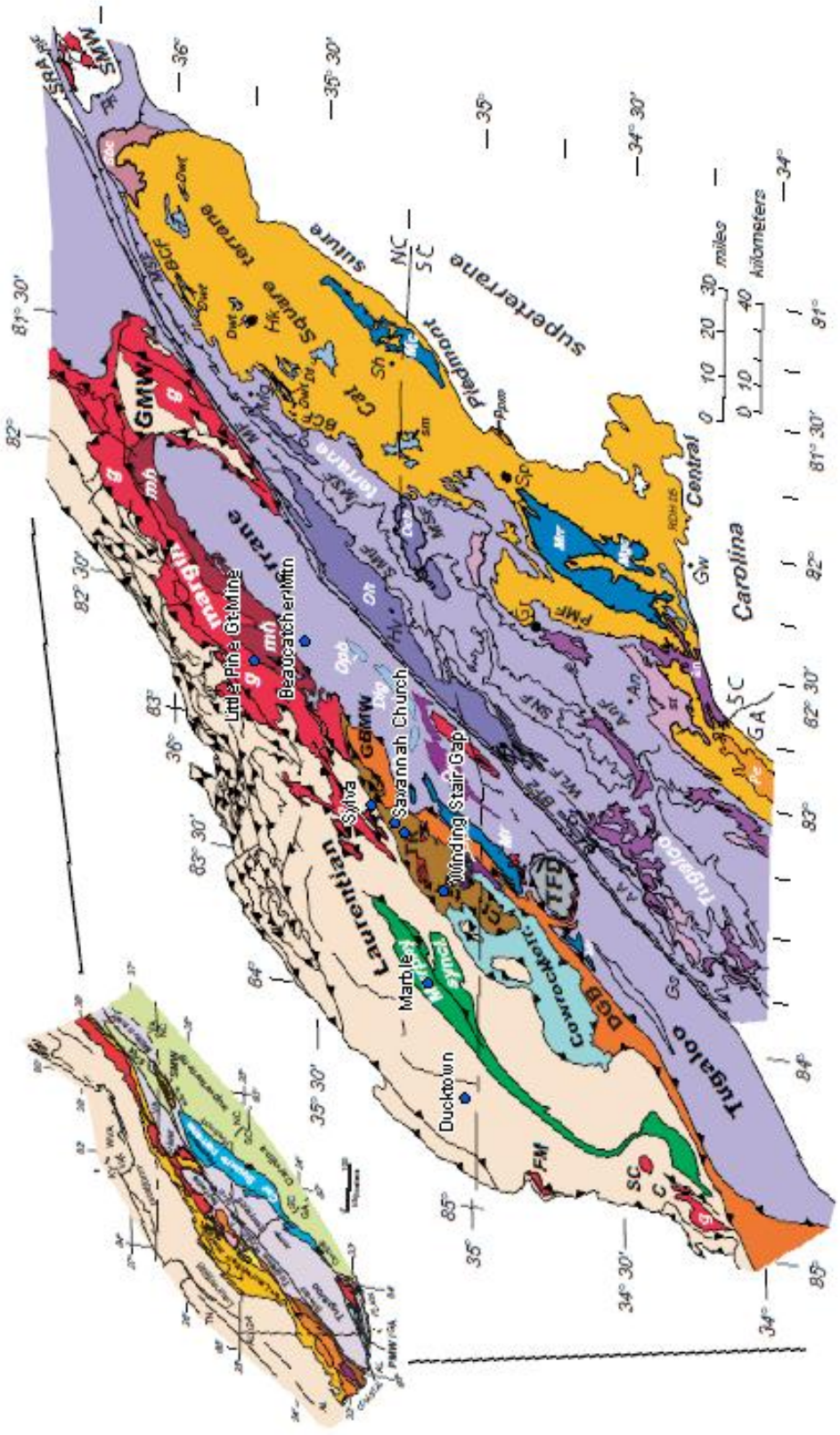

Figure 3a. Map of the different terranes of the BR province (Hatcher et al., 2005) with outcrop sample locations indicated by the blue circles.

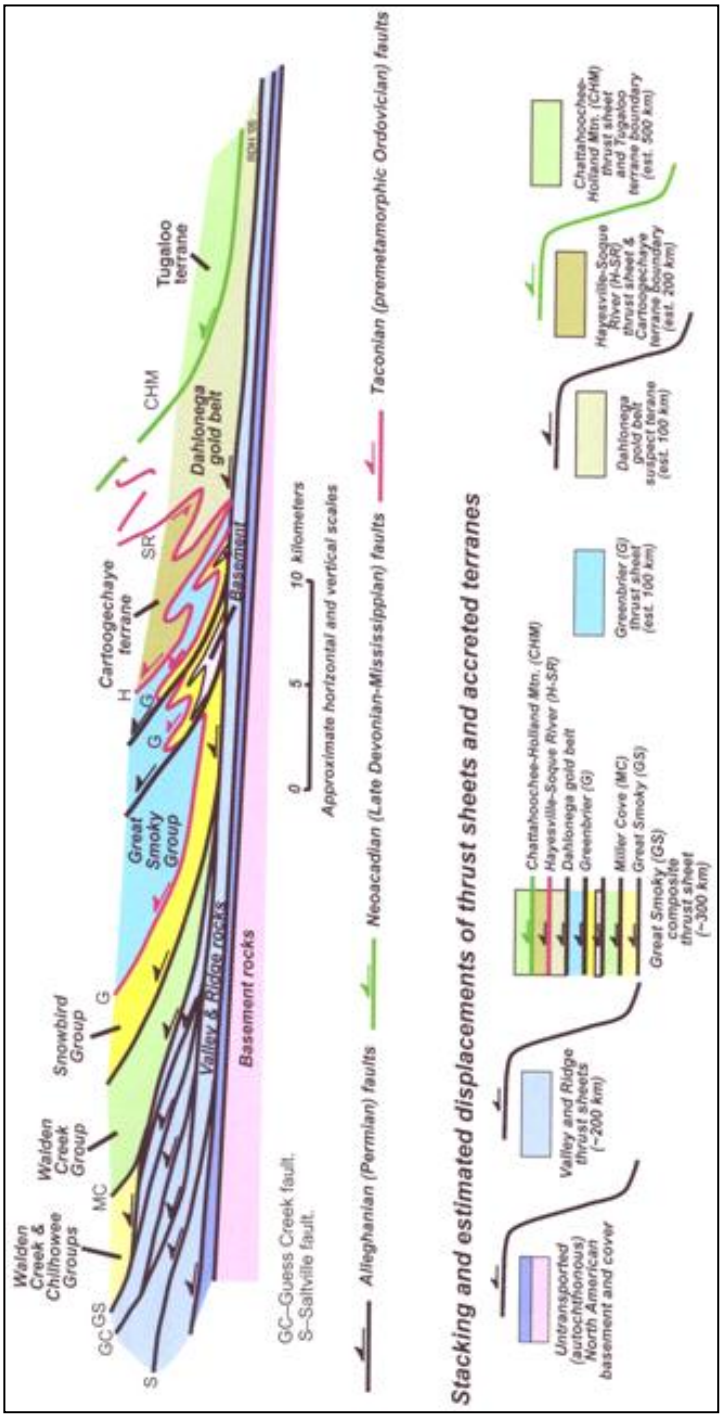

Figure 3b. East – West Cross section of the different terranes and the approximate ages of each (Hatcher et al., 2005).

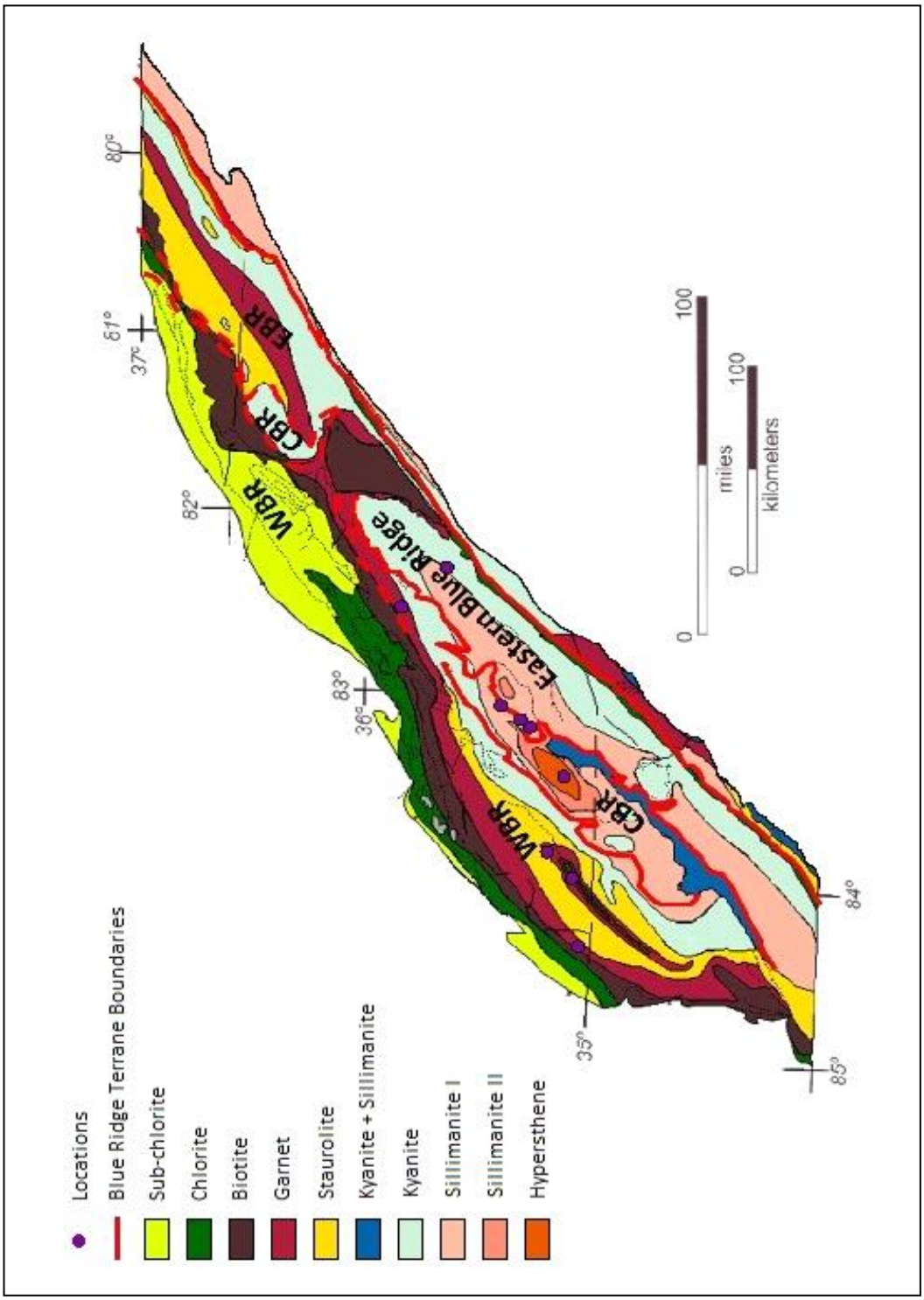

Figure 4. Isograd map of the different Blue Ridge terranes showing the different sampling areas and the Winding Stair Gap along with the major fault zones (HF: Hayesville Fault, CF: Chattahoochee Fault) (Hatcher, 2010; Hadley and Goldsmith, 1963; Carpenter, 1970; Hadley and Nelson, 1971; Rankin et al., 1972; Espenshade et al., 1975; Goldsmith et al., 1988; Merschat and Wiener, 1988; Eckert et al., 1989; Hopson et al., 1989; Butler, 1991; Hatcher and Goldberg, 1991; Quinn, 1991; Nelson et al., 1998; Settles, 2002; Higgins et al., 2003; Merschat, 2003; Tull and Holm, 2005; Hatcher and Merschat, 2006; Hatcher et al., 2007; Tull et al., 2007).

GEOLOGIC SETTING

The main focus for collecting rock samples was a 120 mile stretch along highway 64, State Rt. 23, and highway 74 starting in Ducktown Tennessee, and ending north east of Asheville, North Carolina. Rocks were collected from 6 outcrops along this transect: Ducktown, and Marble, in the western Blue Ridge (WBR), Savannah Church (SVC), Sylva (SV), and Little Pine Garnet Mine in the central Blue Ridge (CBR), and finally Beaucatcher Mountain (BCM - Fig. 5) in the eastern Blue Ridge (EBR). According to Hatcher et al.'s (2005) map showing structural boundaries, the Ducktown outcrop is located in the Western Blue Ridge (WBR). Rocks of Ducktown, TN belong to the Precambrian Great Smoky Group of the Ocoee Supergroup and consist of metagraywackes and mica schists (Hatcher et al., 2005; Nesbitt et al., 1982). The Marble outcrop (also within the WBR) is situated in the Murphy Syncline. Rocks of the Murphy Syncline range in age from Cambrian to Middle Ordivician (Hatcher, 1978). The Sylva outcrop is located in the Cartoogechaye terrane, Savannah Church is located in the Dahlonega Gold Belt, Little Pine Garnet Mine is located in the Grenvillian gneiss margin, and Beaucatcher Mountain is in the Tugaloo terrane (Fig. 3a).

Rocks of the Dahlonega Gold Belt are predominantly pelitic schists and metasandstones (German, 1985; Settles, 2002). The Grenville Gneiss Margin contains gneisses that were formed during the Grenvillian orogeny, after which they underwent several events of folding and deformation during the Paleozoic (Bartholomew and Lewis, 1988). The Cowrock terrane of the central Blue Ridge consists of high - grade gneisses, schists, amphibolites, and migmatites (Hatcher et al., 2005; Absher & Mcsween, 1985; Eckert et al., 1989). The Cartoogechaye terrane, which is overthrust on top of the

Cowrock terrane, consists of metasandstone, pelitic schist, and an assemblage of mafic and ultramafic rocks (Hatcher et al., 2005). The mafic/ultramafic rocks of the Cartoogechaye terrane are interpreted as ophiolitic slices; however the source of the protolith of the metasedimentary rocks is still unclear (Hatcher et al., 2005). The Hayesville fault is the main boundary between the western and central Blue Ridge and is considered to be premetamorphism (Hatcher, 1978). According to Hatcher et al. (2005); Absher & Mcsween, (1985); Eckert et al., (1989); Moecher et al (2004); El-Shazly et al. (2011), all these rocks were metamorphosed under conditions as high as the granulite facies during the Taconic orogeny. The metamorphic grade varies from west to east and the maximum conditions of 850 ˚C and 9.5 kbars were reached in Winding Stair Gap of the central Blue Ridge (El-Shazly et al., 2011).

Objectives

The primary goals of this project are as follows:

- Identify peak metamorphic mineral assemblages in several areas throughout the Blue Ridge Province.
- Constrain peak P-T conditions of metamorphism for areas throughout the Blue Ridge.
- Possibly establish the direction of increasing/decreasing metamorphic grade and why it increases/decreases in that direction.
- Reconstruct the P-T paths for some of the samples studied to help identify the tectonic position of their respective terranes.
- Determine the relationships between metamorphism and major structural/deformational events.

ANALYTICAL TECHNIQUES

Seventeen samples were selected for petrographic analysis: two from Beaucatcher Mountain, five from Little Pine Garnet Mine, three from Savannah Church, four from Sylva, and one each from Marble, and Ducktown. Table 1 lists the coordinates of each sample locality.

Table 1

Location	Latitude	Longitude	Easting	Northing
GFT-5 Ducktown	35.033300	-84.381000	738920	3879872
GFT-7 Marble	35.168300	-83.921300	233934	3895616
Little Pine Gt-Mine	35.770000	-82.622861	353306	3959653
SVC-3	35.292816	-83.275250	293104	3907890
SVC-5	35.259856	-83.310807	289785	3904309
SVC-7	35.259856	-83.310807	289785	3904309
SV-4	35.371450	-83.205160	299673	3916469
SV-7	35.371450	-83.205160	299673	3916469
GFT-23	35.371450	-83.205160	299673	3916469
GFT-24	35.371450	-83.205160	299673	3916469
BCM-2	35.600000	-82.537489	360728	3940672
WSG	35.122400	-83.545094	268076	3889582

The samples selected for detailed analysis included garnet–biotite schists and gneisses, garnet - chlorite schists, staurolite - biotite schists, garnet amphibolites, garnet - hornblende gneisses, and garnet - biotite - hornblende granofelses. Table 2 lists the modal contents of the samples studied. The majority of the rock samples collected for this study were semi - pelitic and are interpreted to represent metamorphosed greywackes. The main mineral assemblage for the semi - pelitic/pelitic samples was characterized by garnet - biotite - plagioclase - ilmenite - quartz ± sillimanite - rutile, which for the more mafic rocks (calc - silicates/admixtures of carbonates and greywackes) is garnet - biotite - amphibole - plagioclase - rutile - quartz ± sillimanite - rutile. After extensive examination of each of the thin sections made from these rocks, samples containing minerals

appropriate for geothermobarometric calculations were chosen for microprobe analysis using the Scanning Electron Microscope (SEM). When doing quantitative analysis on the SEM, it is useful to probe cores and rims of each of these minerals to see if there is any change in composition (zoning). Most of the samples contained more than one crystal of garnet, and in those cases, 4 - 7 garnets were analyzed in each thin section, and multiple analyses of biotite and plagioclase were made to assess homogeneity. To characterize the zoning patterns of the various minerals, compositional x - ray maps were made.

Microprobe analysis was carried out on a JEOL JSM 5310 LV scanning electron microscope equipped with a Link Pentafet EDS at Marshall University. Analytical conditions were 20 kV operating voltage, 95 mAmp condenser lens current, a working distance of 20 mm, and a beam size of 2 μm. Beam current intensity was monitored on pure Co, with a calibration performed every 2 hours maintaining a count rate of 18 - 24 kcps, and a dead time of 35%. Standardization was performed on well - characterized Smithsonian Institution standards, all mounted on the same sample holder. Standards included microcline (Si, K, Al), scapolite (Na, Al, Cl), Kakanui hornblende (Ti), Kakanui pyrope (Mg, Si, Al), diopside (Ca, Mg), chromite (Cr), Roberts Victor garnet 1 and 2 (Ca, Si), Rockport fayalite (Fe, Mn), Johnstown hypersthene (Fe), gahnite (Zn) and INGAR garnet (Fe, Mn). These and additional standards (e.g. Kakanui augite and Lake County plagioclase) were routinely analyzed as unknowns to check on the quality of the analyses. Analytical data were processed using LINK ISIS 3.1 software and a ZAF correction routine. Precision is estimated at1–2% for all oxide weight percentage values, and 10% or better for Na_2O. Mineral formulae were calculated on the basis of 8, 12 and 22 oxygen atoms per formula unit (apfu) for feldspar, garnet and biotite respectively, assuming all

Fe as Fe^{2+} for the latter two minerals. Formulae for anthophyllite/gedrite and hornblende were calculated based on 15 cations less Na and K, and 13 cations less Na + K + Ca respectively (Robinson et al., 1982), using program probe - amph (Tindle, 2000). Formulae for staurolite, chlorite, and ilmenite were calculated on the basis of 23, 28, and 3 oxygens, respectively, using the excel spreadsheet programs of Tindle (2000). All end - member activities for mineral pairs used in conventional thermobarometry were calculated using AXWIN (Holland & Powell, 2005), and the results were used to determine an average P–T condition defined by the intersection of all independent reactions using THERMOCALC 3.26 (Powell & Holland, 2002). Program CSPACE (Torres - Roldan et al., 1999) was used to create compositional phase diagrams for each of the samples studied, and to characterize the peak mineral assemblage at each locality.

PETROGRAPHY AND MINERAL CHEMISTRY

WESTERN BLUE RIDGE

Ducktown:

The rocks exposed at this location are schists and metasandstones that are part of the Copperhill Formation and display transposition and reverse graded bedding (Hatcher, 2010). The mineral assemblage is garnet + biotite + muscovite + quartz + ilmenite with retrograde chlorite for a garnet - chlorite schist. Sample GFT-5 was not used in microprobe analyses due to the lack of plagioclase or any aluminosilicates which are essential for thermobarometry. However, Nesbitt et al. (1982) reported the mineral assemblages quartz + feldspar + biotite + muscovite + ilmenite ± calcite/garnet/staurolite/clinozoisite for metagreywackes and biotite + muscovite + quartz

+ feldspar + garnet ± ilmenite/staurolite for the mica schists. According to Nesbitt et al. (1982) thermobarometry on these Ducktown rocks yielded pressures of 6 kbars and temperatures of 540 ˚C.

Table 2. Modal contents of samples.

	Ducktown	Marble	Little Pine Garnet Mine					Savannah Church			Sylva				BCM
	GFT-5	GFT-7	LP-1	LP-10	LP-7	LP-12	LP-13	SVC-3	SVC-5	SVC-7	SV-4	SV-7	GFT-23	GFT-24	BCM-2
Garnet	20	10	–	15	1	20	10	10	5	15	15	5	8	10	5
Staurolite	–	15	5	–	2	5	–	–	–	–	–	–	–	–	–
Biotite	10	15	15	10	30	tr	tr	30	25	20	15	30	20	32	15
Muscovite	5	10	–	–	1	–	1	–	1	–	–	–	1	–	10
Chlorite	20	5	19	–	10	5	20	–	3	–	–	–	2	–	–
Sill	–	–	1	–	1	1	–	–	–	–	–	–	–	–	–
Hornblende	–	–	–	–	–	–	–	15	–	–	30	1	–	15	–
Gedrite	–	–	10	35	31	39	5	–	–	–	–	–	–	–	–
Anthophyllite	–	–	35	tr	10	15	–	–	–	–	–	–	–	–	–
Talc	–	–	–	–	–	10	57	–	–	–	–	–	–	–	–
Clinozoisite	–	–	–	–	–	–	–	–	–	–	1	3	4	4	–
Epidote	–	–	–	–	–	–	–	–	1	–	–	–	1	3	–
Plagioclase	–	5	–	5	–	1	–	10	10	10	15	10	42	15	35
K-feldspar	–	–	–	–	–	–	–	–	10	1	1	1	–	–	–
Quartz	36	30	1	25	1	1	1	26	39	48	14	36	20	7	30
Rutile	–	–	5	4	1	3	–	–	–	–	1	–	–	1	–
Opaque	3(ilm)	10	7	5	10(ilm)	5(ilm)	5	5	3(ilm)	3(ilm)	3(ilm)	3(ilm)	1(ilm)	1	1
Sphene	–	–	1	–	1	–	1	–	–	–	2	–	tr	5	1
Zircon	1	–	1	–	–	–	–	1	1	1	1	1	1	–	1
Apatite	–	–	–	1	1	–	–	1	1	1	1	–	tr	1	–
Monazite	–	tr	–	–	–	–	–	1	1	1	1	–	–	1	1
Calcite	–	–	–	–	–	–	–	1	–	–	–	10	–	5	1
Xenotime	–	–	–	–	–	tr	tr	tr	tr	–	tr	–	–	–	tr

Marble:

Rocks exposed at the Marble location are staurolite - garnet metasiltstones of the Mineral Bluff Formation and have relict bedding (Hatcher, 2010). The rock used in this study is a staurolite - biotite - garnet schist. The peak mineral assemblage for this rock is quartz + ilmenite + muscovite + biotite + garnet + plagioclase + staurolite (Fig. 5). Sphene and chlorite are retrograde phases.

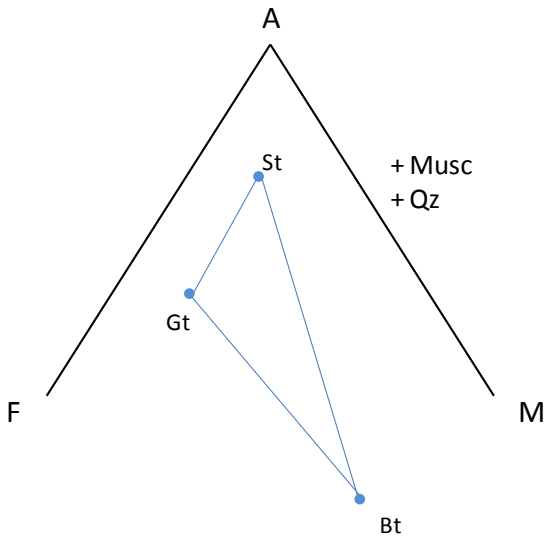

Figure 5. AFM projection from muscovite and quartz for the marble location depicting the peak mineral assemblage as Gt + Bt + St. Garnet and biotite compositions plotted represent the average composition for analyses from sample GFT-7.

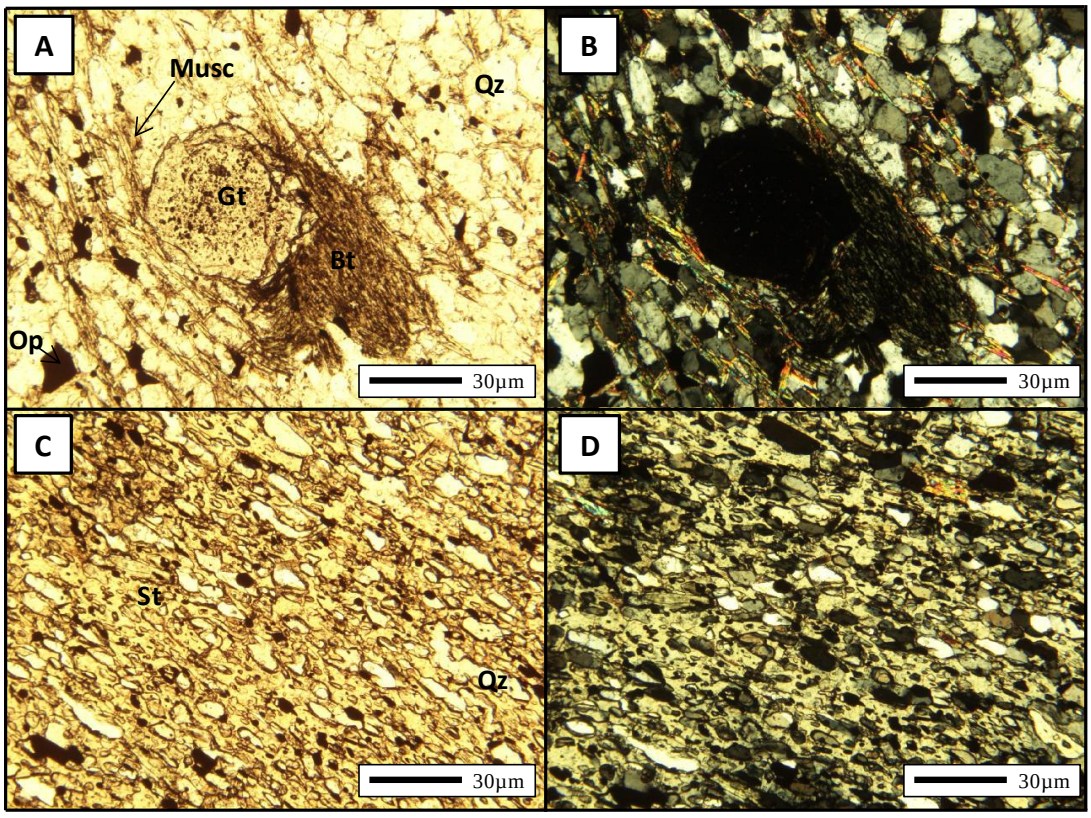

Figure 6. Photomicrographs from Marble (GFT-7). A - B) Garnet crystal full of inclusions of quartz rimmed by biotite and muscovite (A - plane polarized light, B - crossed polarized light). C - D) Porphyroblastic crystal of staurolite exhibiting a poikiloblastic texture with quartz (C - plane polarized light, D - crossed polarized light).

Garnets: Garnets in this location contain many inclusions of quartz, ilmenite, plagioclase, and sphene (Fig. 6 A - B). Some of the garnets are anhedral and resorbed, whereas others are very euhedral in shape. The grain sizes range from 0.35 to 1 mm, the smaller of which are anhedral in shape and contain more fractures. Garnets from Marble are more or less homogenous and are almandine rich with high amounts of spessartine, and only minor increase of spessartine and almandine along their outermost rims (X_{alm} = 0.54 - 0.56, X_{grs} = 0.02 - 0.05, X_{prp} = 0.15 - 0.17, X_{spss} = 0.20 - 0.22; Fig. 7, Table 3).

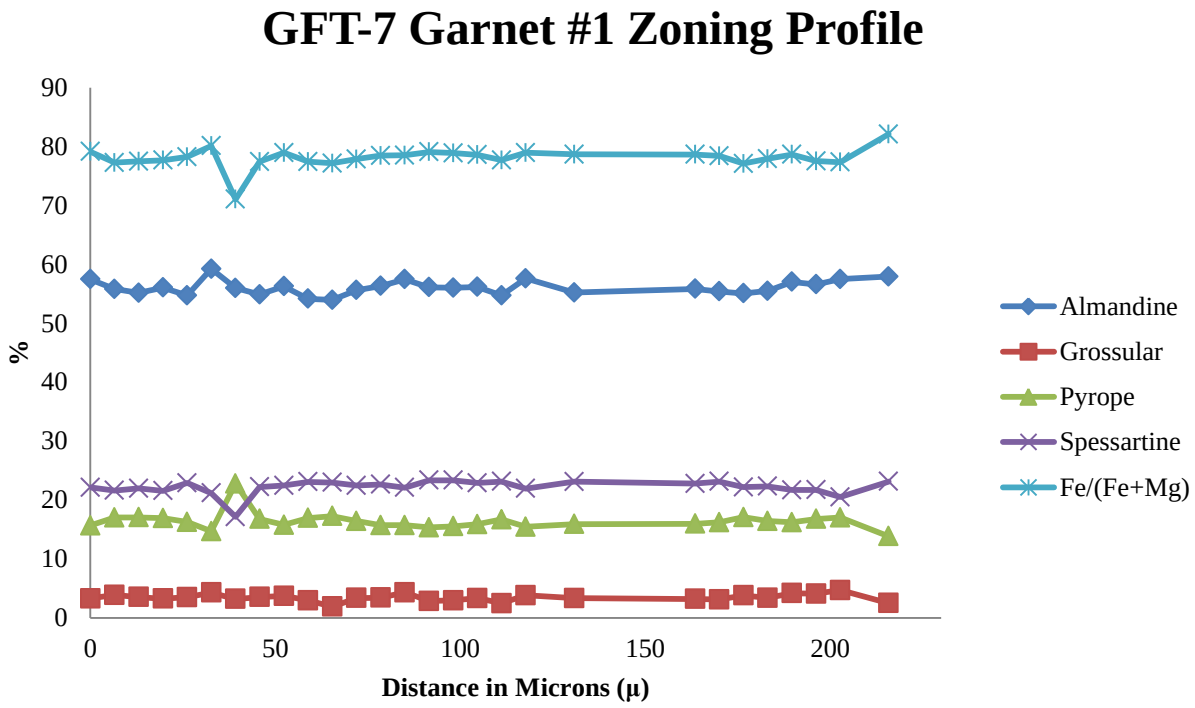

Figure 7. Garnet profile showing consistent compositions throughout garnet minus inclusions (random peaks) and the enrichment of spessartine at the rims.

Table 3. Representative garnet analyses for Marble

	gt3										gt4									
	rim1	rim2	rim3	rim4	rim5	core1	core2	core3	rim6	rim7	rim1	core1	rim2	rim3	rim4	core2	rim6	rim7	core3	core4
SiO2	36.61	36.44	36.51	36.47	37.24	36.78	37.14	36.94	37.04	37.15	37.32	36.83	37.15	37.72	36.50	37.14	36.95	36.55	36.86	36.61
TiO2	0.05	0.05	0.00	0.00	0.07	0.01	0.14	0.12	0.08	0.10	0.01	0.20	0.14	0.00	0.01	0.11	0.01	0.12	0.33	0.12
Al2O3	21.45	20.99	21.28	21.32	21.23	21.33	21.29	21.21	21.04	21.14	21.35	21.33	21.23	21.52	21.43	21.33	21.54	21.51	21.25	20.99
Cr2O3	0.19	0.22	0.24	0.24	0.20	0.20	0.27	0.30	0.19	0.14	0.24	0.19	0.27	0.17	0.34	0.25	0.26	0.34	0.27	0.18
Fe2O3	0.18	0.55	0.30	0.44	0.60	0.54	0.31	0.68	0.43	0.66	0.24	0.52	0.09	0.00	0.41	0.44	0.30	0.39	0.53	0.70
FeO	25.56	25.67	26.17	25.84	25.62	25.90	26.34	25.83	25.78	25.83	25.87	26.27	25.85	25.58	25.55	26.24	26.12	25.39	26.20	25.65
MnO	9.65	9.61	9.48	9.82	9.33	9.22	9.02	9.16	9.62	9.85	9.61	8.99	9.33	9.48	9.68	8.80	9.54	9.62	8.72	9.06
MgO	3.92	4.07	3.78	3.79	4.23	4.04	3.89	4.22	3.94	3.97	3.97	4.08	3.99	4.01	4.08	4.11	3.90	4.25	4.07	4.14
CaO	2.20	1.80	1.98	2.11	2.40	2.39	2.37	2.42	2.02	2.10	2.16	2.26	2.09	2.17	2.21	2.46	2.23	2.25	2.60	2.33
Total	99.80	99.41	99.75	100.02	100.92	100.40	100.78	100.88	100.15	100.93	100.78	100.67	100.14	100.64	100.20	100.86	100.84	100.41	100.82	99.77
Si	2.94	2.94	2.94	2.93	2.96	2.94	2.95	2.94	2.97	2.96	2.97	2.94	2.97	2.99	2.92	2.95	2.94	2.92	2.93	2.94
Al iv	0.06	0.06	0.06	0.07	0.04	0.06	0.05	0.06	0.03	0.04	0.03	0.06	0.03	0.01	0.08	0.05	0.06	0.08	0.07	0.06
Al vi	1.97	1.94	1.96	1.95	1.94	1.95	1.95	1.93	1.95	1.94	1.97	1.94	1.97	2.00	1.95	1.95	1.96	1.95	1.93	1.93
Ti	0.00	0.00	0.00	0.00	0.00	0.00	0.01	0.01	0.00	0.01	0.00	0.01	0.01	0.00	0.00	0.01	0.00	0.01	0.02	0.01
Cr	0.01	0.01	0.02	0.02	0.01	0.01	0.02	0.02	0.01	0.01	0.02	0.01	0.02	0.01	0.02	0.02	0.02	0.02	0.02	0.01
Fe3+	0.01	0.03	0.02	0.03	0.04	0.03	0.02	0.04	0.03	0.04	0.01	0.03	0.01	0.00	0.02	0.03	0.02	0.02	0.03	0.04
Fe2+	1.72	1.73	1.76	1.74	1.70	1.73	1.75	1.72	1.73	1.72	1.72	1.75	1.73	1.70	1.71	1.74	1.74	1.70	1.74	1.72
Mn	0.66	0.66	0.65	0.67	0.63	0.62	0.61	0.62	0.65	0.66	0.65	0.61	0.63	0.64	0.66	0.59	0.64	0.65	0.59	0.62
Mg	0.47	0.49	0.45	0.45	0.50	0.48	0.46	0.50	0.47	0.47	0.47	0.48	0.48	0.47	0.49	0.49	0.46	0.51	0.48	0.50
Ca	0.19	0.16	0.17	0.18	0.20	0.20	0.20	0.21	0.17	0.18	0.18	0.19	0.18	0.18	0.19	0.21	0.19	0.19	0.22	0.20
Xalm	0.55	0.56	0.57	0.56	0.55	0.55	0.57	0.55	0.56	0.56	0.56	0.56	0.57	0.57	0.54	0.56	0.56	0.54	0.56	0.55
Xand	0.01	0.02	0.01	0.01	0.02	0.02	0.01	0.02	0.01	0.02	0.01	0.02	0.00	0.00	0.01	0.01	0.01	0.01	0.02	0.02
Xgrs	0.05	0.03	0.04	0.04	0.04	0.05	0.05	0.04	0.04	0.04	0.05	0.04	0.05	0.06	0.04	0.05	0.05	0.04	0.05	0.04
Xprp	0.16	0.17	0.15	0.15	0.17	0.16	0.16	0.17	0.16	0.16	0.16	0.17	0.16	0.16	0.17	0.17	0.16	0.17	0.16	0.17
Xspss	0.22	0.22	0.22	0.23	0.21	0.21	0.21	0.21	0.22	0.22	0.22	0.21	0.21	0.21	0.22	0.20	0.22	0.22	0.20	0.21
Xuv	0.01	0.01	0.01	0.01	0.01	0.01	0.01	0.01	0.01	0.00	0.01	0.01	0.01	0.01	0.01	0.01	0.01	0.01	0.01	0.01

Biotites: Sample GFT7 contains both brown biotite and green/brown biotite. Both types of biotite are very euhedral and very coarse grained (porphyroblastic texture), ranging from 3.5 to 4 mm in size. These also contain inclusions of quartz, plagioclase, and ilmenite. The fine grained variety of biotite (0.05 to 0.35 mm) is always brown. There was no detected compositional difference between the two biotite varieties (assuming all Fe is Fe^{2+}) and both were homogenous (Table 4). Their compositions are Al^{iv} = 2.62 - 2.83, Al^{vi} = 0.43 - 0.59, Fe/(Fe + Mg) = 0.34 - 0.36, Ti^{iv} = 0.10 - 0.20 (Fig. 8).

Table 4. Representative biotite analyses for Marble

	gt5bt1 (brown)								gt5bt2 (green)						
	core1	rim1	core2	rim2	rim3	core3	rim4	rim5	rim1	core1	core2	core3	core4	rim2	core5
SiO2	37.63	37.47	37.26	37.17	36.37	36.69	36.92	36.90	36.93	37.13	35.96	36.86	36.32	39.81	36.80
TiO2	1.30	1.36	1.47	1.27	1.43	1.36	1.39	1.45	1.37	1.26	1.26	1.48	1.48	1.29	1.50
Al2O3	18.66	18.42	18.39	18.36	18.21	18.54	18.53	18.32	18.34	18.66	17.90	18.22	17.91	18.92	18.27
FeO	14.56	14.59	14.97	14.76	15.32	14.41	14.24	14.67	14.98	14.78	14.46	15.00	14.77	13.58	15.09
MnO	0.21	0.12	0.16	0.12	0.00	0.11	0.17	0.10	0.15	0.12	0.08	0.18	0.10	0.11	0.07
MgO	15.29	14.75	15.07	15.17	14.57	14.69	15.02	14.86	15.19	14.89	14.15	14.57	14.76	13.23	14.89
CaO	0.02	0.10	0.06	0.02	0.08	0.00	0.00	0.06	0.05	0.01	0.06	0.08	0.15	0.13	0.00
Na2O	0.66	1.07	0.91	1.01	0.78	1.31	0.79	0.90	0.95	1.20	0.79	0.96	1.03	0.98	0.67
K2O	9.10	9.07	9.01	9.09	8.61	8.99	9.02	9.05	8.62	8.54	8.54	8.88	8.76	8.13	8.78
Cr2O3	0.00	0.00	0.00	0.01	0.01	0.02	0.00	0.07	0.00	0.06	0.00	0.00	0.07	0.00	0.10
Total	97.44	96.95	97.30	96.97	95.38	96.13	96.07	96.37	96.59	96.64	93.21	96.24	95.36	96.18	96.18
Si	5.36	5.38	5.35	5.35	5.34	5.34	5.35	5.35	5.34	5.35	5.40	5.36	5.34	5.61	5.35
Al iv	2.64	2.62	2.65	2.65	2.66	2.66	2.65	2.65	2.66	2.65	2.60	2.64	2.66	2.39	2.65
Al vi	0.50	0.50	0.45	0.47	0.50	0.52	0.52	0.48	0.46	0.52	0.57	0.48	0.45	0.75	0.47
Ti	0.14	0.15	0.16	0.14	0.16	0.15	0.15	0.16	0.15	0.14	0.14	0.16	0.16	0.14	0.16
Cr	0.00	0.00	0.00	0.00	0.00	0.00	0.00	0.01	0.00	0.01	0.00	0.00	0.01	0.00	0.01
Fe	1.74	1.75	1.80	1.78	1.88	1.75	1.73	1.78	1.81	1.78	1.82	1.82	1.82	1.60	1.83
Mn	0.03	0.01	1.80	0.01	0.00	0.01	0.02	0.01	0.02	0.01	0.01	0.02	0.01	0.01	0.01
Mg	3.25	3.16	3.22	3.26	3.19	3.19	3.25	3.21	3.27	3.20	3.17	3.16	3.24	2.78	3.22
Li*	0.72	0.69	0.66	0.65	0.52	0.57	0.61	0.60	0.61	0.64	0.46	0.60	0.52	1.06	0.59
Ca	0.00	0.02	0.01	0.00	0.01	0.00	0.00	0.01	0.01	0.00	0.01	0.01	0.02	0.02	0.00
Na	0.18	0.30	0.25	0.28	0.22	0.37	0.22	0.25	0.27	0.33	0.23	0.27	0.29	0.27	0.19
K	1.65	1.66	1.65	1.67	1.61	1.67	1.67	1.67	1.59	1.57	1.64	1.65	1.64	1.46	1.63
Al total	3.13	3.12	3.11	3.12	3.15	3.18	3.17	3.13	3.12	3.17	3.17	3.12	3.11	3.14	3.13
Fe/Fe+Mg	0.35	0.36	0.36	0.35	0.37	0.35	0.35	0.36	0.36	0.36	0.36	0.37	0.36	0.37	0.36

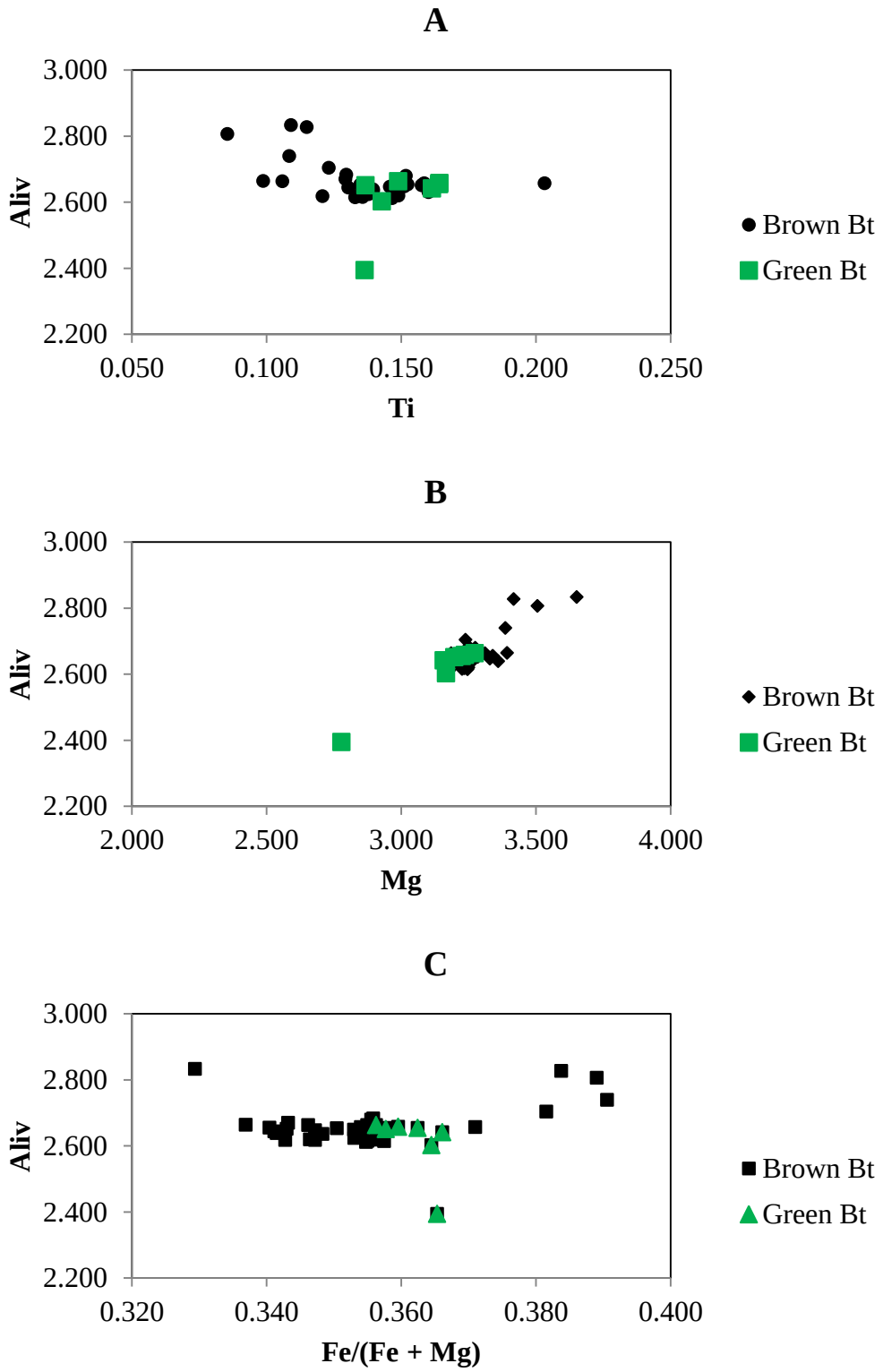

Figure 8. Compositions of biotites from GFT-7 (Marble) plotted on (A) Al^{iv} vs. Ti, (B) Al^{iv} vs. Mg, and (C) Al^{iv} vs. Fe/(Fe + Mg).

Other Minerals: Minor amounts of plagioclase occur in these rocks as fine - grained (~ 0.1 mm) anhedral crystals. The plagioclase crystals are albite rich (X_{ab} = 0.80, X_{an} = 0.20; Table 5). Staurolite displays a poikiloblastic texture and is also very coarse grained (~4 mm; Fig. 6 C & D). The staurolite crystals contain inclusions of quartz, biotite, muscovite and ilmenite. They are also resorbed and highly fractured with chlorite filling in the cracks.

Table 5. Representative feldspar analyses for Marble

	gt4plg1					
	P1	P2	P3	P4	P5	P6
SiO2	62.43	61.03	62.11	62.24	62.42	61.06
TiO2	0.01	0.00	0.03	0.00	0.03	0.04
Al2O3	23.26	22.94	23.35	23.64	23.86	23.47
FeO	0.14	0.13	0.04	0.08	0.03	0.02
MnO	0.00	0.00	0.00	0.00	0.00	0.00
MgO	0.61	0.51	0.84	0.68	0.70	0.33
CaO	4.54	4.61	4.45	4.54	4.55	4.62
Na2O	9.34	9.33	9.63	9.17	9.67	9.39
K2O	0.18	0.15	0.23	0.07	0.05	0.11
Total	100.51	98.70	100.67	100.41	101.31	99.04
Si	2.76	2.75	2.74	2.75	2.74	2.74
Al	1.21	1.22	1.22	1.23	1.23	1.24
Ti	0.00	0.00	0.00	0.00	0.00	0.00
Fe	0.01	0.00	0.00	0.00	0.00	0.00
Mg	0.04	0.03	0.05	0.04	0.05	0.02
Ca	0.22	0.22	0.21	0.21	0.21	0.22
Na	0.80	0.81	0.82	0.79	0.82	0.82
K	0.01	0.01	0.01	0.00	0.00	0.01
X_{an}	0.21	0.21	0.20	0.21	0.21	0.21
X_{ab}	0.78	0.78	0.79	0.78	0.79	0.78
X_{or}	0.01	0.01	0.01	0.00	0.00	0.01

Little Pine Garnet Mine:

Rock types exposed at the Little Pine Garnet Mine location include mafic/ultramafic rocks interbedded with quartzofeldspathic gneisses and quartz veins (Fig. 9). Samples from the garnet mine are characterized by the mineral assemblages: fine to medium grained staurolite + gedrite/anthophyllite + biotite + rutile + sillimanite +

quartz + sphene ± plagioclase, with chlorite and late ilmenite (LP-1: mafic/ultramafic rock; Fig. 10), garnet + gedrite/anthophyllite + biotite + rutile + quartz ± plagioclase and late ilmenite, (LP-10: quartzofeldspathic gneiss), garnet + staurolite + gedrite/anthophyllite + biotite + rutile + sillimanite + sphene + quartz ± chlorite, late ilmenite, and muscovite (LP-7: mafic/ultramafic rock) all of which are interpreted as retrograde phases (Fig. 11), and coarse grained garnet – talc – anthophyllite ± gedrite ± staurolite ± rutile ± quartz, with late chlorite (LP-12 , LP-13: mafic/ultramafic rock; Fig. 12).

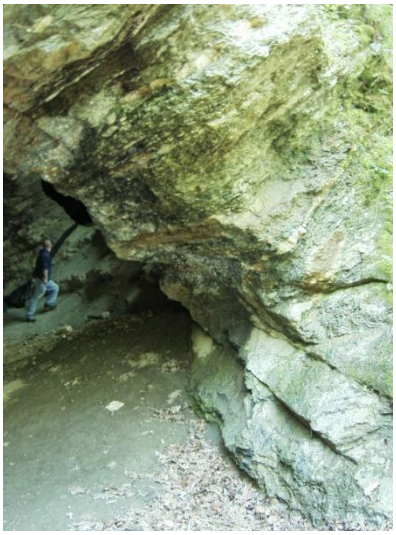

Figure 9. Little Pine Garnet mine showing mafic/ultramafic rocks interbedded with gneisses and quartz veins

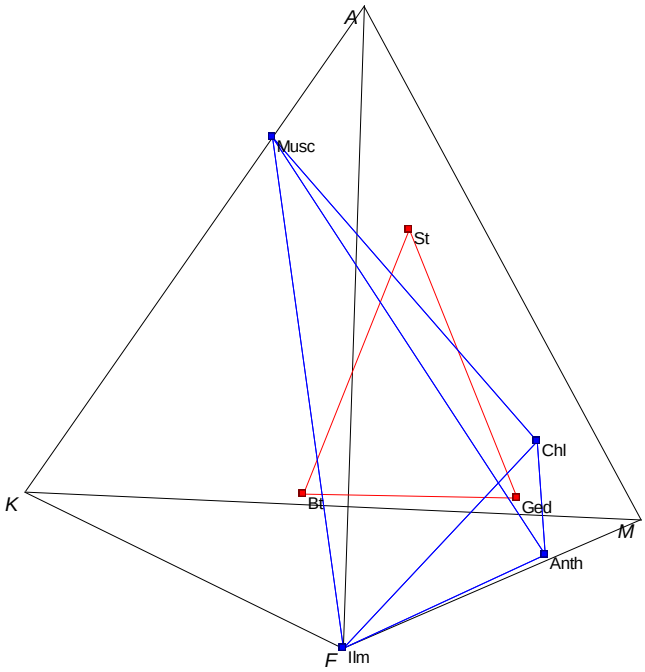

Figure 10. AFMK projection from quartz showing the mineral assemblages St + Bt + Ged and Anth + Ilm + Chl + Ms representing two stages of evolution of sample LP-1, respectively. Diagram rotated to clarify reactions.

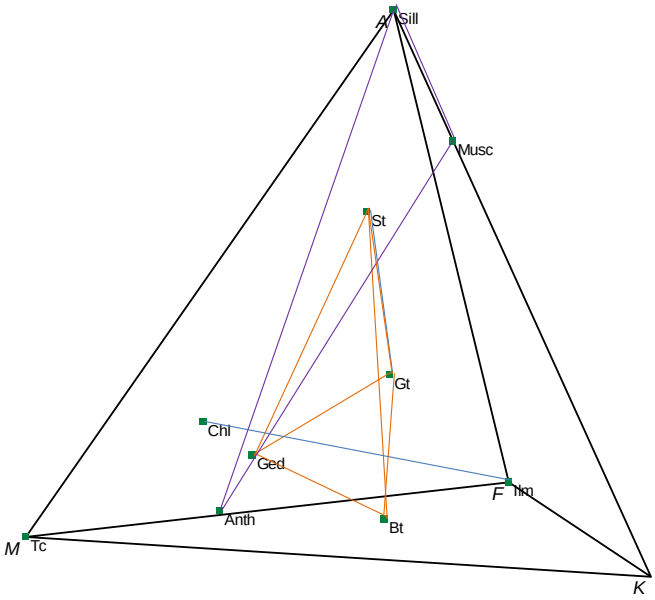

Figure 11. AFMK projection from quartz showing the mineral assemblages Gt + St + Ged + Bt, Anth + Sill ± Ms, and Chl + Ilm characteristic of the three stages of evolution of sample LP-7 (diagram has been rotated to better show the assemblages).

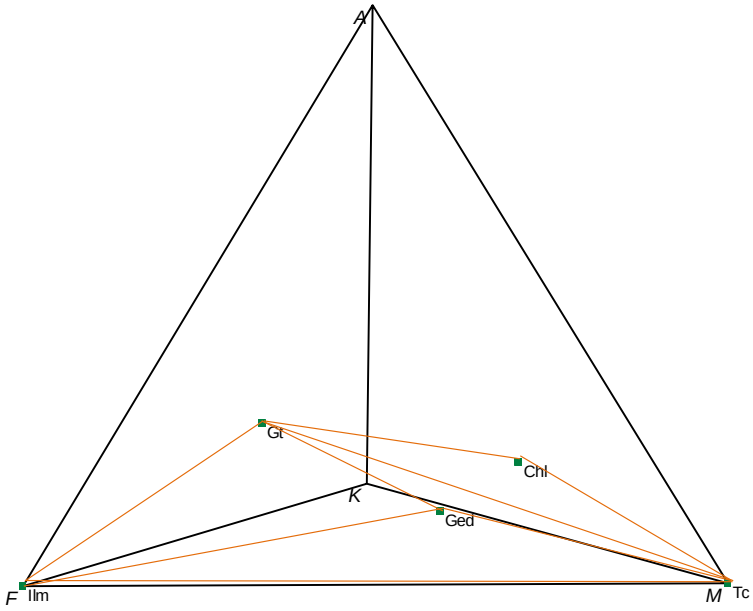

Figure 12. AFMK projection from Qz showing the mineral assemblages of LP-13.

Garnets: Two types of garnet occur in different rocks from this location, fine to medium grained garnets (1 – 5 mm) occurring in biotite – amphibole ± chlorite matrix and coarse grained garnets (about 16 - 25 mm in diameter) occurring in a talc matrix. Both varieties are similar in composition; however, the larger garnets are slightly more enriched in almandine (fine grained garnets from LP-7: X_{alm} = 0.59 - 64, X_{grs} = 0.05 - 0.07, X_{prp} = 0.26 - 0.30, X_{spss} = 0.01 - 0.02, coarse grained garnets from LP-12: X_{alm} = 0.63 - 67, X_{grs} = 0.05 - 0.09, X_{prp} = 0.22 - 0.30, X_{spss} = 0.01 - 0.02; Table 6). The garnets contain inclusions of biotite, quartz, amphibole, rutile, and ilmenite. Fractures in the garnets are filled with biotite and plagioclase. The smaller garnets exhibit mortar textures and seem to be slightly zoned, having a small increase in pyrope in the core and an increase in almandine towards the rim (Figs. 13, 14). Garnets were abundant in LP-10, 12, and 13, but scarce in LP-1 and LP-7.

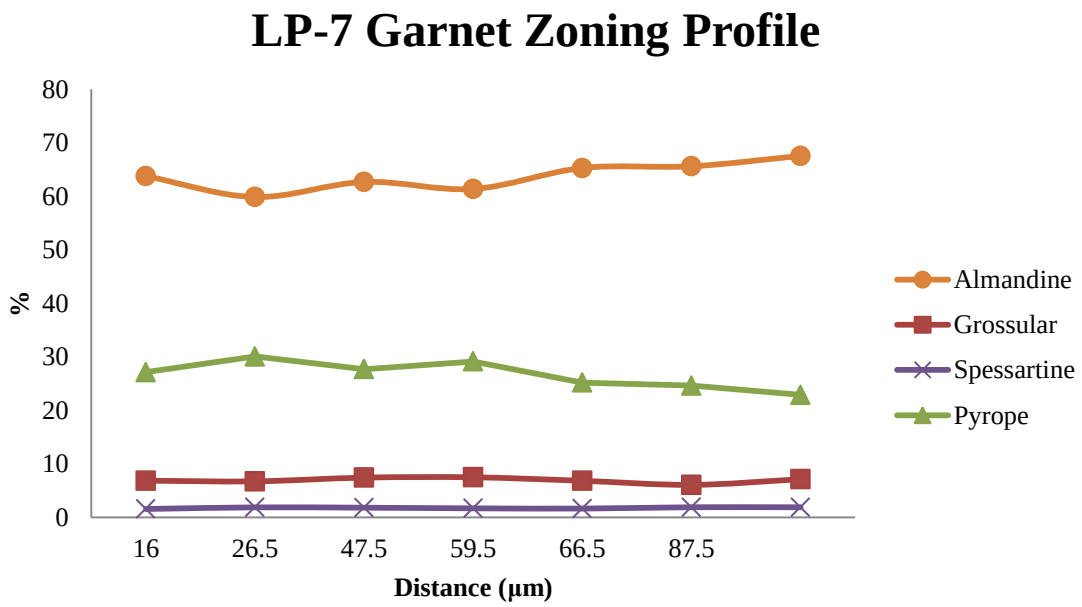

Figure 13. Zoning profile for the finer grained garnet showing slight increases in pyrope in the core and increases in almandine towards the rims (profile was started 16µm from the edge of the garnet).

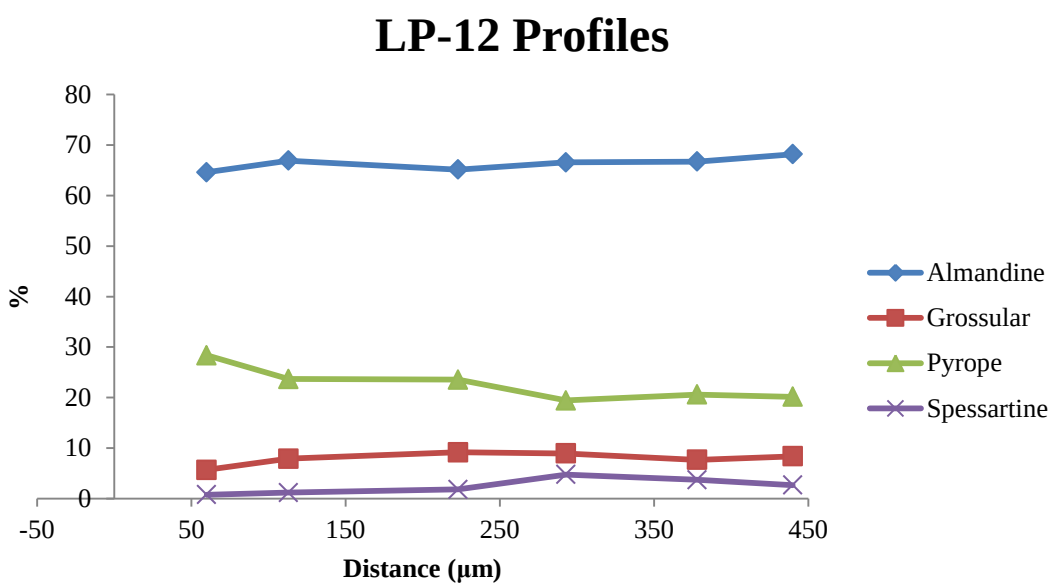

Figure 14. Zoning profile for the coarser grained garnet showing slight increases in pyrope in the core and increases in almandine towards the rims (profile was started at 50µm from the edge of the garnet).

Table 6. Representative garnet analyses for Little Pine Garnet Mine

	lp7									lp12						
	r1	c1	r2	c2	r3	c3	r4	c4	r5	r1	c1	r2	core2	c3	r3	r4
SiO2	37.32	37.79	37.97	37.94	38.04	37.81	37.31	38.56	38.30	37.94	38.66	39.22	35.60	37.36	35.13	34.25
TiO2	0.00	0.20	0.01	0.00	0.00	0.13	0.01	0.05	0.00	0.11	0.07	0.12	0.12	0.00	0.10	0.00
Al2O3	21.87	22.41	22.19	22.18	22.12	22.35	21.96	22.38	22.12	22.45	22.12	22.52	20.56	21.54	19.91	19.82
Cr2O3	0.07	0.11	0.22	0.08	0.25	0.18	0.03	0.03	0.00	0.00	0.00	0.04	0.06	0.00	0.09	0.03
Fe2O3	0.08	0.10	0.00	0.13	0.22	0.32	0.49	0.47	0.10	0.00	0.21	0.00	0.05	0.08	0.00	0.16
FeO	29.48	29.13	30.04	29.73	29.37	28.89	30.60	28.97	29.51	29.45	30.46	29.88	29.19	29.67	27.95	27.41
MnO	0.71	0.70	0.70	0.85	0.67	0.75	0.76	0.85	0.67	0.37	0.36	0.35	0.50	0.71	0.37	0.79
MgO	6.96	7.48	6.91	7.07	7.49	7.80	6.67	7.77	7.39	7.67	7.36	7.60	5.65	6.07	5.47	5.53
CaO	2.45	2.82	2.67	2.59	2.61	2.72	2.41	2.95	2.45	2.13	2.26	2.15	2.74	3.19	2.59	2.87
Total	98.94	100.75	100.71	100.58	100.77	100.95	100.22	102.04	100.54	100.13	101.49	101.86	94.46	98.61	91.62	90.86
Si	2.95	2.93	2.95	2.95	2.95	2.92	2.93	2.95	2.97	2.95	2.98	2.98	2.97	2.97	3.00	2.96
Al iv	0.05	0.07	0.05	0.05	0.05	0.08	0.07	0.05	0.03	0.05	0.02	0.02	0.03	0.03	0.00	0.04
Al vi	1.99	1.98	1.99	1.99	1.97	1.96	1.97	1.96	1.99	2.00	1.98	2.01	1.99	1.99	2.00	1.99
Ti	0.00	0.01	0.00	0.00	0.00	0.01	0.00	0.00	0.00	0.01	0.00	0.01	0.01	0.00	0.01	0.00
Cr	0.00	0.01	0.01	0.00	0.02	0.01	0.00	0.00	0.00	0.00	0.00	0.00	0.00	0.00	0.01	0.00
Fe3+	0.00	0.01	0.00	0.01	0.01	0.02	0.03	0.03	0.01	0.00	0.01	0.00	0.00	0.01	0.00	0.01
Fe2+	1.95	1.89	1.95	1.93	1.90	1.87	2.01	1.85	1.91	1.92	1.96	1.92	2.03	1.97	2.02	1.98
Mn	0.05	0.05	0.05	0.06	0.04	0.05	0.05	0.06	0.04	0.02	0.02	0.02	0.03	0.05	0.03	0.06
Mg	0.82	0.86	0.80	0.82	0.86	0.90	0.78	0.89	0.85	0.89	0.84	0.86	0.70	0.72	0.70	0.71
Ca	0.21	0.23	0.22	0.22	0.22	0.22	0.20	0.24	0.20	0.18	0.19	0.18	0.24	0.27	0.24	0.27
Total	8.03	8.03	8.02	8.03	8.03	8.04	8.04	8.03	8.02	8.02	8.01	8.00	8.01	8.01	7.99	8.02
Xalm	0.64	0.61	0.64	0.63	0.62	0.60	0.65	0.60	0.63	0.63	0.65	0.64	0.67	0.65	0.68	0.65
Xand	0.00	0.00	0.00	0.00	0.01	0.01	0.01	0.01	0.00	0.00	0.01	0.00	0.00	0.00	0.00	0.01
Xgrs	0.07	0.07	0.07	0.07	0.06	0.06	0.05	0.07	0.07	0.06	0.06	0.06	0.08	0.09	0.08	0.08
Xprp	0.28	0.30	0.27	0.28	0.29	0.31	0.27	0.30	0.29	0.30	0.28	0.29	0.24	0.24	0.23	0.24
Xspss	0.02	0.02	0.02	0.02	0.01	0.02	0.02	0.02	0.01	0.01	0.01	0.01	0.01	0.02	0.01	0.02
Xuv	0.00	0.00	0.01	0.00	0.01	0.01	0.00	0.00	0.00	0.00	0.00	0.00	0.00	0.00	0.00	0.00

Amphiboles: Two types of amphiboles were found to coexist in several samples from the Little Pine Garnet Mine outcrop: the orthoamphiboles anthophyllite and gedrite (Table 8, Fig. 15), following the nomenclature scheme of Leake et al. (1997). Both contained inclusions of monazite, quartz, plagioclase, rutile, and ilmenite (Fig. 16 H). The amphiboles are 2 - 3.5 mm in size. Occasionally, these amphiboles are rimmed with sillimanite (Fig. 17 B). Gedrites are in some cases rimmed by biotite/chlorite (Figs. 16 J & N), and in other cases by very fine - grained sillimanite (Fig. 16 C). Despite their chemical compositions and classification, almost all "gedrites" were characterized by an average extinction angle of about 7 ˚C (Table 7), suggesting that they maybe some variety of the clinoamphiboles grunerite instead. In order for the amphibole to be a classified as a grunerite using the nomenclature scheme of Leake et al. (1997), the Si content in the formula would have to be 7 – 8 apfu and the Mg/(Fe + Mg) would have to be 0 - 0.5, which is not the case in all amphiboles analyzed (Table 8). The average Al^{iv} content for the gedrites is 1.41 - 1.5 for cores and 1.6 - 1.74 for rims, suggesting some slight zoning pattern (Table 8). Gedrites in LP-1, 7, and 10 are pleochroic, going from a bluish green to green (Fig. 16 B, C, M, N) whereas the gedrite from LP-13 (talc – rich) is colorless. LP-12 has gedrites that are both pleochroic and colorless. Most of the gedrite crystals are prismatic or tabular in shape (Figs. 16 K, L). On the other hand, anthophyllite is colorless, and is always fibrous or bladed. Based on textural relationships between the two amphiboles, it seems that gedrite was the earlier phase (Fig. 16 A) and that anthophyllite formed later and is occasionally cutting across the foliation. Anthophyllite

is abundant in LP-1, LP-7, and LP-12 but is less abundant or missing in LP-10 and LP-13.

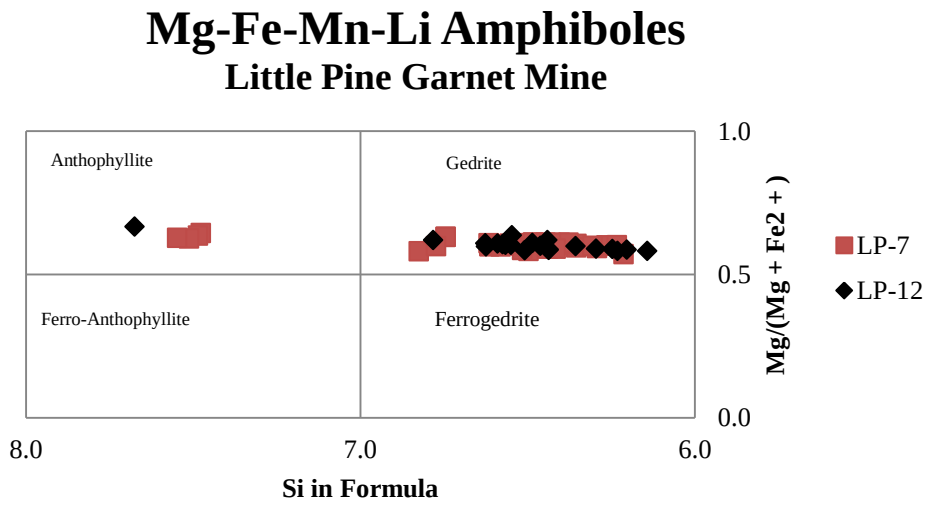

Figure 15. Graph showing the classification of the amphiboles based on the amount of Si and the Mg/(Mg + Fe) ratio from sample from Little Pine Garnet Mine.

Table 7. Extinction angles obtained on gedrite crystals from the Little Pine Garnet Mine

LP7	LP1	LP10	LP12
10.0	7.0	9.0	7.0
5.0	5.0	6.5	7.0
7.0			5.5
6.0			6.0
7.0			8.0
7.5			
9.0			
5.0			
8.0			
8.0			
4.5			
6.0			
10.0			
4.0			
8.0			

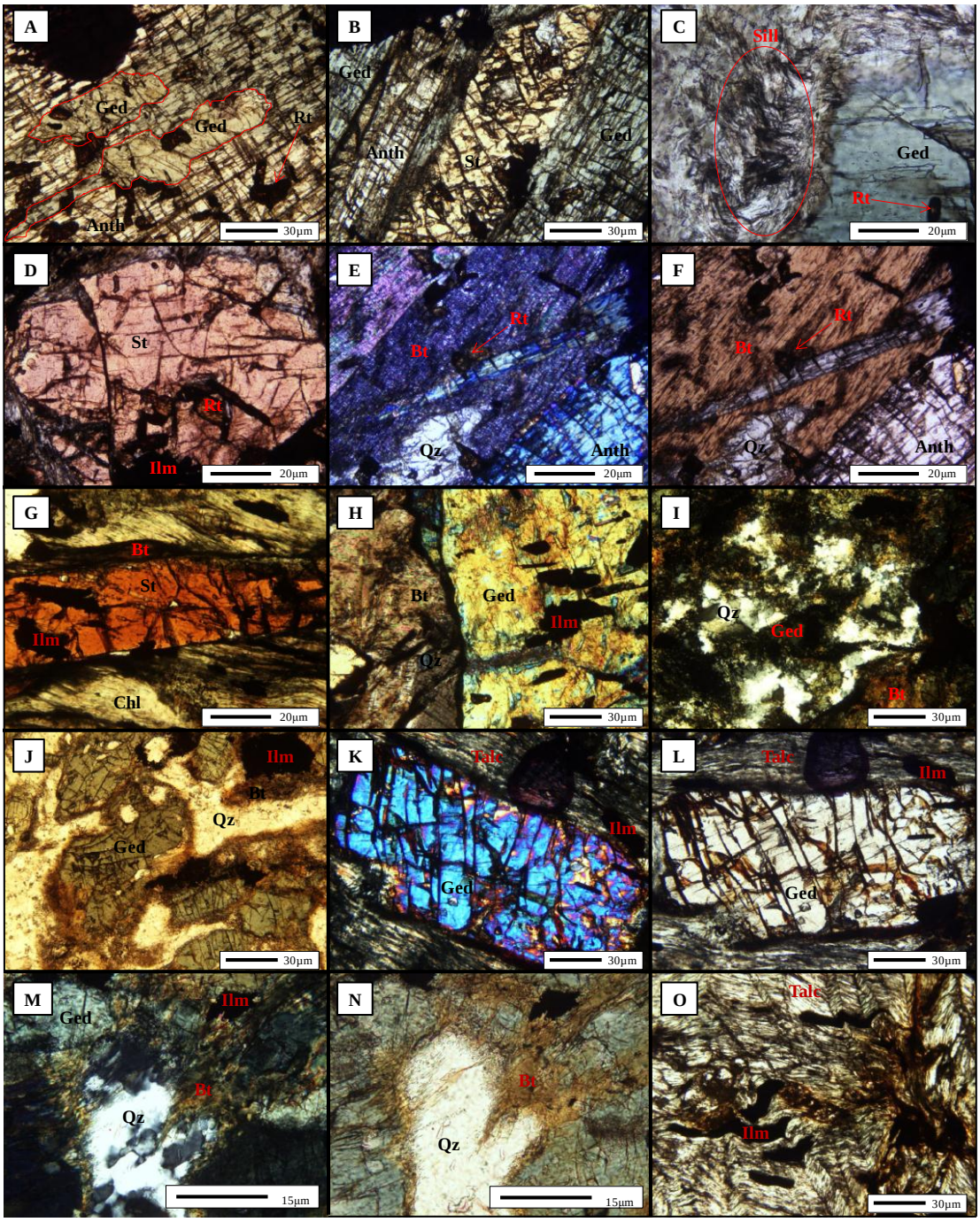

Figure 16. Photomicrographs of several different textural relationships at Little Pine Garnet Mine. A) Anthophyllite crystal with interior being composed of gedrite, both with rutile inclusions (PPL), B) Staurolite included in a crystal of gedrite (PPL), C) Gedrite crystal rimmed by sillimanite next to chlorite (PPL), D) Staurolite crystal with inclusions of rutile and ilmenite, rimmed by chlorite (PL), E - F) Biotite crystal with inclusions of anthophyllite and quartz (E - XPL, F - PL), G) Elongated staurolite crystal with oriented inclusions of ilmenite and apatite, surrounded by chlorite and biotite, H) Gedrite being replaced by opaques and with inclusions of oriented crystals of ilmenite (XPL), I - J) Gedrite crystals with inclusions of quartz and reaction rims of biotite/chlorite (I - XPL, J - PL), K - L) Gedrite crystal with inclusions of ilmenite surrounded by talc and being replaced by an opaque (K - XPL, L - PL), M - N) Gedrite reacting with quartz and being replaced by biotite/chlorite and sillimanite (M - XPL, N - PPL),. O) Talc with

stringers of oddly shaped ilmenite showing stress (PPL light). A - F: LP-1, G - H: LP-7, I - J: LP-10, K - N: LP-12, O: LP-13.

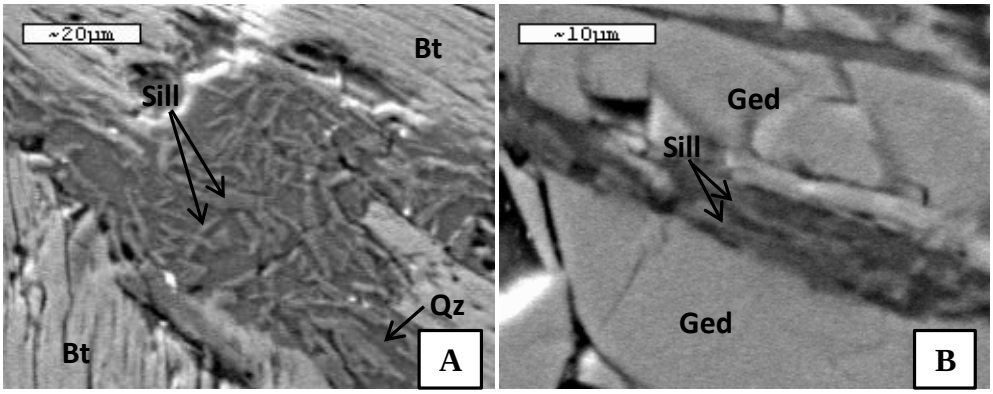

Figure 17. Backscatter electron images of A) sillimanite forming at the rims of biotite and B) sillimanite forming at the rims of a gedrite crystal.

Table 8. Representative amphibole analyses for gedrite and anthophyllite from the Little Pine Garnet Mine (g - gedrite, m - anthophyllite)

	g4	g6	g10	g13	g12	g14	g16	m1	m2	m3	m4
SiO2	44.54	45.64	43.20	44.17	43.54	43.86	44.06	51.93	51.39	51.64	51.27
TiO2	0.10	0.13	0.32	0.07	0.07	0.04	0.19	0.00	0.03	0.00	0.07
Al2O3	13.25	14.44	16.24	14.52	14.90	15.58	14.01	4.15	4.21	3.77	3.73
Cr2O3	0.02	0.00	0.00	0.07	0.08	0.00	0.17	0.09	0.10	0.10	0.00
FeO	20.38	18.47	18.90	19.10	19.71	18.30	19.99	19.57	19.78	20.49	19.98
MnO	0.14	0.21	0.16	0.22	0.10	0.19	0.01	0.03	0.15	0.09	0.08
MgO	16.19	15.87	15.97	16.79	16.22	16.19	16.13	19.98	19.40	19.22	18.94
CaO	0.36	0.34	0.32	0.29	0.36	0.31	0.26	0.23	0.07	0.31	0.15
Na2O	2.92	2.78	3.00	3.07	2.88	3.02	3.04	2.08	1.89	1.87	1.88
K2O	0.00	0.03	0.05	0.00	0.05	0.00	0.00	0.00	0.00	0.03	0.00
Total	97.91	97.90	98.17	98.29	97.91	97.49	97.86	98.07	97.03	97.53	96.10
Si	6.52	6.59	6.26	6.40	6.35	6.38	6.44	7.48	7.49	7.51	7.55
Al iv	1.48	1.41	1.74	1.60	1.65	1.62	1.56	0.52	0.51	0.49	0.45
Al vi	0.80	1.04	1.04	0.88	0.92	1.05	0.85	0.18	0.21	0.16	0.19
Ti	0.01	0.01	0.04	0.01	0.01	0.00	0.02	0.00	0.00	0.00	0.01
Cr	0.00	0.00	0.00	0.01	0.01	0.00	0.02	0.01	0.01	0.01	0.00
Fe2+	2.49	2.23	2.29	2.32	2.41	2.23	2.44	2.36	2.41	2.49	2.46
Mn	0.02	0.03	0.02	0.03	0.01	0.02	0.00	0.00	0.02	0.01	0.01
Mg	3.53	3.41	3.45	3.63	3.53	3.51	3.51	4.29	4.21	4.17	4.16
Ca	0.06	0.05	0.05	0.04	0.06	0.05	0.04	0.04	0.01	0.05	0.02
Na	0.83	0.78	0.84	0.86	0.82	0.85	0.86	0.58	0.53	0.53	0.54
K	0.00	0.01	0.01	0.00	0.01	0.00	0.00	0.00	0.00	0.01	0.00
Total Al	2.29	2.46	2.77	2.48	2.56	2.67	2.41	0.70	0.72	0.65	0.65
Fe/(Fe+Mg)	0.41	0.39	0.40	0.39	0.41	0.39	0.41	0.35	0.36	0.37	0.37
(Ca+Na) (B)	0.19	0.31	0.20	0.17	0.16	0.23	0.19	0.19	0.16	0.18	0.20
Na (B)	0.13	0.26	0.15	0.13	0.10	0.18	0.15	0.15	0.15	0.14	0.17
(Na+K) (A)	0.70	0.53	0.70	0.74	0.72	0.67	0.71	0.43	0.38	0.40	0.36

Biotites: The biotite crystals are kinked and most are at least about 1 mm in size. Inclusions found in the biotite crystals are ilmenite, monazite, and rutile. Biotite crystals were homogenous with the composition Al^{iv} = 2.48 - 2.81, Al^{vi} = 0.29 - 0.53, Fe/(Fe + Mg) = 0.22 - 0.26, Ti^{iv} = 0.12 - 0.16 (Table 9, Fig. 18). Some of the biotites are partially replaced by chlorite along their rims and occasionally sillimanite as well (Fig. 17 A). Biotite was not abundant in the talc bearing assemblages (or completely missing, LP-12, 13) and was abundant in the other samples (LP-1, 7, 10).

Table 9. Representative biotite analyses for Little Pine Garnet Mine

	lp12							lp7						
	c1	r1	c2	r2	r3	r4	c3	c1	r2	c2	r3	c3	r4	c4
SiO2	38.71	38.14	38.40	38.45	36.92	38.49	37.82	37.58	37.92	37.26	37.53	37.57	37.76	38.43
TiO2	1.14	1.23	1.24	1.48	1.15	1.12	1.37	1.36	1.20	1.11	1.26	1.37	1.26	1.48
Al2O3	18.19	18.17	17.56	17.25	18.57	17.99	18.17	17.43	18.02	19.38	17.18	17.41	17.61	17.79
FeO	10.61	10.68	10.62	9.88	10.67	10.21	10.49	10.09	8.88	10.46	10.28	10.75	9.82	10.80
MnO	0.06	0.00	0.00	0.00	0.00	0.00	0.05	0.00	0.05	0.11	0.00	0.00	0.00	0.00
MgO	17.31	17.87	17.71	17.69	18.92	17.53	17.45	18.19	18.52	20.47	18.46	18.17	18.34	19.10
CaO	0.05	0.21	0.21	0.33	0.19	0.07	0.12	0.00	0.08	0.07	0.03	0.00	0.08	0.00
Na2O	0.77	0.40	1.14	0.42	0.20	1.24	0.77	1.34	1.22	1.09	1.30	1.26	1.42	1.03
K2O	8.21	7.58	8.09	8.01	6.72	8.41	8.31	8.50	8.36	7.37	8.32	8.47	8.64	8.76
Cr2O3	0.00	0.07	0.00	0.00	0.09	0.00	0.00	0.00	0.03	0.01	0.01	0.06	0.00	0.00
Total	95.07	94.35	94.96	93.51	93.43	95.07	94.56	94.49	94.28	97.33	94.36	95.07	94.92	97.38
Si	5.49	5.44	5.47	5.52	5.33	5.47	5.42	5.41	5.42	5.19	5.41	5.39	5.41	5.36
Al iv	2.51	2.56	2.53	2.48	2.67	2.53	2.58	2.59	2.58	2.81	2.59	2.61	2.59	2.64
Al vi	0.53	0.50	0.42	0.45	0.49	0.48	0.49	0.37	0.46	0.37	0.33	0.34	0.38	0.29
Ti	0.12	0.13	0.13	0.16	0.12	0.12	0.15	0.15	0.13	0.12	0.14	0.15	0.14	0.16
Cr	0.00	0.01	0.00	0.00	0.01	0.00	0.00	0.00	0.00	0.00	0.00	0.01	0.00	0.00
Fe	1.26	1.28	1.27	1.19	1.29	1.21	1.26	1.21	1.06	1.22	1.24	1.29	1.18	1.26
Mn	0.01	0.00	0.00	0.00	0.00	0.00	0.01	0.00	0.01	0.01	0.00	0.00	0.00	0.00
Mg	3.66	3.80	3.76	3.79	4.07	3.71	3.73	3.91	3.95	4.25	3.97	3.89	3.91	3.97
Li*	0.89	0.80	0.84	0.86	0.61	0.85	0.75	0.71	0.77	0.64	0.71	0.71	0.74	0.83
Ca	0.01	0.03	0.03	0.05	0.03	0.01	0.02	0.00	0.01	0.01	0.01	0.00	0.01	0.00
Na	0.21	0.11	0.31	0.12	0.06	0.34	0.21	0.37	0.34	0.29	0.36	0.35	0.39	0.28
K	1.48	1.38	1.47	1.47	1.24	1.52	1.52	1.56	1.52	1.31	1.53	1.55	1.58	1.56
Al total	3.04	3.06	2.95	2.92	3.16	3.01	3.07	2.96	3.04	3.18	2.92	2.95	2.97	2.93
Fe/Fe+Mg	0.26	0.25	0.25	0.24	0.24	0.25	0.25	0.24	0.21	0.22	0.24	0.25	0.23	0.24

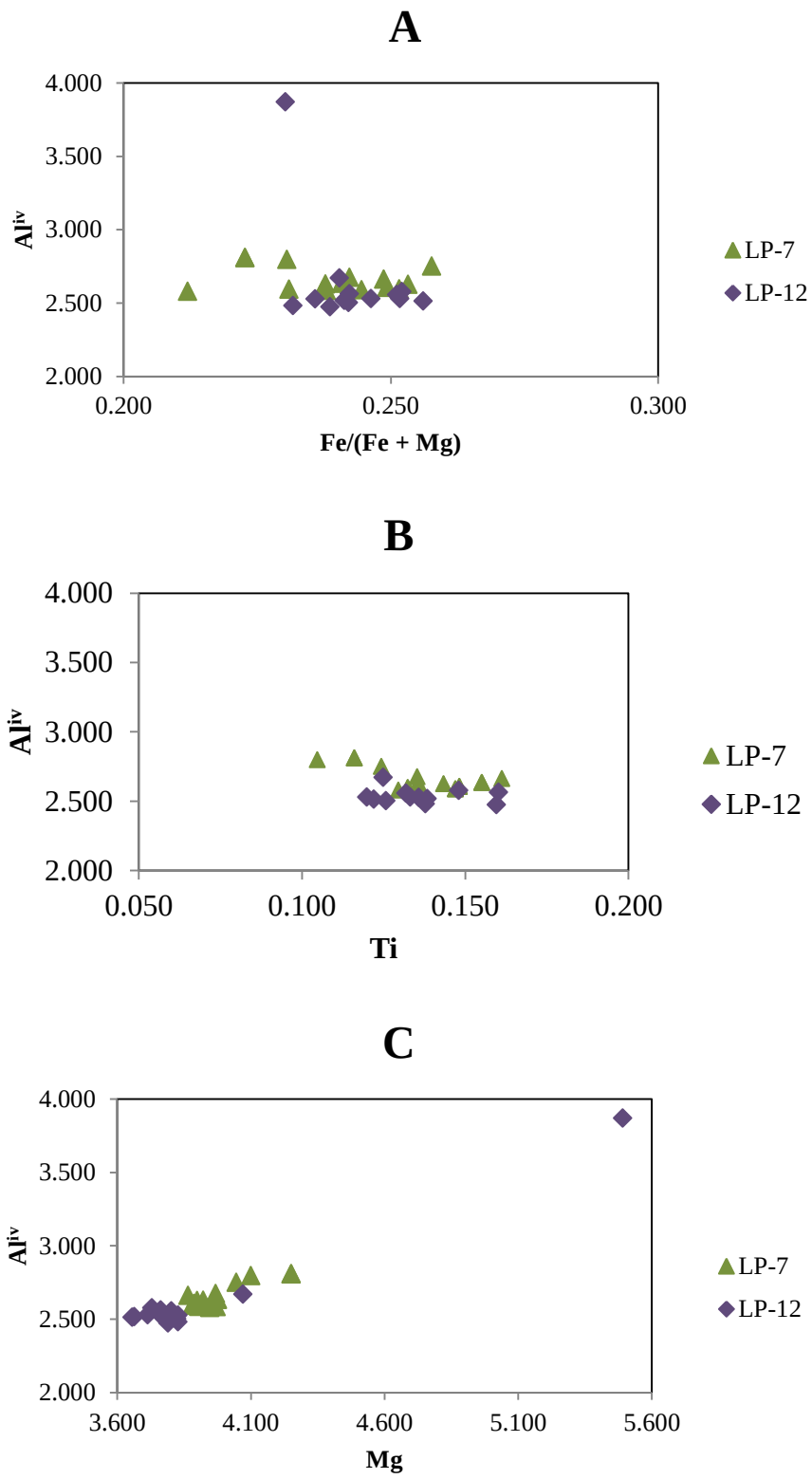

Figure 18. Compositions of biotites from Little Pine Garnet Mine plotted on (A) Al^{iv} vs. Ti, (B) Al^{iv} vs. Mg, and (C) Al^{iv} vs. Fe/(Fe + Mg).

Staurolite: Staurolite crystals in this location contain inclusions of apatite and ilmenite (Fig. 16 D, G). Inclusions in the staurolite are oriented with the biotite foliation (Fig. 16 G). Some of these inclusions are elongated whereas others are granular. Some of the staurolite crystals are surrounded by chlorite. The staurolites in these samples are characterized by a relatively high Mg content (Fe/(Fe + Mg) = 0.58 – 0.62; Table 10).

Table 10. Representative staurolite analyses from Little Pine Garnet Mine (LP-7)

	s1	s2	s3	s4	s5	s6	s7	s8	s9	s10	s11
SiO2	26.17	26.22	26.12	26.24	25.65	25.78	26.00	25.80	27.69	26.21	25.39
TiO2	0.44	0.56	0.53	0.51	0.54	0.71	0.62	0.57	0.63	0.58	0.67
Al2O3	52.07	52.21	52.30	52.08	51.16	51.97	51.75	51.16	52.25	52.38	50.31
FeO	13.42	13.44	13.61	13.89	13.06	12.98	12.94	13.45	12.06	13.39	12.96
MnO	0.09	0.11	0.03	0.18	0.04	0.04	0.01	0.08	0.05	0.01	0.04
MgO	5.09	4.95	4.97	4.82	5.07	5.30	5.30	5.30	5.13	5.35	5.13
CaO	0.00	0.00	0.00	0.04	0.00	0.05	0.00	0.00	0.00	0.05	0.00
Na2O	0.95	1.08	1.11	1.14	0.92	1.03	0.91	0.92	0.79	1.07	0.81
K2O	0.08	0.05	0.05	0.03	0.00	0.07	0.02	0.06	0.02	0.06	0.04
Total	98.32	98.61	98.72	98.94	96.44	97.93	97.55	97.32	98.62	99.10	95.36
Si	3.65	3.65	3.63	3.65	3.64	3.61	3.65	3.64	3.81	3.63	3.65
Al	8.56	8.56	8.57	8.53	8.56	8.57	8.55	8.51	8.47	8.54	8.52
Ti	0.05	0.06	0.06	0.05	0.06	0.08	0.06	0.06	0.06	0.06	0.07
Fe	1.57	1.56	1.58	1.62	1.55	1.52	1.52	1.59	1.39	1.55	1.56
Mn	0.01	0.01	0.00	0.02	0.00	0.00	0.00	0.01	0.01	0.00	0.01
Mg	1.06	1.03	1.03	1.00	1.07	1.10	1.11	1.11	1.05	1.10	1.10
Ca	0.00	0.00	0.00	0.01	0.00	0.01	0.00	0.00	0.00	0.01	0.00
Na	0.26	0.29	0.30	0.31	0.25	0.28	0.25	0.25	0.21	0.29	0.23
K	0.01	0.01	0.01	0.01	0.00	0.01	0.00	0.01	0.00	0.01	0.01
Fe/(Fe+Mg)	0.60	0.60	0.61	0.62	0.59	0.58	0.58	0.59	0.57	0.58	0.59

Other Minerals: Feldspars are very scarce in this location and crystals that are present are anhedral and small in size (about 0.1 mm). They are homogenous in composition and are albite rich (X_{ab} = 0.63 - 0.77, X_{an} = 0.20 - 0.31, X_{or} = 0.01; Table 11). The opaque minerals are oriented with the crenulations creating odd shaped crystals (Fig. 16 O). Chlorite has Fe/(Fe + Mg) of about 0.25 and forms felted masses with ilmenite "inclusions" that seem to pseudomorph biotite and/or gedrite (Table 12; Fig.

16C). Rutile is almost restricted to the staurolite and garnet crystals. Talc is found surrounding gedrite crystals.

Table 11. Representative feldspar analyses for Little Pine Garnet Mine

	lp7					lp12	
	p2	p3	p4	p5	p6	p1	p2
SiO2	55.55	56.30	61.83	58.59	60.39	55.99	54.58
TiO2	0.01	0.00	0.00	0.09	0.06	0.00	0.28
Al2O3	29.68	26.66	24.64	27.06	24.41	31.46	24.21
FeO	0.91	0.96	0.51	0.75	0.51	0.51	2.12
MgO	1.19	1.30	0.63	1.05	1.10	1.82	2.44
CaO	6.05	6.46	4.31	6.34	4.95	4.03	4.89
Na2O	7.45	8.06	9.05	7.81	7.32	6.39	6.92
K2O	0.11	0.24	0.06	0.28	0.20	0.08	1.20
Total	100.96	99.98	101.03	101.96	98.95	100.27	96.64
Si	2.47	2.54	2.72	2.58	2.70	2.47	2.56
Al	1.56	1.42	1.28	1.40	1.29	1.64	1.34
Ti	0.00	0.00	0.00	0.00	0.00	0.00	0.01
Fe	0.03	0.04	0.02	0.03	0.02	0.02	0.08
Mg	0.08	0.09	0.04	0.07	0.07	0.12	0.17
Ca	0.29	0.31	0.20	0.30	0.24	0.19	0.25
Na	0.64	0.70	0.77	0.67	0.64	0.55	0.63
K	0.01	0.01	0.00	0.02	0.01	0.00	0.07
X_{an}	0.31	0.30	0.21	0.30	0.27	0.26	0.26
X_{ab}	0.69	0.68	0.79	0.68	0.72	0.74	0.66
X_{or}	0.01	0.01	0.00	0.02	0.01	0.01	0.08

Table 12. Representative chlorite analyses from Little Pine Garnet Mine

LP-7	cl1	cl2	cl3	cl4	cl5	cl6	cl7	cl8	cl9	cl10	cl11	cl12	cl13
SiO2	26.94	27.62	27.96	29.31	27.45	26.56	26.01	26.84	26.50	28.03	27.53	27.37	26.59
TiO2	0.26	0.08	0.18	0.39	0.44	0.34	0.19	0.16	0.21	0.17	0.15	0.18	0.02
Al2O3	23.06	23.45	21.69	19.98	23.40	22.72	22.03	22.84	23.64	23.56	22.69	22.94	22.45
Cr2O3	0.24	0.00	0.19	0.00	0.00	0.08	0.00	0.02	0.00	0.00	0.00	0.00	0.00
FeO	13.75	13.52	13.45	13.54	13.69	13.70	14.02	13.58	15.22	14.62	13.73	13.29	12.90
MnO	0.00	0.00	0.00	0.00	0.04	0.00	0.00	0.00	0.01	0.07	0.11	0.03	0.00
MgO	24.50	25.11	24.31	22.16	25.32	23.70	23.16	24.17	22.77	23.50	24.73	25.02	23.36
CaO	0.00	0.00	0.00	0.00	0.00	0.07	0.09	0.15	0.00	0.19	0.11	0.04	0.07
Na2O	0.81	1.06	0.85	0.99	0.76	0.79	1.41	0.85	0.80	1.09	0.73	0.91	1.01
K2O	0.03	0.17	0.41	0.62	0.03	0.12	0.00	0.09	0.08	0.46	0.21	0.20	0.12
Total	89.58	91.02	89.04	86.99	91.13	88.08	86.92	88.70	89.22	91.68	89.99	89.99	86.51
Si	5.16	5.18	5.38	5.79	5.16	5.18	5.12	5.19	5.14	5.25	5.25	5.20	5.25
Al iv	2.84	2.82	2.62	2.21	2.84	2.82	2.88	2.81	2.86	2.75	2.75	2.80	2.75
Al vi	2.44	2.45	2.37	2.50	2.42	2.48	2.35	2.47	2.61	2.55	2.42	2.41	2.56
Ti	0.04	0.01	0.03	0.06	0.06	0.05	0.03	0.02	0.03	0.02	0.02	0.03	0.00
Cr	0.04	0.00	0.03	0.00	0.00	0.01	0.00	0.00	0.00	0.00	0.00	0.00	0.00
Fe2+	2.43	2.41	2.37	2.25	2.37	2.44	2.69	2.43	2.66	2.53	2.42	2.38	2.35
Mn	0.00	0.00	0.00	0.00	0.01	0.00	0.00	0.00	0.00	0.01	0.02	0.01	0.00
Mg	7.00	7.01	6.97	6.53	7.10	6.89	6.80	6.97	6.58	6.56	7.03	7.08	6.88
Ca	0.00	0.00	0.00	0.00	0.00	0.01	0.02	0.03	0.00	0.04	0.02	0.01	0.01
Na	0.60	0.77	0.63	0.76	0.56	0.60	1.08	0.64	0.60	0.79	0.54	0.67	0.77
K	0.01	0.08	0.20	0.31	0.02	0.06	0.00	0.04	0.04	0.22	0.10	0.10	0.06
Al total	5.28	5.28	4.99	4.70	5.26	5.30	5.23	5.28	5.47	5.30	5.17	5.22	5.31
Fe/Fe+Mg	0.26	0.26	0.25	0.26	0.25	0.26	0.28	0.26	0.29	0.28	0.26	0.25	0.25

CENTRAL BLUE RIDGE

Savannah Church:

Figure 19. Savannah Church outcrop showing gneisses and migmatites crosscut by pegmatitic dyke.

Rocks exposed at this location are mafic amphibolites, calc - silicates, and biotite gneisses and migmatites cross cut by pegmatitic dikes (Hatcher, 2010; Fig. 19). The mineral assemblage for the Savannah church gneisses is garnet + biotite + plagioclase + ilmenite + quartz ± orthoclase (SVC-5 and SVC-7, respectively; Fig. 20). Hornblende occurs in one sample (SVC-3 a migmatitic gneiss) as part of the peak assemblage, whereas chlorite ± muscovite are both retrograde phases.

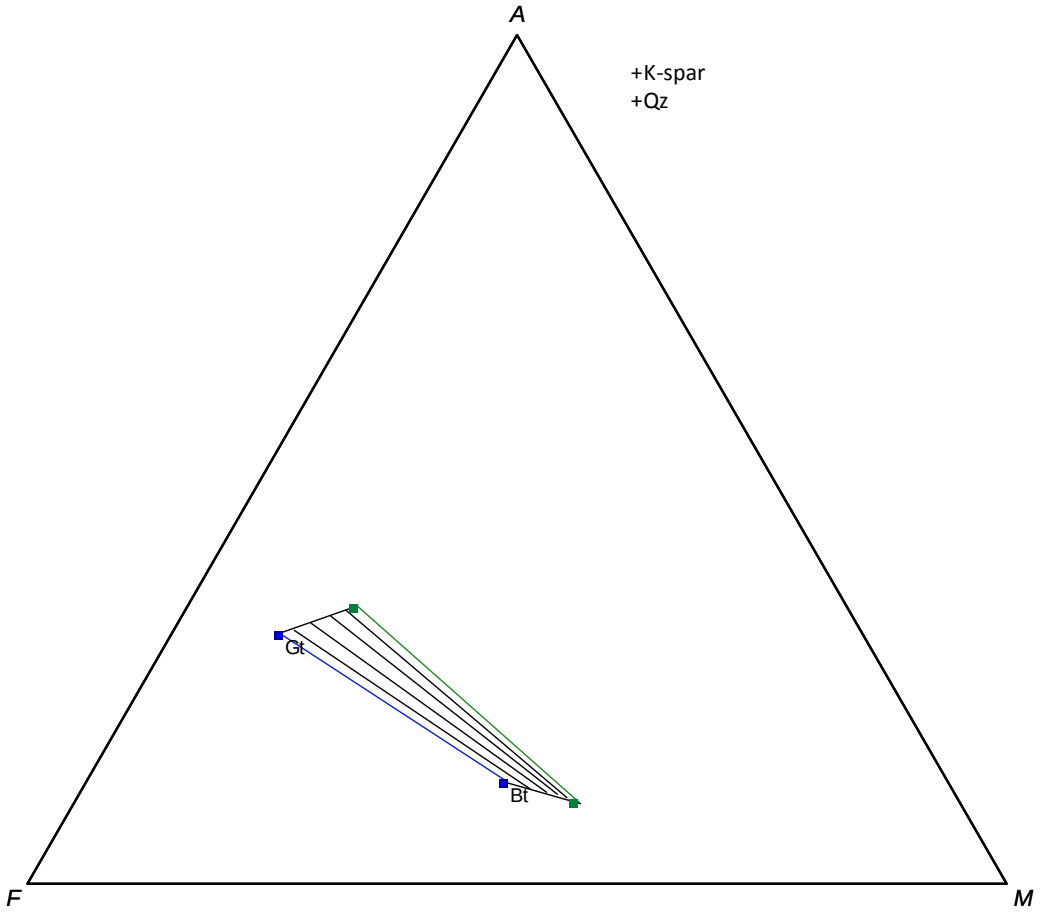

Figure 20. AFM projection from K - feldspar showing the peak mineral assemblage Gt + Bt for the Savannah Church location (Blue and green tie lines: average compositions in SVC-5, and SVC-7, respectively).

Garnets: Garnets at the Savannah Church location are resorbed and contain many inclusions of quartz, biotite, plagioclase, ilmenite, rutile, zircon, pyrite, monazite, and xenotime (Figs. 21; 22 A, B). The grain sizes range from 0.30 to 0.75 mm with the majority of them being on the smaller end.

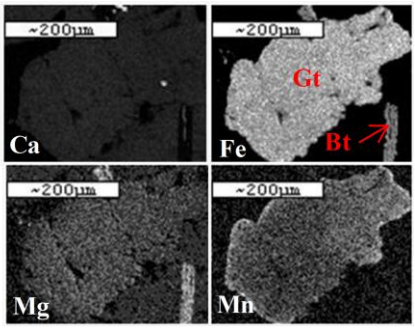

Figure 21. X - Ray map of one of the garnets from Savannah Church. Notice rims are enriched in Mn (Spessartine).

Almost all of the garnet crystals from this area are in contact with biotite, which sometimes completely surrounds it (Figs. 22 C, D and E). These garnets were within otherwise equigranular grains of quartz, with slightly larger garnet crystals scattered in between the folded foliation of biotite. Compositionally, these garnets are almandine rich with small to moderate amounts of pyrope and grossular, and substantial amounts of spessartine (X_{alm} = 0.65 - 0.70, X_{prp} = 0.12 - 0.24, X_{grs} = 0.06 - 0.09, X_{spss} = 0.05 - 0.16). These garnets are slightly zoned with the cores being more enriched in pyrope and depleted in grossular relative to their rims (Figs. 23, 24). A few crystals show a small increase of manganese towards one or more of their rims (Fig. 23).

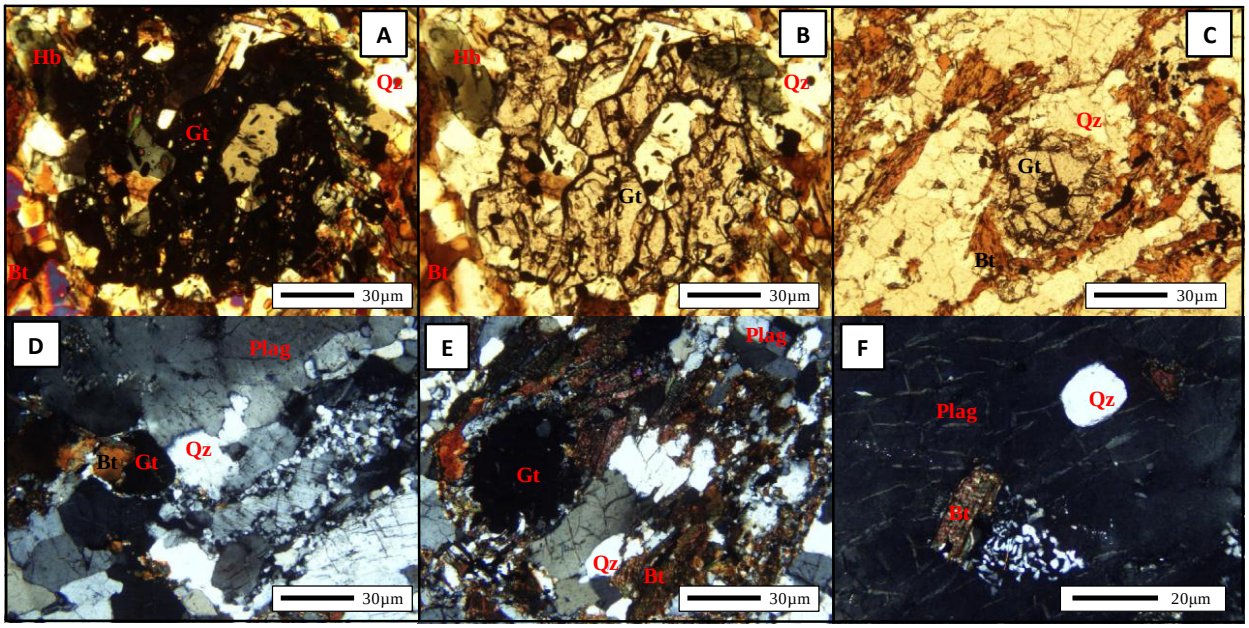

Figure 22: SVC-3: A - B) Resorbed garnet with inclusions of biotite, amphibole, quartz, and ilmenite (A - crossed polarized light, B - plane polarized light, SVC-7: C) .Garnet situated between folded foliation of biotite, D) Garnet with a quartz rind showing mortar texture, E) Resorbed garnet crystal with inclusions of quartz, also with a quartz rind and showing mylonitization, F) Quartz and biotite included in a plagioclase crystal which displays a myrmekitic intergrowth with quartz.

Table 13. Representative garnet analyses for Savannah Church

	svc5-gt3										svc7-gt4							
	core1	rim1	rim2	core2	core3	rim3	rim4	core4	rim5	rim6	rim1	core1	rim2	core2	rim3	core3	rim4	core5
SiO2	36.24	36.08	36.66	37.13	37.13	36.56	36.67	36.30	36.45	37.19	39.72	39.81	39.44	39.42	40.40	41.17	39.88	41.32
TiO2	0.00	0.05	0.10	0.04	0.00	0.03	0.00	0.00	0.17	0.13	0.12	0.05	0.00	0.04	0.00	0.08	0.06	0.03
Al2O3	21.57	21.15	21.27	21.18	21.78	21.40	21.94	21.37	21.24	21.54	23.06	22.99	22.75	23.04	23.41	23.91	23.11	24.13
Cr2O3	0.00	0.14	0.13	0.27	0.20	0.15	0.04	0.15	0.06	0.22	0.04	0.05	0.13	0.04	0.06	0.12	0.12	0.11
FeO	31.55	30.68	31.20	31.09	31.36	31.45	32.07	30.49	30.75	30.12	26.85	25.44	25.95	25.45	26.28	26.07	25.94	26.07
MnO	3.55	4.73	4.42	3.68	3.81	4.23	3.90	4.04	4.57	5.84	1.58	1.26	2.74	1.25	1.49	1.32	1.59	1.19
MgO	3.52	2.83	3.29	3.39	3.78	2.97	3.40	3.21	3.38	2.89	4.95	5.43	3.83	5.44	5.03	5.69	4.62	6.12
CaO	2.56	2.86	2.67	2.50	2.77	2.78	2.60	2.77	2.68	2.75	2.75	2.73	3.03	2.63	2.91	2.78	2.79	2.68
Total	98.99	98.53	99.98	99.29	100.84	99.57	100.64	98.33	99.55	100.70	99.05	97.76	97.86	97.31	99.58	101.14	98.11	101.65
Si	2.94	2.95	2.95	2.99	2.95	2.95	2.93	2.95	2.94	2.96	3.03	3.05	3.05	3.03	3.05	3.04	3.05	3.04
Al iv	0.06	0.05	0.05	0.01	0.05	0.05	0.07	0.05	0.06	0.04	0.00	0.00	0.00	0.00	0.00	0.00	0.00	0.00
Al vi	2.00	1.99	1.97	2.00	1.99	1.99	2.00	2.01	1.97	1.99	2.11	2.11	2.11	2.13	2.12	2.12	2.13	2.13
Ti	0.00	0.00	0.01	0.00	0.00	0.00	0.00	0.00	0.01	0.01	0.01	0.00	0.00	0.00	0.00	0.00	0.00	0.00
Cr	0.00	0.01	0.01	0.02	0.01	0.01	0.00	0.01	0.00	0.01	0.00	0.00	0.01	0.00	0.00	0.01	0.01	0.01
Fe2+	2.14	2.10	2.10	2.11	2.08	2.13	2.14	2.10	2.08	2.03	1.92	1.85	1.90	1.86	1.88	1.84	1.90	1.83
Mn	0.24	0.33	0.30	0.25	0.26	0.29	0.26	0.28	0.31	0.39	0.10	0.08	0.18	0.08	0.10	0.08	0.10	0.07
Mg	0.43	0.34	0.39	0.41	0.45	0.36	0.41	0.39	0.41	0.34	0.56	0.62	0.44	0.62	0.57	0.63	0.53	0.67
Ca	0.22	0.25	0.23	0.22	0.24	0.24	0.22	0.24	0.23	0.23	0.22	0.22	0.25	0.22	0.23	0.22	0.23	0.21
Fe/Mg	5.03	6.10	5.32	5.20	4.66	5.96	5.29	5.39	5.11	5.89	3.40	2.99	4.31	2.98	3.33	2.94	3.62	2.73
X_{Alm}	0.70	0.69	0.69	0.71	0.68	0.70	0.70	0.69	0.68	0.67	0.68	0.67	0.69	0.67	0.68	0.66	0.69	0.66
X_{Grs}	0.08	0.08	0.07	0.06	0.07	0.08	0.07	0.08	0.07	0.07	0.08	0.08	0.09	0.08	0.08	0.08	0.08	0.07
X_{Prp}	0.14	0.12	0.13	0.14	0.15	0.12	0.14	0.13	0.14	0.12	0.20	0.22	0.16	0.22	0.20	0.23	0.19	0.24
X_{Sps}	0.08	0.11	0.10	0.08	0.09	0.10	0.09	0.09	0.11	0.13	0.04	0.03	0.06	0.03	0.03	0.03	0.04	0.03

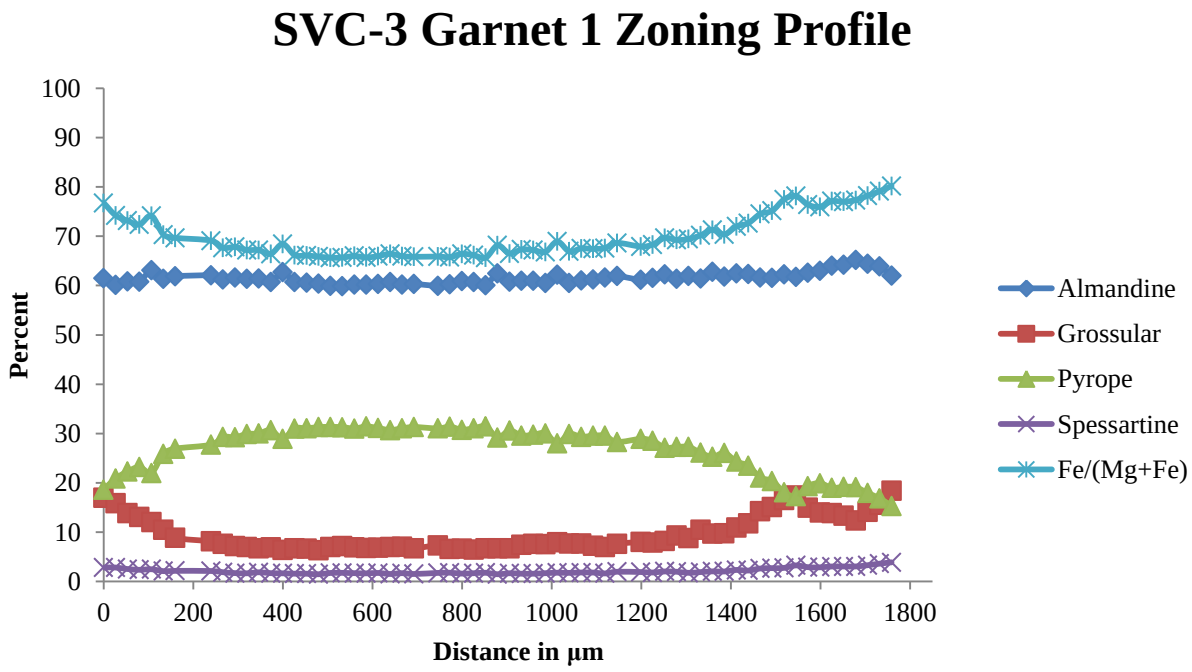

Figure 23: Garnet profile from Savannah Church showing slight enrichment of pyrope and decrease of grossular in the cores.

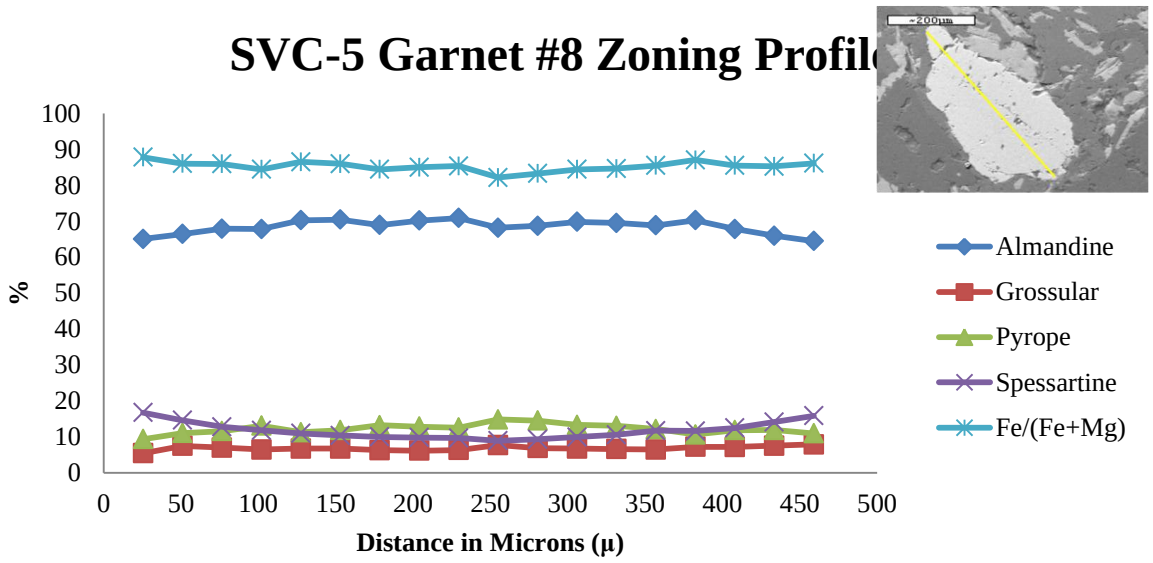

Figure 24. Garnet profile from Savannah Church showing slight enrichment of pyrope and almandine in the cores and spessartine in the rims.

Biotite: Biotite occurs as inclusions in garnet and plagioclase as well as in the matrix (Fig. 22 F). The biotite grain sizes range from 0.2 to 4 mm and are oriented to define the foliation, although many crystals either completely or partially envelop the garnets. The biotites contain inclusions of rutile, ilmenite, quartz, xenotime, and monazite (Fig. 25A), and are locally replaced by chlorite along their rims (Fig. 25B). All crystals of biotite are homogenous and similar in composition with Al^{iv} = 2.63 - 2.75, Al^{vi} = 0.49 - 0.58, Fe/(Fe + Mg) = 0.49 - 0.53, Ti^{iv} = 0.23 - 0.41 (Table 14, Fig. 26).

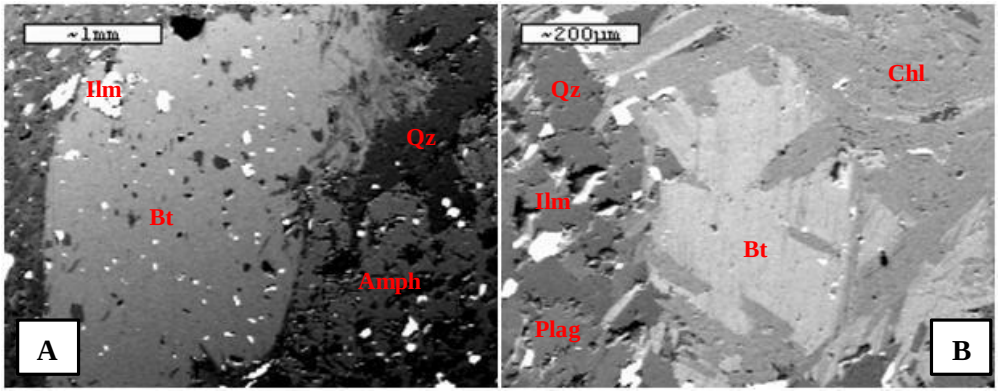

Figure 25: A) Large biotite crystal full of inclusions of ilmenite and quartz, B) Textural relationship between biotite being replaced by chlorite. Both images are from sample SVC-7.

A

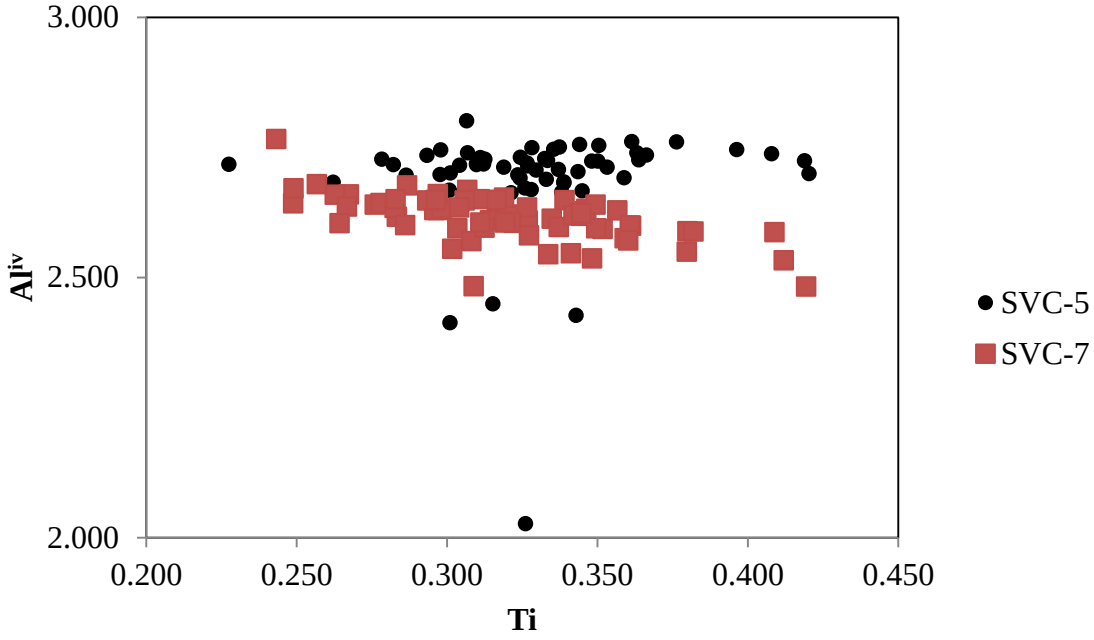
3.000
2.500
2.000
Aliv
0.200
0.250
0.300
0.350
0.400
0.450
Ti
SVC-5
SVC-7

B

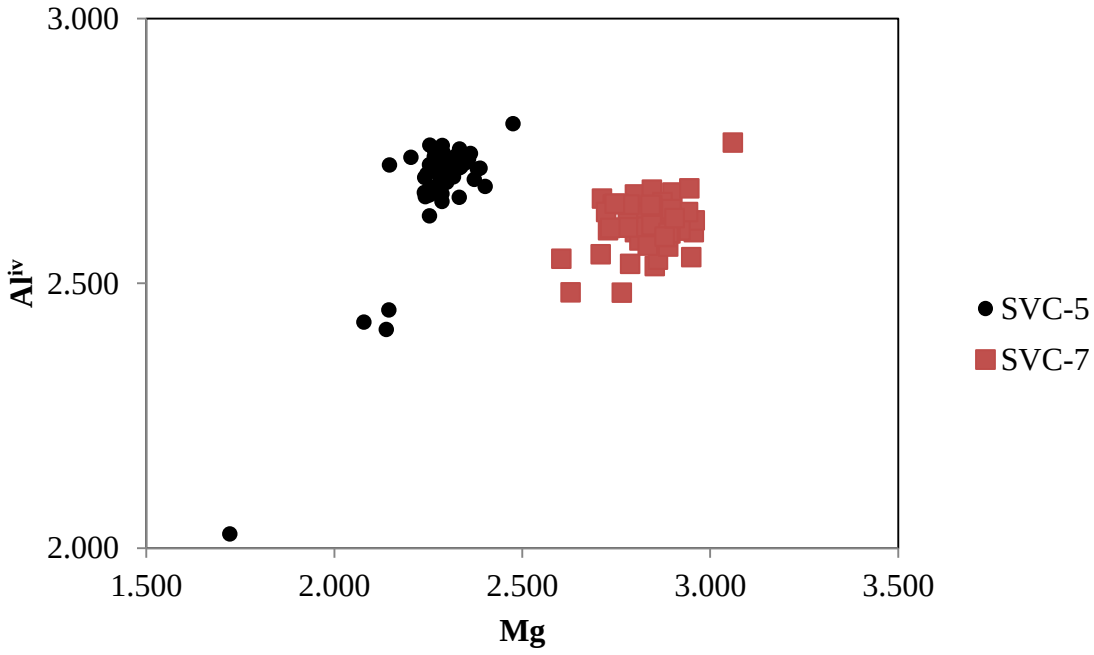
3.000
2.500
2.000
Aliv
1.500
2.000
2.500
3.000
3.500
Mg
SVC-5
SVC-7

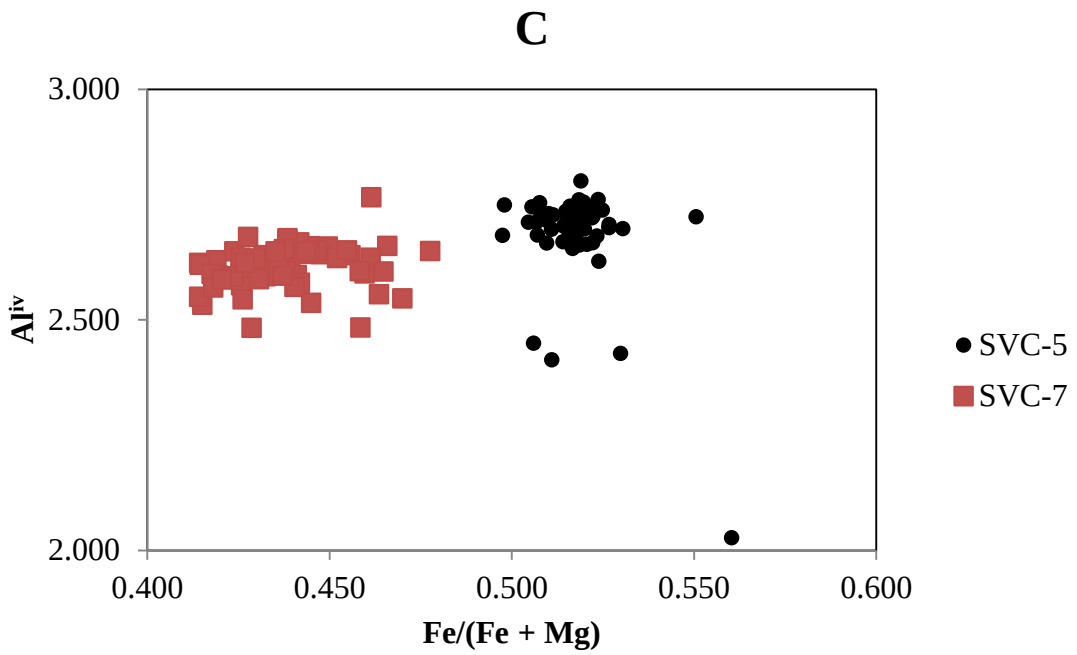

Figure 26. Compositions of biotites from Savannah Church plotted on (A) Al^{iv} vs. Ti, (B) Al^{iv} vs. Mg, and (C) Al^{iv} vs. Fe/(Fe + Mg).

Other Minerals: Plagioclase is found throughout the sample, and is characterized by an anhedral shape, and in some cases rims the garnet. Inclusions of biotite, quartz, and monazite are occasionally found, however the plagioclase is very often devoid of inclusions. Plagioclase crystals range in size from 0.1 to 0.5 mm. Compositionally, the plagioclase crystals were unzoned, however some plagioclase rims exhibited exsolution lamellae of Kspar, giving rise to an antiperthitic texture (Fig. 27). The feldspars are albite rich (X_{ab} = 0.73 - 0.82, X_{an} = 0.18 - 0.26; Table 15).

Table 14. Representative biotite analyses for Savannah Church

	svc5													svc7										
	gt5						gt6							gt5bt1										
	c1	r1	r2	r3	c2	c3	c1	r1	r2	c2	r3	r4	c3	core1	rim1	rim2	rim3	rim4	core3	core4	rim5	rim6	core2	core4	rim7
SiO2	34.79	34.82	35.10	34.98	34.98	34.42	34.34	34.80	34.72	35.11	35.34	34.91	37.58	36.06	36.00	36.22	35.55	35.97	35.28	36.17	36.42	35.10	34.93	35.98	35.64
TiO2	3.07	2.63	2.76	2.71	2.95	3.45	3.09	3.19	2.72	3.08	3.00	3.20	2.69	2.52	2.52	2.65	2.39	2.17	2.42	2.23	2.59	2.05	2.56	2.35	2.42
Al2O3	17.82	17.69	18.10	18.20	17.78	17.86	17.71	18.33	18.22	17.75	18.48	18.19	17.24	17.03	16.58	16.67	16.28	16.89	16.64	16.51	16.98	16.61	16.10	16.75	16.69
FeO	20.74	20.26	20.09	19.69	19.09	19.44	18.99	19.12	19.74	19.92	19.63	19.50	17.98	18.00	17.52	17.66	17.46	16.64	17.63	17.96	17.84	18.99	17.86	17.31	17.15
MnO	0.11	0.21	0.13	0.24	0.15	0.09	0.21	0.06	0.07	0.04	0.21	0.14	0.17	0.12	0.08	0.06	0.09	0.00	0.07	0.06	0.00	0.04	0.00	0.14	0.00
MgO	9.50	10.21	10.40	10.36	9.86	9.99	9.91	10.06	10.14	10.27	10.33	10.05	9.65	12.93	12.61	12.82	12.45	12.87	12.72	12.97	12.99	12.72	12.14	12.84	12.92
CaO	0.09	0.21	0.03	0.06	0.08	0.04	0.00	0.00	0.02	0.07	0.02	0.00	0.00	0.00	0.07	0.00	0.00	0.12	0.07	0.19	0.01	0.17	0.23	0.00	0.17
Na2O	0.73	0.15	0.13	0.67	0.29	0.34	0.27	0.55	0.48	0.96	0.92	0.41	0.60	1.40	0.95	0.77	0.69	0.73	0.82	0.57	1.09	0.68	0.92	0.56	0.95
K2O	9.48	9.47	9.53	9.67	9.40	9.50	9.29	9.58	9.12	9.41	9.22	9.55	8.87	8.81	8.75	8.67	8.40	8.84	8.71	8.67	8.75	7.22	8.77	8.33	8.10
Cr2O3	0.02	0.02	0.12	0.08	0.21	0.15	0.03	0.13	0.11	0.07	0.11	0.00	0.00	0.00	0.07	0.02	0.00	0.00	0.16	0.00	0.19	0.03	0.24	0.00	0.14
Li2O*	0.43	0.44	0.52	0.49	0.49	0.33	0.30	0.44	0.41	0.52	0.59	0.47	1.23	0.80	0.78	0.84	0.65	0.77	0.57	0.83	0.90	0.52	0.47	0.78	0.68
Total	96.78	96.12	96.92	97.16	95.27	95.61	94.15	96.28	95.76	97.20	97.86	96.42	96.03	97.67	95.93	96.39	93.97	95.01	95.11	96.15	97.74	94.13	94.24	95.05	94.87
Si	5.28	5.30	5.28	5.26	5.34	5.25	5.31	5.26	5.28	5.28	5.25	5.27	5.59	5.32	5.39	5.39	5.43	5.41	5.35	5.40	5.35	5.36	5.37	5.41	5.38
Al iv	2.72	2.70	2.72	2.74	2.66	2.75	2.69	2.74	2.72	2.72	2.75	2.73	2.41	2.68	2.61	2.61	2.57	2.59	2.65	2.60	2.65	2.64	2.63	2.59	2.62
Al vi	0.46	0.47	0.49	0.49	0.53	0.47	0.54	0.53	0.54	0.42	0.49	0.51	0.61	0.29	0.32	0.31	0.36	0.41	0.32	0.31	0.29	0.35	0.28	0.38	0.34
Ti	0.35	0.30	0.31	0.31	0.34	0.40	0.36	0.36	0.31	0.35	0.34	0.36	0.30	0.28	0.28	0.30	0.27	0.25	0.28	0.25	0.29	0.24	0.30	0.27	0.27
Cr	0.00	0.00	0.01	0.01	0.02	0.02	0.00	0.02	0.01	0.01	0.01	0.00	0.00	0.00	0.01	0.00	0.00	0.00	0.02	0.00	0.02	0.00	0.03	0.00	0.02
Fe	2.63	2.58	2.53	2.48	2.44	2.48	2.46	2.42	2.51	2.50	2.44	2.46	2.24	2.22	2.20	2.20	2.23	2.09	2.23	2.24	2.19	2.43	2.30	2.18	2.16
Mn	0.01	0.03	0.02	0.03	0.02	0.01	0.03	0.01	0.01	0.00	0.03	0.02	0.02	0.01	0.01	0.01	0.01	0.00	0.01	0.01	0.00	0.00	0.00	0.02	0.00
Mg	2.15	2.32	2.33	2.32	2.24	2.27	2.28	2.27	2.30	2.30	2.29	2.26	2.14	2.85	2.82	2.84	2.83	2.89	2.87	2.89	2.85	2.90	2.78	2.88	2.91
Li*	0.26	0.27	0.32	0.30	0.30	0.20	0.19	0.27	0.25	0.32	0.35	0.28	0.74	0.47	0.47	0.50	0.40	0.47	0.35	0.50	0.53	0.32	0.29	0.47	0.41
Ca	0.01	0.03	0.01	0.01	0.01	0.01	0.00	0.00	0.00	0.01	0.00	0.00	0.00	0.00	0.01	0.00	0.00	0.02	0.01	0.03	0.00	0.03	0.04	0.00	0.03
Na	0.22	0.05	0.04	0.20	0.09	0.10	0.08	0.16	0.14	0.28	0.27	0.12	0.17	0.40	0.28	0.22	0.20	0.21	0.24	0.16	0.31	0.20	0.27	0.16	0.28
K	1.83	1.84	1.83	1.86	1.83	1.85	1.83	1.85	1.77	1.80	1.75	1.84	1.68	1.66	1.67	1.65	1.64	1.70	1.68	1.65	1.64	1.41	1.72	1.60	1.56
Al total	3.19	3.17	3.21	3.23	3.20	3.21	3.23	3.27	3.27	3.14	3.24	3.24	3.02	2.96	2.93	2.92	2.93	3.00	2.97	2.91	2.94	2.99	2.92	2.97	2.97
Fe/Fe+Mg	0.55	0.53	0.52	0.52	0.52	0.52	0.52	0.52	0.52	0.52	0.52	0.52	0.51	0.44	0.44	0.44	0.44	0.42	0.44	0.44	0.44	0.46	0.45	0.43	0.43

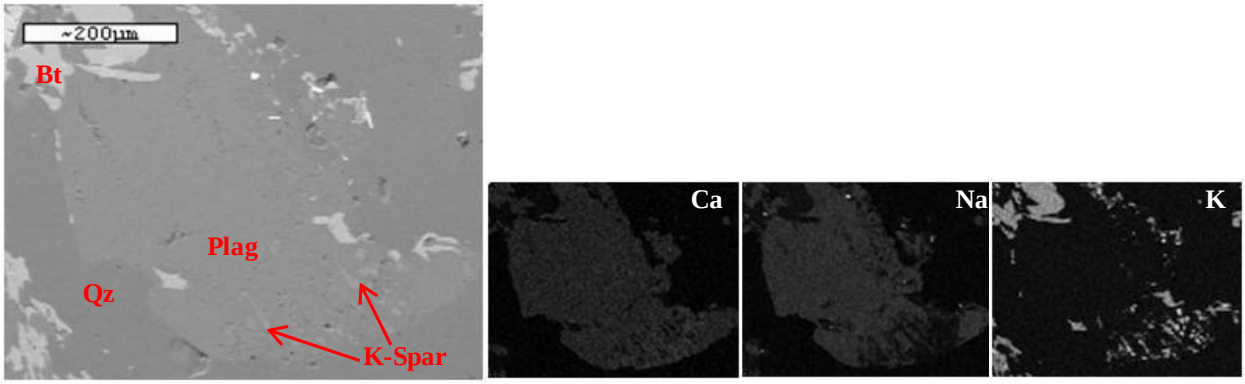

Figure 27. Plagioclase displaying antiperthitic texture along the rims. A) BSE image; B, C, and D: X - ray maps.

Table 15. Representative feldspar analyses for Savannah Church

	svc7								svc5								
	gt1								Plag1 at Gt6					Plag1 at Gt7			
	p8	p5	p6	p3	p2	p8	p3	p5	P1	P2	P3	P4	P5	P1	P2	P3	P4
SiO2	61.85	61.30	62.14	61.93	62.20	61.85	61.93	61.30	60.90	62.60	60.39	61.10	62.98	61.45	61.37	61.92	62.72
TiO2	0.02	0.00	0.00	0.06	0.03	0.02	0.06	0.00	0.01	0.08	0.00	0.00	0.00	0.03	0.00	0.09	0.14
Al2O3	24.78	24.31	23.73	23.97	24.19	24.78	23.97	24.31	23.31	22.23	23.07	23.66	24.09	23.82	23.79	23.73	24.59
FeO	0.17	0.16	0.00	0.04	0.15	0.17	0.04	0.16	0.20	0.17	0.71	0.14	0.27	0.27	0.20	0.09	0.27
MnO	0.00	0.00	0.00	0.00	0.00	0.00	0.00	0.00	0.00	0.00	0.00	0.00	0.00	0.00	0.00	0.00	0.00
MgO	0.72	0.49	0.32	0.46	0.66	0.72	0.46	0.49	0.42	0.11	1.09	0.54	0.60	0.61	0.52	0.56	0.47
CaO	4.17	4.04	3.57	3.76	3.56	4.17	3.76	4.04	4.73	4.37	4.58	4.97	4.98	5.23	5.24	4.98	5.12
Na2O	8.97	8.84	9.13	8.78	9.00	8.97	8.78	8.84	8.42	8.36	8.45	8.40	8.35	8.20	8.19	8.41	8.53
K2O	0.16	0.11	0.22	0.13	0.05	0.16	0.13	0.11	0.27	0.19	0.34	0.27	0.09	0.17	0.30	0.06	0.03
Total	100.84	99.26	99.11	99.13	99.85	100.84	99.13	99.26	98.25	98.11	98.62	99.07	101.36	99.77	99.60	99.83	101.86
Si	2.72	2.73	2.77	2.76	2.75	2.72	2.76	2.73	2.75	2.82	2.73	2.74	2.75	2.73	2.74	2.75	2.73
Al	1.28	1.28	1.25	1.26	1.26	1.28	1.26	1.28	1.24	1.18	1.23	1.25	1.24	1.25	1.25	1.24	1.26
Ti	0.00	0.00	0.00	0.00	0.00	0.00	0.00	0.00	0.00	0.00	0.00	0.00	0.00	0.00	0.00	0.00	0.00
Fe	0.01	0.01	0.00	0.00	0.01	0.01	0.00	0.01	0.01	0.01	0.03	0.01	0.01	0.01	0.01	0.00	0.01
Mg	0.05	0.03	0.02	0.03	0.04	0.05	0.03	0.03	0.03	0.01	0.07	0.04	0.04	0.04	0.03	0.04	0.03
Ca	0.20	0.19	0.17	0.18	0.17	0.20	0.18	0.19	0.23	0.21	0.22	0.24	0.23	0.25	0.25	0.24	0.24
Na	0.76	0.76	0.79	0.76	0.77	0.76	0.76	0.76	0.74	0.73	0.74	0.73	0.71	0.71	0.71	0.72	0.72
K	0.01	0.01	0.01	0.01	0.00	0.01	0.01	0.01	0.02	0.01	0.02	0.02	0.01	0.01	0.02	0.00	0.00
Xan	0.20	0.20	0.18	0.19	0.18	0.20	0.19	0.20	0.23	0.22	0.23	0.24	0.25	0.26	0.26	0.25	0.25
Xab	0.79	0.79	0.81	0.80	0.82	0.79	0.80	0.79	0.75	0.77	0.75	0.74	0.75	0.73	0.73	0.75	0.75
Xor	0.01	0.01	0.01	0.01	0.00	0.01	0.01	0.01	0.02	0.01	0.02	0.02	0.01	0.01	0.02	0.00	0.00

Sylva:

The rocks of Sylva are deformed migmatitic biotite gneisses, calc silicates, and mafic amphibolites cut by quartz - feldspar veins and dykes (Fig. 28). The mineral assemblage for the

Figure 28. Migmatites and dikes at Sylva.

Sylva area is garnet + biotite + quartz + hornblende + plagioclase + rutile + clinozoisite + ilmenite + sphene ± orthoclase for a calc silicate/greywacke (SV-4), garnet + biotite + quartz + plagioclase + clinozoisite + ilmenite ± orthoclase for another metagraywacke (SV-7, GFT-23) and garnet + biotite + quartz + hornblende + plagioclase + rutile + clinozoisite/epidote + ilmenite for a calc silicate (GFT-24). The peak mineral assemblage is garnet + hornblende + biotite + ilmenite + plagioclase + quartz ± K - feldspar (Fig. 29).

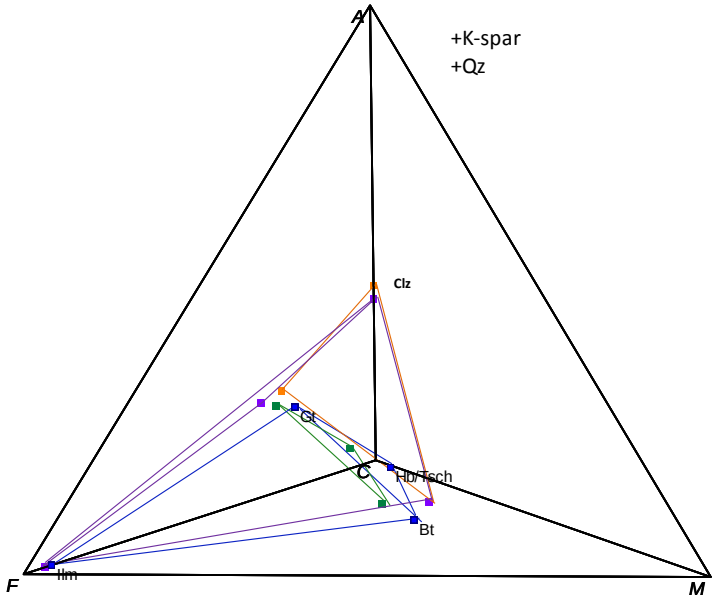

Figure 29. AFMC projection from Qz and K - spar displaying the peak mineral assemblages Gt + Hb (Tsch) + Bt + Ilm, and Czo + Hb + Gt, + Ilm for Sylva (Tie lines: Blue - SV-4, Green - SV-7, Purple - GFT-23, Orange - GFT-24).

Garnets: The garnets in this sample are resorbed with many inclusions of quartz, xenotime, rutile, monazite, clinozoisite, biotite, and hornblende/tschermakite. The grain sizes range from 0.2 to 1.5 mm. Many crystals are surrounded by plagioclase + quartz sometimes separating them from biotite (Fig. 30A, B, D). These garnets are almandine - rich (X_{alm} = 0.48 - 0.59) with substantial amounts of pyrope (X_{prp} = 0.22 - 0.24) and

grossular (X_{grs} = 0.21 - 0.23), but minor amounts of spessartine (X_{spss} = 0.02; Table 16). Compositionally, the garnets are homogenous, showing minor increase in Mn + Fe and decrease in Mg along some of their rims (Figs. 31B, 32).

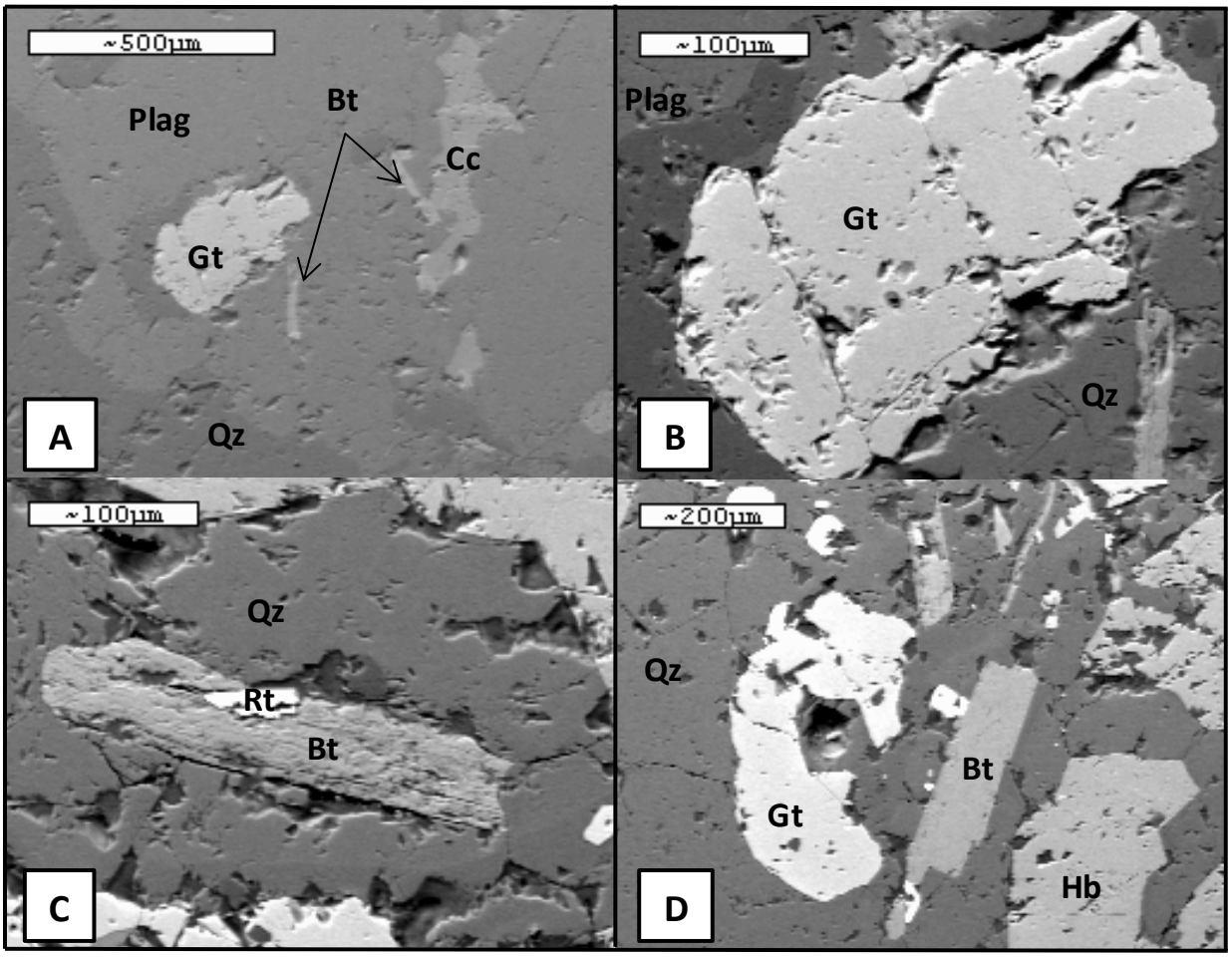

Figure 30. Backscatter electron images taken using the SEM. A - B are from SV - 7, C - D are from SV-4 of Sylva. A) Garnet surrounded by quartz and plagioclase (plagioclase has inclusions of biotite), B) Closer view of garnet with fractures, C) Biotite crystal surrounded by quartz with a rutile inclusion, D) Gt with core missing surrounded by quartz near a biotite .

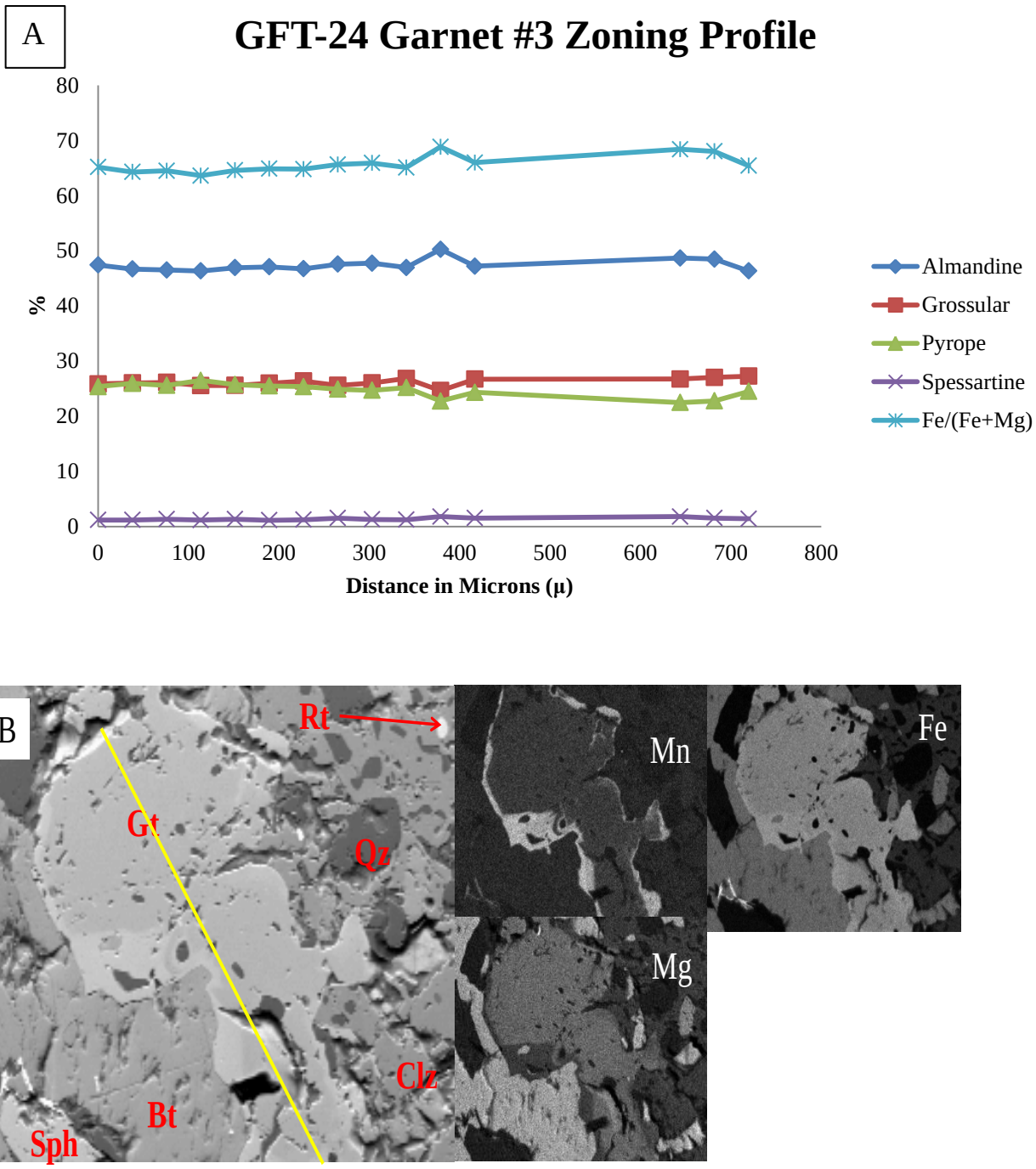

Figure 31.A) Zoning profile from one of the garnets found in GFT-24 from Sylva. Notice it is pretty homogenous throughout, B) X - ray map for the same garnet with a yellow line indicating where the zoning profile was taken. Notice the garnet becomes manganese and iron rich along the rims, especially where it is in contact with biotite.

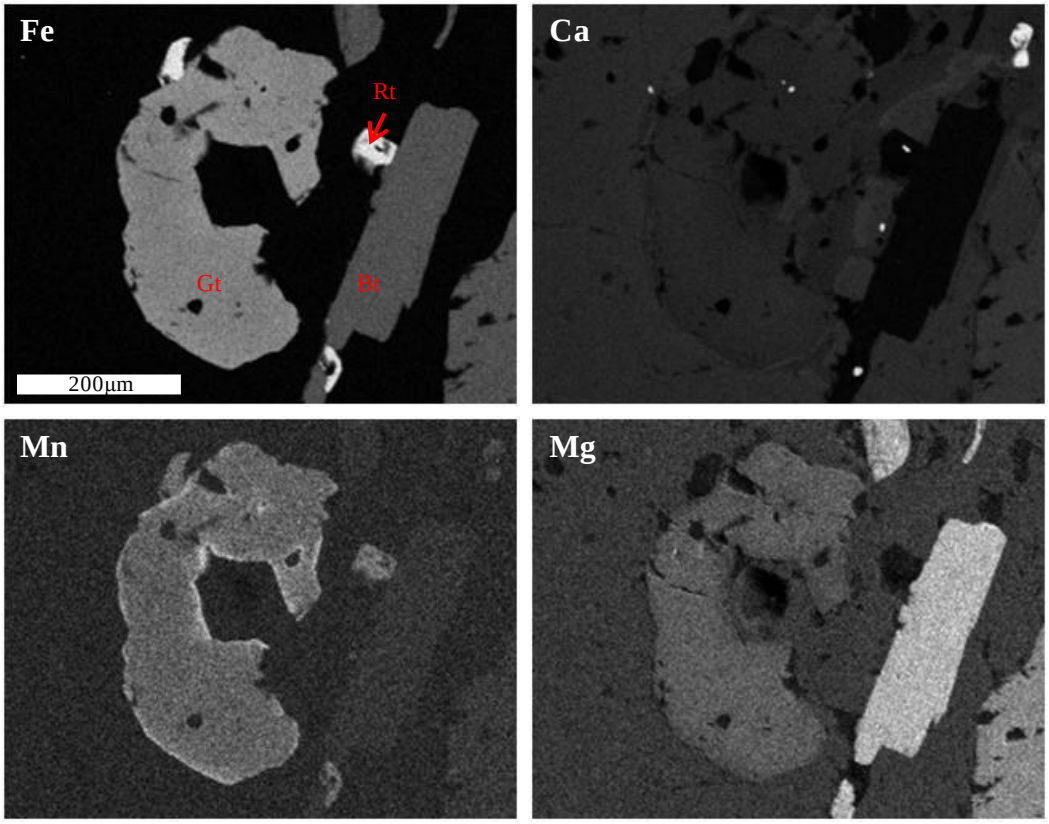

Figure 32. X - ray map showing zoning components in a garnet crystal from the Sylva location. Notice the enrichment of Mn along the rims.

Biotite: Biotite occurs as inclusions in the garnet as well as a matrix mineral as mostly euhedral crystals. Their sizes range between 0.1 and 0.4 mm. They frequently contain rutile inclusions (fully and partially; Fig. 30 C), and are commonly in contact with hornblende (tschermakite, Fig. 33 E). A few of the biotite crystals showed a symplectic texture with quartz (Fig 33 F). Some of the biotite crystals were completely surrounded by plagioclase (Fig. 33 D). Despite the occurrence of two textural varieties of biotite (green and brown), they showed no chemical differences with Al^{iv} = 2.42 - 2.68, Al^{vi} = 0.4 - 0.52, Fe/(Fe + Mg) = 0.40 - 0.44, and Ti^{vi} = 0.16 - 0.21 (Table 17, Fig. 34).

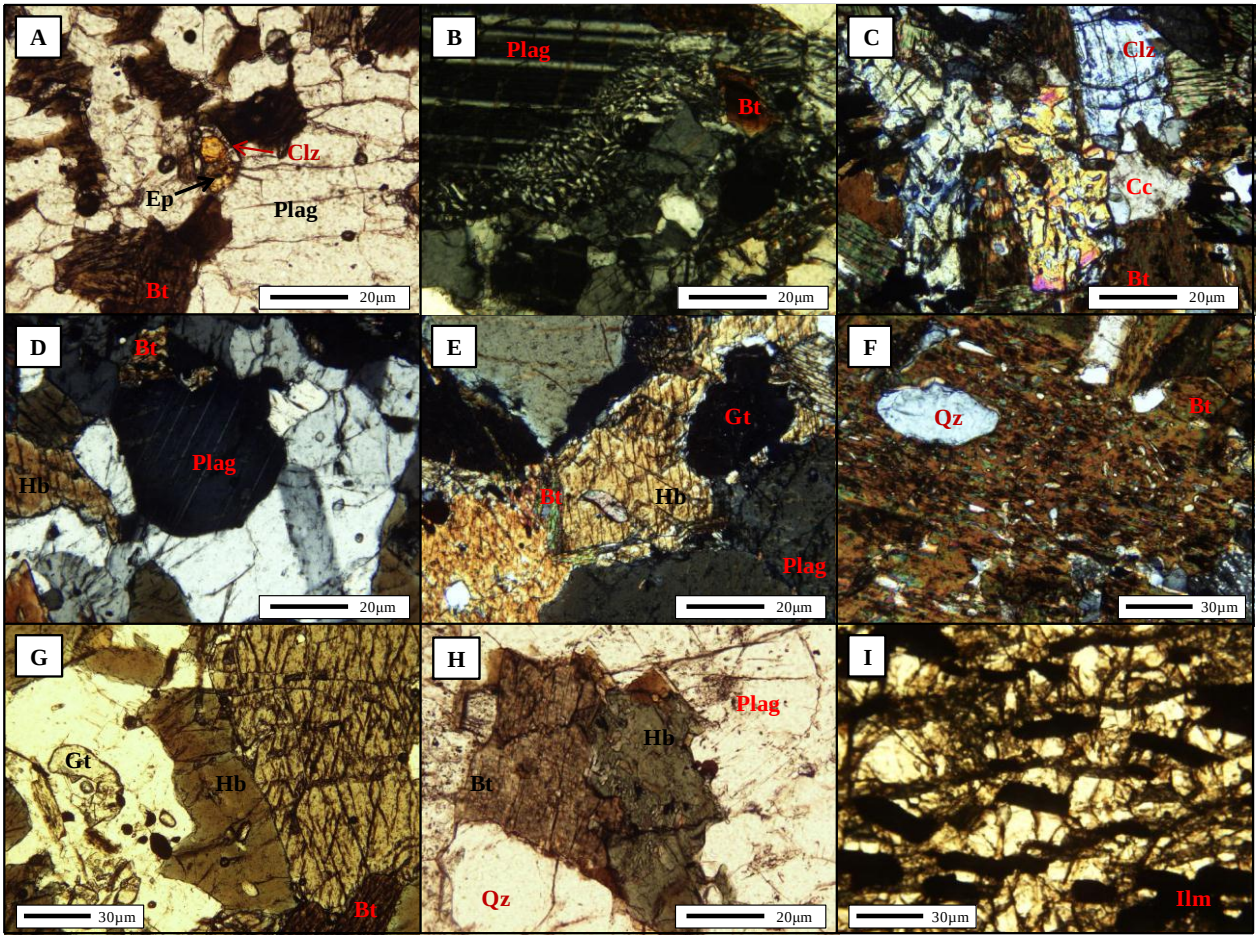

Figure 33. Selected textural relationships from Sylva. GFT-23: A) Epidote rimmed by clinozoisite, GFT-24: B) myrmekitic texture in plagioclase crystal with quartz, C) clinozoisite crystals exhibiting a symplectic texture with quartz, D) Biotite crystal included in a crystal of plagioclase, SV-4: E) Garnet crystal with a quartz ring around it and surrounded by tschermakite, F) Biotite displaying a symplectic texture with quartz, G) anhedral and resorbed garnet crystal near hornblende with truncated edges (possibly indicating partial melting), SV-7: H) Hornblende and biotite with symplectic texture with quartz, with the hornblende being replaced by biotite, I) oriented opaques in garnet.

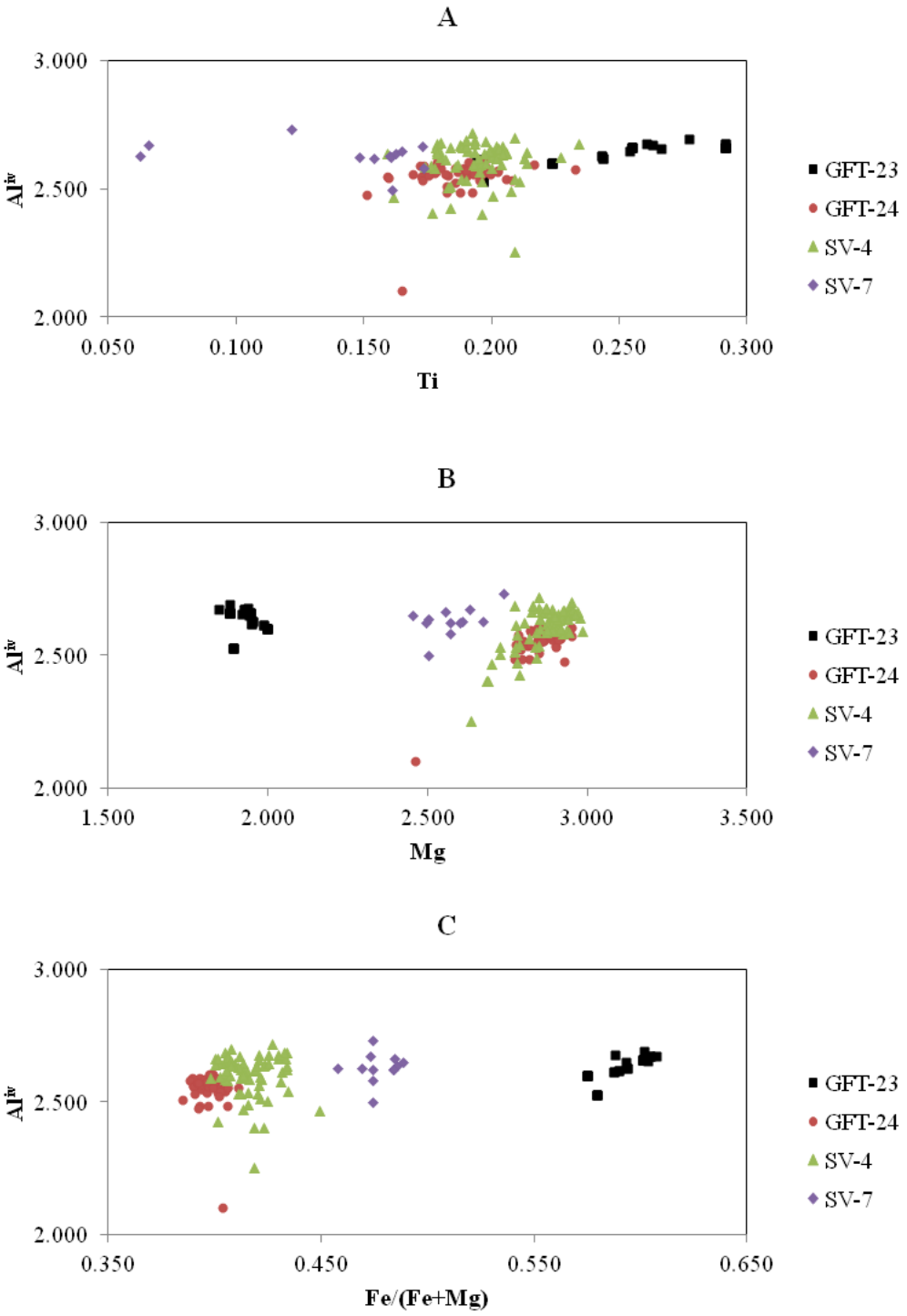

Figure 34. Compositions of biotites from Sylva plotted on (A) Al^{iv} vs. Ti, (B) Al^{iv} vs. Mg, and (C) Al^{iv} vs. Fe/(Fe + Mg).

Table 16. Representative garnet analyses for Sylva

	sv4-gt2										sv7-gt1									
	rim1	rim2	rim3	rim4	rim5	core1	core2	rim6	core3	rim7	core1	rim1	rim2	core2	rim3	rim4	rim5	core3	rim6	rim7
SiO2	37.79	37.79	37.43	37.28	36.72	37.31	36.90	37.85	37.69	37.56	38.00	37.11	37.96	38.15	38.05	37.79	38.12	38.28	38.51	38.24
TiO2	0.11	0.03	0.12	0.18	0.22	0.14	0.01	0.18	0.06	0.06	0.04	0.08	0.10	0.12	0.08	0.08	0.06	0.06	0.17	0.09
Al2O3	22.55	22.66	22.62	22.25	21.79	22.40	21.98	22.59	22.06	22.23	22.02	21.78	22.04	22.24	22.29	22.09	22.44	22.69	22.46	22.38
Cr2O3	0.20	0.25	0.21	0.21	0.26	0.05	0.05	0.07	0.23	0.12	0.05	0.05	0.08	0.18	0.01	0.18	0.12	0.05	0.09	0.07
Fe2O3	0.17	0.03	0.20	0.36	0.32	0.25	0.42	0.32	0.44	0.45	0.15	0.00	0.00	0.00	0.00	0.00	0.00	0.00	0.00	0.00
FeO	24.05	23.93	22.19	23.06	22.13	23.93	22.82	23.84	23.72	23.87	25.95	26.93	26.20	26.68	24.41	26.31	25.95	25.39	25.56	26.63
MnO	0.96	0.81	0.66	0.77	0.81	1.28	0.91	1.03	0.89	0.94	1.15	2.62	1.32	2.23	0.94	1.34	1.31	1.03	1.02	1.54
MgO	6.25	6.33	5.86	5.62	5.20	5.76	5.64	5.90	6.06	6.13	5.12	3.67	4.77	4.59	5.49	4.87	5.00	5.34	5.49	4.56
CaO	8.54	8.63	10.74	10.05	10.67	8.72	9.62	9.27	8.88	8.67	7.89	6.92	7.66	7.17	8.16	7.74	7.81	8.08	8.09	7.50
Total	100.60	100.46	100.04	99.78	98.13	99.86	98.35	101.05	100.03	100.02	100.35	99.17	100.12	101.36	99.44	100.40	100.82	100.93	101.40	101.01
Si	2.92	2.92	2.90	2.91	2.91	2.91	2.92	2.91	2.93	2.92	2.96	2.96	2.97	2.96	2.96	2.95	2.95	2.95	2.96	2.96
Al iv	0.08	0.08	0.10	0.09	0.09	0.09	0.08	0.09	0.07	0.08	0.04	0.04	0.03	0.04	0.04	0.05	0.05	0.05	0.04	0.04
Al vi	1.97	1.98	1.97	1.95	1.95	1.97	1.97	1.96	1.95	1.96	1.99	2.00	2.00	1.99	2.01	1.98	2.00	2.01	1.99	2.01
Ti	0.01	0.00	0.01	0.01	0.01	0.01	0.00	0.01	0.00	0.00	0.00	0.00	0.01	0.01	0.00	0.00	0.00	0.00	0.01	0.01
Cr	0.01	0.02	0.01	0.01	0.02	0.00	0.00	0.00	0.01	0.01	0.00	0.00	0.00	0.01	0.00	0.01	0.01	0.00	0.01	0.00
Fe2+	1.55	1.55	1.44	1.50	1.47	1.56	1.51	1.54	1.54	1.55	1.69	1.81	1.72	1.74	1.61	1.72	1.70	1.66	1.65	1.75
Mn	0.06	0.05	0.04	0.05	0.05	0.08	0.06	0.07	0.06	0.06	0.08	0.18	0.09	0.15	0.06	0.09	0.09	0.07	0.07	0.10
Mg	0.72	0.73	0.68	0.65	0.61	0.67	0.66	0.68	0.70	0.71	0.59	0.44	0.56	0.53	0.64	0.57	0.58	0.61	0.63	0.53
Ca	0.71	0.71	0.89	0.84	0.91	0.73	0.81	0.76	0.74	0.72	0.66	0.59	0.64	0.60	0.68	0.65	0.65	0.67	0.67	0.62
X_{alm}	49.01	48.76	44.41	46.87	45.86	49.03	47.22	48.20	48.80	48.83	55.12	59.28	56.71	56.97	53.43	55.84	55.60	54.30	53.99	57.80
X_{and}	0.51	0.08	0.61	1.09	0.98	0.76	1.29	0.96	1.33	1.36	0.43	0.00	0.00	0.00	0.00	0.00	0.00	0.00	0.00	0.00
X_{grs}	23.09	23.58	29.48	27.13	29.31	24.13	26.46	25.09	23.18	23.00	21.65	19.82	21.37	19.60	22.93	21.38	21.57	22.46	22.23	20.79
X_{prp}	24.64	24.98	23.34	22.48	21.12	23.02	22.77	23.24	23.96	24.33	20.07	14.75	18.74	17.93	21.51	19.20	19.55	20.79	21.26	17.79
X_{spss}	2.14	1.81	1.50	1.76	1.87	2.91	2.09	2.30	2.01	2.12	2.57	5.98	2.94	4.95	2.10	3.01	2.91	2.28	2.24	3.41
X_{uv}	0.61	0.80	0.66	0.67	0.85	0.15	0.17	0.20	0.73	0.37	0.16	0.17	0.24	0.55	0.04	0.57	0.37	0.17	0.28	0.22

Table 17. Representative biotite analyses from Sylva.

	SV-4														SV-7							
	bt2-2				bt1-1					bt1-2					bt1							
	rim1	core1	rim2	core2	rim1	core1	rim2	rim3	core2	rim1	core1	rim2	rim4	core2	c1	r1	r2	c2	r3	r4	r5	c3
SiO2	35.80	37.19	37.72	37.02	35.51	36.28	36.55	35.81	35.89	35.15	35.16	35.81	36.53	35.76	35.92	36.31	37.12	35.02	34.96	34.75	36.02	35.62
TiO2	1.81	1.91	1.65	1.88	1.58	1.66	1.79	1.60	1.70	1.56	1.58	1.69	1.42	1.73	1.42	1.55	1.44	1.41	1.51	1.42	1.32	1.41
Al2O3	17.33	17.58	16.92	17.07	17.31	16.86	17.83	17.47	17.13	17.31	17.81	17.89	16.34	17.63	18.10	17.75	17.61	17.59	17.77	17.54	18.38	17.92
FeO	16.75	16.05	15.11	16.40	17.11	17.01	17.03	17.17	16.60	17.14	16.78	17.33	17.36	17.36	18.42	18.59	18.21	18.45	18.81	18.19	18.72	19.07
MnO	0.00	0.09	0.04	0.09	0.03	0.02	0.03	0.00	0.21	0.00	0.09	0.03	0.06	0.05	0.13	0.05	0.16	0.20	0.19	0.18	0.08	0.11
MgO	13.00	12.42	12.65	12.94	12.74	12.42	13.04	13.01	12.81	12.54	12.73	12.71	11.96	12.93	11.70	11.56	11.32	10.96	11.24	10.69	11.21	11.43
CaO	0.10	0.25	0.10	0.04	0.15	0.23	0.12	0.17	0.09	0.07	0.06	0.00	0.52	0.13	0.00	0.11	0.58	0.70	0.33	1.52	0.35	0.29
Na2O	0.88	0.97	1.24	0.72	1.41	0.74	1.03	1.02	0.89	0.62	0.96	0.93	0.86	0.79	0.75	0.72	0.45	0.67	0.81	0.50	0.55	0.20
K2O	9.47	9.04	8.76	9.36	9.78	9.06	9.33	9.18	9.13	9.62	9.44	9.42	8.59	9.90	9.19	8.83	8.42	9.47	9.12	9.26	9.09	9.00
Cr2O3	0.02	0.00	0.01	0.05	0.00	0.05	0.00	0.02	0.00	0.04	0.00	0.00	0.07	0.02	0.04	0.08	0.00	0.00	0.01	0.02	0.06	0.00
Li2O*	0.72	1.12	1.27	1.07	0.64	0.86	0.94	0.73	0.75	0.54	0.54	0.73	0.93	0.71	0.76	0.87	1.10	0.50	0.48	0.42	0.79	0.67
Total	95.88	96.61	95.48	96.64	96.26	95.20	97.68	96.17	95.20	94.58	95.16	96.54	94.65	97.02	96.01	95.92	95.83	95.74	95.64	95.55	95.46	95.37
Si	5.36	5.47	5.58	5.46	5.34	5.46	5.36	5.35	5.41	5.36	5.32	5.34	5.53	5.32	5.37	5.42	5.50	5.36	5.33	5.35	5.38	5.38
Al iv	2.64	2.53	2.42	2.54	2.66	2.54	2.64	2.65	2.59	2.64	2.68	2.66	2.47	2.68	2.63	2.58	2.50	2.64	2.67	2.65	2.62	2.62
Al vi	0.43	0.52	0.52	0.43	0.40	0.45	0.44	0.43	0.45	0.48	0.50	0.48	0.45	0.42	0.56	0.54	0.58	0.54	0.53	0.54	0.61	0.57
Ti	0.20	0.21	0.18	0.21	0.18	0.19	0.20	0.18	0.19	0.18	0.18	0.19	0.16	0.19	0.16	0.17	0.16	0.16	0.17	0.16	0.15	0.16
Cr	0.00	0.00	0.00	0.01	0.00	0.01	0.00	0.00	0.00	0.00	0.00	0.00	0.01	0.00	0.00	0.01	0.00	0.00	0.00	0.00	0.01	0.00
Fe	2.10	1.97	1.87	2.02	2.15	2.14	2.09	2.15	2.09	2.19	2.12	2.16	2.20	2.16	2.30	2.32	2.26	2.36	2.40	2.34	2.34	2.41
Mn	0.00	0.01	0.00	0.01	0.00	0.00	0.00	0.00	0.03	0.00	0.01	0.00	0.01	0.01	0.02	0.01	0.02	0.03	0.02	0.02	0.01	0.01
Mg	2.90	2.72	2.79	2.85	2.86	2.79	2.85	2.90	2.88	2.85	2.87	2.82	2.70	2.87	2.61	2.57	2.50	2.50	2.56	2.45	2.50	2.57
Li*	0.44	0.66	0.76	0.64	0.39	0.52	0.55	0.44	0.45	0.33	0.33	0.43	0.57	0.43	0.45	0.52	0.66	0.31	0.29	0.26	0.47	0.41
Ca	0.02	0.04	0.02	0.01	0.02	0.04	0.02	0.03	0.01	0.01	0.01	0.00	0.08	0.02	0.00	0.02	0.09	0.12	0.05	0.25	0.06	0.05
Na	0.26	0.28	0.36	0.21	0.41	0.22	0.29	0.30	0.26	0.18	0.28	0.27	0.25	0.23	0.22	0.21	0.13	0.20	0.24	0.15	0.16	0.06
K	1.81	1.70	1.65	1.76	1.87	1.74	1.75	1.75	1.75	1.87	1.82	1.79	1.66	1.88	1.75	1.68	1.59	1.85	1.77	1.82	1.73	1.73
Al total	3.06	3.05	2.95	2.97	3.07	2.99	3.08	3.08	3.04	3.11	3.18	3.14	2.92	3.09	3.19	3.12	3.08	3.18	3.20	3.18	3.24	3.19
Fe/Fe+Mg	0.42	0.42	0.40	0.42	0.43	0.43	0.42	0.43	0.42	0.43	0.43	0.43	0.45	0.43	0.47	0.47	0.47	0.49	0.48	0.49	0.48	0.48

Amphiboles: Amphiboles from Sylva classify as "tschermakite" following the nomenclature of Leake et al. (1997; Fig. 35). The tschermakite (Hb) crystals were slightly zoned with rims generally having a higher Si and lower Al^{iv} compared to the cores (Table 18). Many of the crystals were subhedral and ranged in size from 0.2 mm - 1.5 mm. The tschermakite crystals were pleochroic from green to darker bluish green, having areas (zones) where it is more of a green - brown (Fig. 33 G, H).

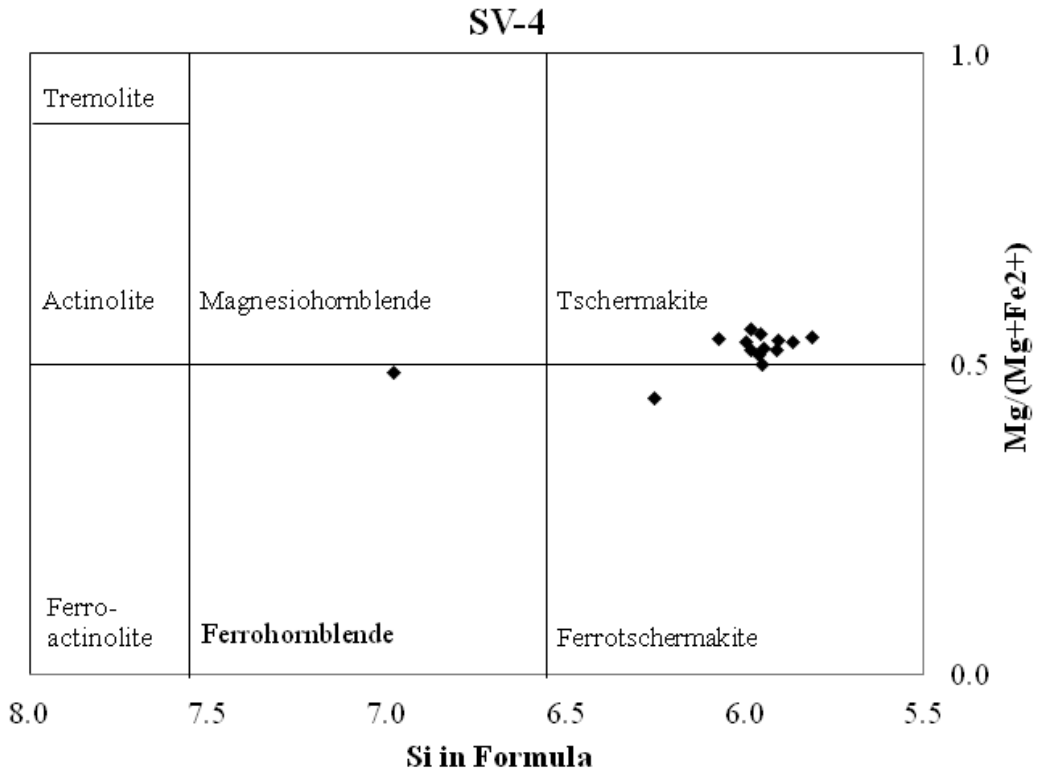

Figure 35. Graph showing the classification of the amphiboles based on the amount of Si and the Mg/(Mg + Fe) ratio from sample SV-4 from Sylva.

Table 18. Representative Amphibole analyses for Sylva

	a1rim	a2rim	a3rim	a4rim	a5core	a6core	a7rim	a8rim	a9core
SiO2	42.04	39.74	41.07	40.19	39.86	40.07	40.50	40.94	40.36
TiO2	1.26	2.35	1.28	1.35	2.23	1.68	1.00	1.43	2.18
Al2O3	14.98	14.18	14.81	14.54	14.35	14.67	15.57	15.03	14.52
FeO	15.71	15.66	15.21	15.10	15.12	15.53	15.41	15.41	15.71
MnO	0.15	0.13	0.12	0.14	0.11	0.19	0.18	0.15	0.17
MgO	11.00	10.64	10.65	10.56	10.56	10.84	10.06	10.23	10.21
CaO	12.23	11.86	11.92	11.96	11.83	11.99	11.97	11.92	11.94
Na2O	1.39	1.26	1.13	1.60	1.35	1.42	1.53	1.49	1.54
K2O	0.73	1.34	0.62	1.01	1.41	1.10	0.62	0.87	1.27
Cr2O3	0.21	0.06	0.10	0.10	0.09	0.06	0.00	0.13	0.11
Total	99.70	97.21	96.91	96.55	96.91	97.55	96.83	97.60	98.01
Si	6.04	5.92	6.05	6.01	5.96	5.92	6.01	6.04	5.98
Al iv	1.96	2.08	1.95	1.99	2.04	2.08	1.99	1.96	2.02
Al vi	0.58	0.40	0.62	0.57	0.48	0.48	0.73	0.66	0.52
Ti	0.14	0.26	0.14	0.15	0.25	0.19	0.11	0.16	0.24
Cr	0.02	0.01	0.01	0.01	0.01	0.01	0.00	0.01	0.01
Fe3+	0.80	0.75	0.84	0.61	0.60	0.81	0.67	0.61	0.52
Fe2+	1.09	1.20	1.04	1.28	1.29	1.11	1.24	1.29	1.42
Mn	0.02	0.02	0.02	0.02	0.01	0.02	0.02	0.02	0.02
Mg	2.36	2.36	2.34	2.35	2.35	2.39	2.22	2.25	2.26
Ca	1.88	1.89	1.88	1.92	1.89	1.90	1.90	1.88	1.90
Na	0.39	0.36	0.32	0.46	0.39	0.41	0.44	0.43	0.44
K	0.13	0.25	0.12	0.19	0.27	0.21	0.12	0.16	0.24
Al Total	2.54	2.49	2.57	2.56	2.53	2.55	2.72	2.61	2.54
Fe/Fe+Mg	0.44	0.45	0.44	0.45	0.45	0.45	0.46	0.46	0.46

*Other Minerals***:** Feldspars from Sylva are andesines (X_{ab} = 0.37 - 0.60, X_{an} = 0.50 - 0.62) and are unzoned (Table 19). There is a large difference between the feldspars from this location. SV-4 seems to have more of the anorthite component than SV-7 which is explained by it being a calc - silicate. The plagioclase crystals contain inclusions of garnet and biotite. The plagioclase has exsolution lamellae of orthoclase and displayed a myrmekitic texture with intergrowths of quartz (Fig. 33 B). Clinozoisite crystals were very euhedral in shape and ranged in size from 0.3 to1.5 mm, some with a symplectic texture with quartz (Fig. 33 C). In one case, epidote was rimmed by clinozoisite (Fig. 33 A).

Table 19. Representative analyses for feldspars at Sylva

	SV4-gt2plg1												SV7-gt1plag1					
	p1	p2	p3	p4	p5	p6	p7	p8	p9	p10	p11	p12	p1	p2	p3	p4	p4	p5
SiO2	54.34	56.67	53.71	53.90	54.25	55.98	53.25	57.08	57.18	54.38	54.10	54.35	59.05	58.25	58.33	58.27	58.28	55.33
TiO2	0.00	0.17	0.00	0.00	0.00	0.00	0.00	0.03	0.05	0.13	0.02	0.00	0.00	0.07	0.08	0.12	0.02	0.00
Al2O3	28.26	26.69	28.34	28.36	28.60	27.13	29.29	26.58	26.66	27.91	28.86	28.06	26.02	26.27	25.84	25.89	26.64	27.18
FeO	0.10	0.45	0.26	0.06	0.07	0.19	0.26	0.33	0.13	0.42	0.07	0.12	0.03	0.00	0.00	0.00	0.11	0.06
MnO	0.00	0.00	0.00	0.00	0.00	0.00	0.00	0.00	0.00	0.00	0.00	0.00						
MgO	1.32	0.87	1.25	0.81	1.09	0.98	1.13	0.99	0.84	0.88	0.92	1.04	0.79	0.80	0.66	1.02	0.62	1.08
CaO	10.24	7.92	10.12	10.35	10.22	8.70	11.05	7.92	7.86	9.74	10.74	10.08	7.94	8.08	7.60	8.55	8.38	9.65
Na2O	5.81	6.72	5.47	5.71	5.78	6.57	5.52	6.78	7.23	5.83	5.65	5.92	7.28	6.90	7.19	6.31	6.94	5.94
K2O	0.19	0.19	0.14	0.10	0.12	0.14	0.15	0.15	0.16	0.21	0.22	0.12	0.12	0.17	0.12	0.12	0.22	0.12
Total	100.27	99.67	99.28	99.29	100.12	99.68	100.65	99.85	100.12	99.50	100.59	99.68	101.23	100.54	99.84	100.28	101.21	99.37
Si	2.45	2.55	2.44	2.45	2.45	2.53	2.40	2.56	2.56	2.47	2.43	2.46	2.61	2.59	2.61	2.60	2.58	2.51
Al	1.50	1.42	1.52	1.52	1.52	1.44	1.56	1.41	1.41	1.49	1.53	1.50	1.36	1.38	1.36	1.36	1.39	1.45
Ti	0.00	0.01	0.00	0.00	0.00	0.00	0.00	0.00	0.00	0.00	0.00	0.00	0.00	0.00	0.00	0.00	0.00	0.00
Fe	0.00	0.02	0.01	0.00	0.00	0.01	0.01	0.01	0.00	0.02	0.00	0.00	0.00	0.00	0.00	0.00	0.00	0.00
Mg	0.09	0.06	0.08	0.05	0.07	0.07	0.08	0.07	0.06	0.06	0.06	0.07	0.05	0.05	0.04	0.07	0.04	0.07
Ca	0.49	0.38	0.49	0.50	0.49	0.42	0.53	0.38	0.38	0.47	0.52	0.49	0.38	0.39	0.36	0.41	0.40	0.47
Na	0.51	0.59	0.48	0.50	0.51	0.57	0.48	0.59	0.63	0.51	0.49	0.52	0.62	0.60	0.62	0.55	0.60	0.52
K	0.01	0.01	0.01	0.01	0.01	0.01	0.01	0.01	0.01	0.01	0.01	0.01	0.01	0.01	0.01	0.01	0.01	0.01
X_{an}	0.49	0.39	0.50	0.50	0.49	0.42	0.52	0.39	0.37	0.47	0.51	0.48	0.37	0.39	0.37	0.42	0.40	0.47
X_{ab}	0.50	0.60	0.49	0.50	0.50	0.57	0.47	0.60	0.62	0.51	0.48	0.51	0.62	0.60	0.63	0.57	0.59	0.52
X_{or}	0.01	0.01	0.01	0.01	0.01	0.01	0.01	0.01	0.01	0.01	0.01	0.01	0.01	0.01	0.01	0.01	0.01	0.01

EASTERN BLUE RIDGE

Beaucatcher Mountain

The rocks exposed at Beaucatcher Mountain consist of migmatites, garnet - biotite gneisses and granofelses, mafic amphibolites (hornblende schists), with some pegmatitic dykes (Fig. 36). The mineral assemblage for Beaucatcher Mountain is garnet + biotite + quartz + sillimanite + plagioclase + hornblende + muscovite + ilmenite (Fig. 37).

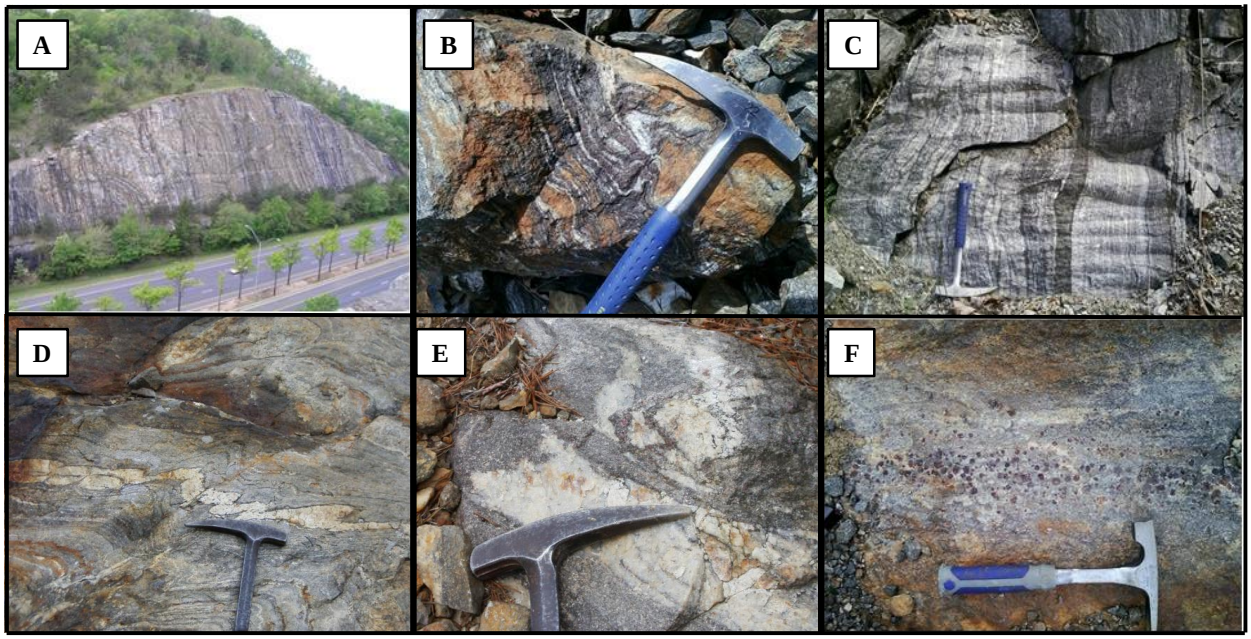

Figure 36. A - F: Beaucatcher Mountain, A) view of Beaucatcher Mountain looking southwest, B) migmatization in a gneiss, C) Bt gneiss with mafic unit, D) folded leucosome in migmatite showing top to the north sense of shear, E) garnet rich restite and leucosome showing evidence of ptygmatic folding, F) peritectic garnets in a migmatite.

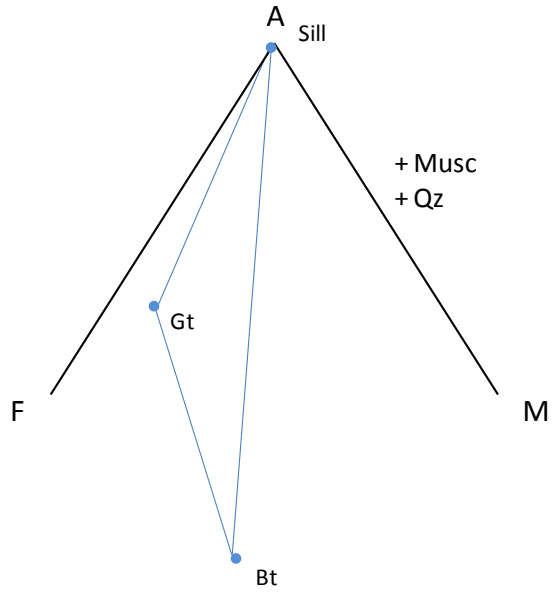

Figure 37. AFM diagram projected from Ms and Qz, displaying the peak mineral assemblage Gt + Bt + Sill for Beaucatcher Mountain.

Garnet: Several garnets are highly fractured and contain very few inclusions. All of the garnets are in contact with biotite, in some cases, completely surrounded by it. The garnets range in size from 0.3 to 0.75 mm. Beaucatcher mountain garnets are almandine

rich with small amounts of pyrope, grossular, and spessartine (X_{alm} = 0.73 - 0.75, X_{prp} =0.09 - 0.12, X_{grs} = 0.03 - 0.05, X_{spss} = 0.07 - 0.14; Table 20). They show weak zoning patterns in which the rims are more enriched in Mn and depleted in Mg and Fe compared to the cores (Fig. 38).

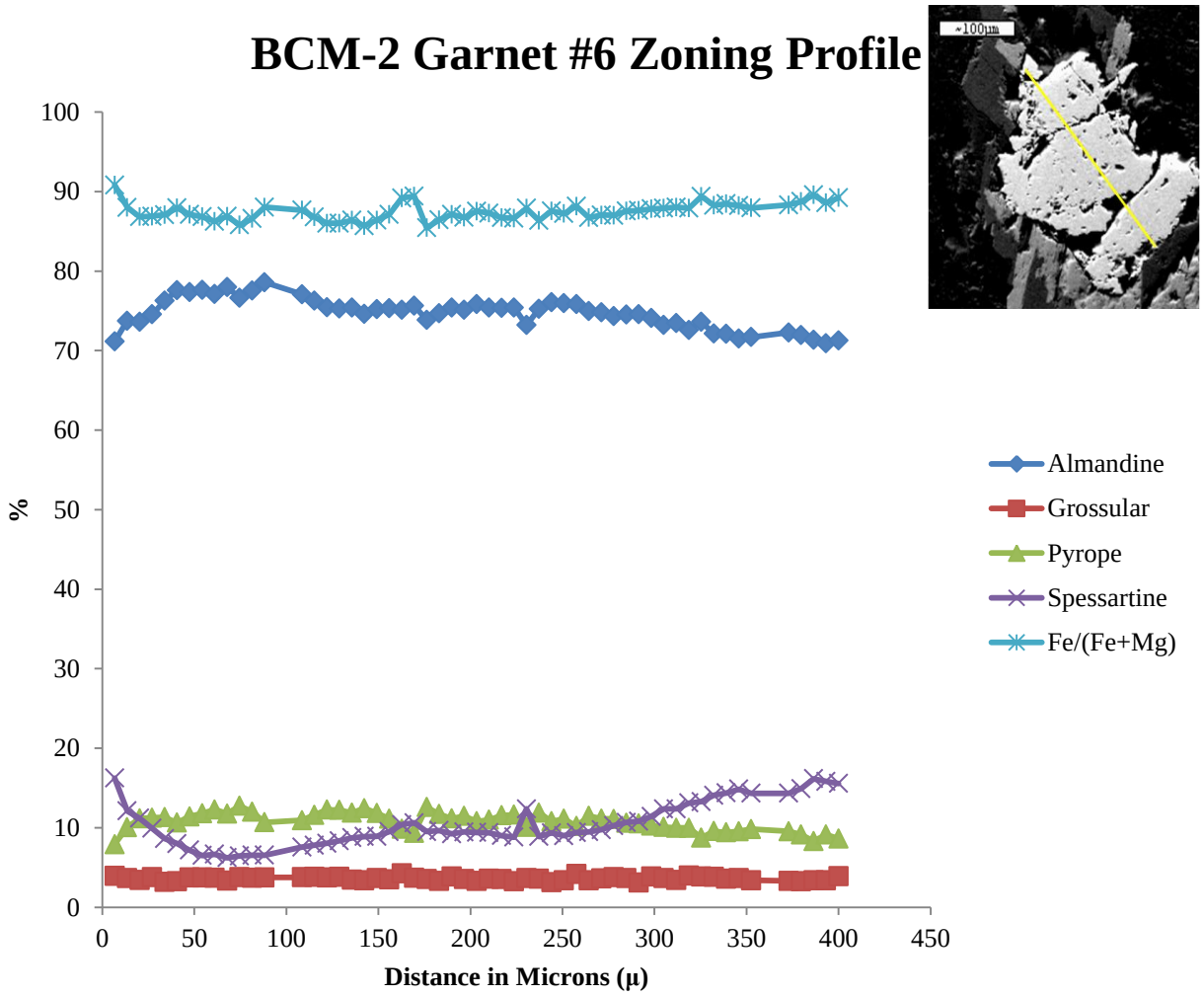

Figure 38: Garnet profile showing enrichment of almandine in cores and spessartine in the rims.

Table 20. Representative garnet analyses for Beaucatcher Mountain

	gt3rim1	gt3core1	gt3rim2	gt3rim3	gt3core2	gt3rim4	gt3rim5	gt3rim6	gt4core1	gt4rim1	gt4rim2	gt4rim3	gt4rim4	gt4rim5	gt5core1	gt5rim1	gt5rim2	gt6rim1
SiO2	37.18	37.54	37.05	37.47	37.65	37.14	37.34	37.32	37.51	36.73	36.99	37.06	37.53	37.31	38.03	37.70	37.21	38.13
TiO2	0.00	0.00	0.00	0.00	0.00	0.04	0.00	0.00	0.00	0.01	0.03	0.00	0.03	0.08	0.13	0.00	0.00	0.00
Al2O3	22.25	22.49	22.18	22.41	22.30	21.99	22.55	22.00	22.28	21.84	21.93	22.02	22.44	22.29	22.79	22.52	22.20	22.51
Cr2O3	0.11	0.20	0.30	0.16	0.06	0.16	0.00	0.25	0.03	0.12	0.16	0.23	0.38	0.21	0.16	0.19	0.12	0.08
FeO	32.21	33.15	29.84	31.43	32.86	30.40	32.69	29.55	32.52	29.70	27.66	28.28	30.55	31.53	32.80	32.25	31.57	33.46
MnO	4.54	2.81	6.98	4.59	3.36	6.43	3.28	6.43	3.87	7.16	8.49	8.32	6.29	5.32	2.66	3.69	3.69	3.00
MgO	2.80	3.58	2.37	3.08	3.25	2.29	3.39	2.19	2.88	2.10	1.77	1.96	2.54	2.64	3.78	3.27	3.02	3.05
CaO	1.37	1.25	1.23	1.82	1.21	1.32	1.42	1.31	1.51	1.34	2.00	1.64	1.41	1.36	1.43	1.39	1.31	1.49
Total	100.39	101.02	99.90	100.91	100.62	99.77	100.64	99.05	100.60	99.00	99.02	99.50	101.17	100.74	101.77	100.98	99.07	101.72
Si	2.95	2.95	2.95	2.95	2.97	2.97	2.95	2.98	2.97	2.96	2.97	2.97	2.95	2.95	2.95	2.96	2.97	2.97
Al iv	0.05	0.05	0.05	0.05	0.03	0.03	0.05	0.02	0.03	0.04	0.03	0.03	0.05	0.05	0.05	0.04	0.03	0.03
Al vi	2.05	2.04	2.06	2.05	2.06	2.05	2.06	2.08	2.06	2.05	2.07	2.06	2.05	2.04	2.05	2.06	2.07	2.06
Ti	0.00	0.00	0.00	0.00	0.00	0.00	0.00	0.00	0.00	0.00	0.00	0.00	0.00	0.00	0.01	0.00	0.00	0.00
Cr	0.01	0.01	0.02	0.01	0.00	0.01	0.00	0.02	0.00	0.01	0.01	0.01	0.02	0.01	0.01	0.01	0.01	0.00
Fe2+	2.21	2.25	2.08	2.14	2.24	2.12	2.23	2.10	2.23	2.09	1.96	1.99	2.10	2.17	2.21	2.20	2.21	2.26
Mn	0.31	0.19	0.47	0.31	0.22	0.43	0.22	0.44	0.26	0.49	0.58	0.56	0.42	0.36	0.17	0.24	0.25	0.20
Mg	0.33	0.42	0.28	0.36	0.38	0.27	0.40	0.26	0.34	0.25	0.21	0.23	0.30	0.31	0.44	0.38	0.36	0.35
Ca	0.12	0.11	0.11	0.15	0.10	0.11	0.12	0.11	0.13	0.12	0.17	0.14	0.12	0.12	0.12	0.12	0.11	0.12
X_{alm}	0.84	0.88	0.78	0.82	0.87	0.79	0.87	0.79	0.85	0.78	0.72	0.74	0.80	0.82	0.88	0.86	0.86	0.88
X_{grs}	0.04	0.03	0.03	0.05	0.04	0.04	0.05	0.03	0.05	0.04	0.06	0.04	0.03	0.04	0.04	0.04	0.04	0.05
X_{prp}	0.13	0.17	0.11	0.14	0.15	0.10	0.16	0.10	0.13	0.09	0.08	0.09	0.11	0.12	0.17	0.15	0.14	0.14
X_{spss}	0.12	0.07	0.18	0.12	0.09	0.16	0.09	0.16	0.10	0.18	0.21	0.21	0.16	0.14	0.07	0.10	0.10	0.08
X_{uv}	0.00	0.01	0.01	0.01	0.00	0.01	0.00	0.01	0.00	0.00	0.01	0.01	0.01	0.01	0.01	0.01	0.00	0.00

Biotite: Biotite crystals range in size from 0.05 to 2 mm, with the larger grains being more euhedral. The inclusions found in the biotite crystals were zircon, ilmenite, monazite, quartz, and plagioclase. Some of the crystals had pleochroic halos and there were several biotite crystals that were being replaced by muscovite. The biotite crystals were homogenous with compositions of Al^{iv} = 2.62 - 2.70, Al^{vi} = 0.49 - 0.81, Fe/(Fe + Mg) = 0.54 - 0.58, Ti^{iv} = 0.09 - 0.3 (Table 21, Fig. 39).

Table 21. Representative biotite anaylses for Beaucatcher Mountain

	Bt1Rim	bt1core	bt2rim	bt2core	bt3rim	bt3core	bt4rim	bt4core	bt5rim	bt5core	bt6rim	bt6core	bhbt
SiO2	34.24	34.55	35.04	35.45	35.44	34.38	34.41	34.58	34.92	35.43	35.39	35.74	35.75
TiO2	2.43	2.57	1.11	1.18	2.18	2.25	2.32	2.25	2.13	2.03	1.92	1.97	0.83
Al2O3	17.91	17.46	18.87	18.67	17.70	17.64	17.59	17.99	18.03	17.75	17.78	18.39	19.34
FeO	20.75	21.33	21.12	21.10	21.59	21.46	21.39	21.43	21.74	21.46	20.53	20.98	20.37
MnO	0.06	0.14	0.15	0.04	0.06	0.16	0.21	0.14	0.17	0.15	0.12	0.15	0.12
MgO	9.08	8.86	9.65	9.90	9.51	9.16	9.05	9.08	9.27	9.04	9.77	9.75	9.27
CaO	0.08	0.11	0.10	0.08	0.07	0.00	0.02	0.00	0.00	0.32	0.01	0.10	0.06
Na2O	1.30	0.85	1.03	1.09	1.25	1.01	1.28	1.23	1.06	1.06	0.96	1.10	1.36
K2O	8.35	8.53	8.54	8.83	8.66	8.52	8.50	8.65	8.58	8.18	8.49	8.77	8.71
Cr2O3	0.17	0.03	0.04	0.07	0.11	0.00	0.00	0.07	0.00	0.11	0.07	0.00	0.00
Total	94.38	94.42	95.67	96.39	96.55	94.58	94.79	95.43	95.90	95.54	95.05	96.96	95.82
Si	5.30	5.35	5.32	5.33	5.34	5.32	5.32	5.31	5.32	5.38	5.38	5.34	5.38
Al iv	2.70	2.65	2.68	2.67	2.66	2.68	2.68	2.69	2.68	2.62	2.62	2.66	2.62
Al vi	0.56	0.53	0.70	0.65	0.49	0.54	0.52	0.56	0.56	0.56	0.57	0.58	0.81
Ti	0.28	0.30	0.13	0.13	0.25	0.26	0.27	0.26	0.24	0.23	0.22	0.22	0.09
Cr	0.02	0.00	0.00	0.01	0.01	0.00	0.00	0.01	0.00	0.01	0.01	0.00	0.00
Fe	2.69	2.76	2.68	2.66	2.72	2.78	2.77	2.75	2.77	2.73	2.61	2.62	2.56
Mn	0.01	0.02	0.02	0.00	0.01	0.02	0.03	0.02	0.02	0.02	0.02	0.02	0.02
Mg	2.09	2.04	2.18	2.22	2.14	2.11	2.09	2.08	2.11	2.05	2.22	2.17	2.08
Li*	0.17	0.23	0.31	0.38	0.38	0.20	0.20	0.23	0.29	0.38	0.37	0.42	0.43
Ca	0.01	0.02	0.02	0.01	0.01	0.00	0.00	0.00	0.00	0.05	0.00	0.02	0.01
Na	0.39	0.25	0.30	0.32	0.37	0.30	0.38	0.37	0.31	0.31	0.28	0.32	0.40
K	1.65	1.68	1.65	1.69	1.66	1.68	1.68	1.69	1.67	1.59	1.65	1.67	1.67
Al total	3.27	3.18	3.38	3.31	3.15	3.22	3.21	3.25	3.24	3.18	3.19	3.24	3.43
Fe/Fe+Mg	0.56	0.57	0.55	0.54	0.56	0.57	0.57	0.57	0.57	0.57	0.54	0.55	0.55

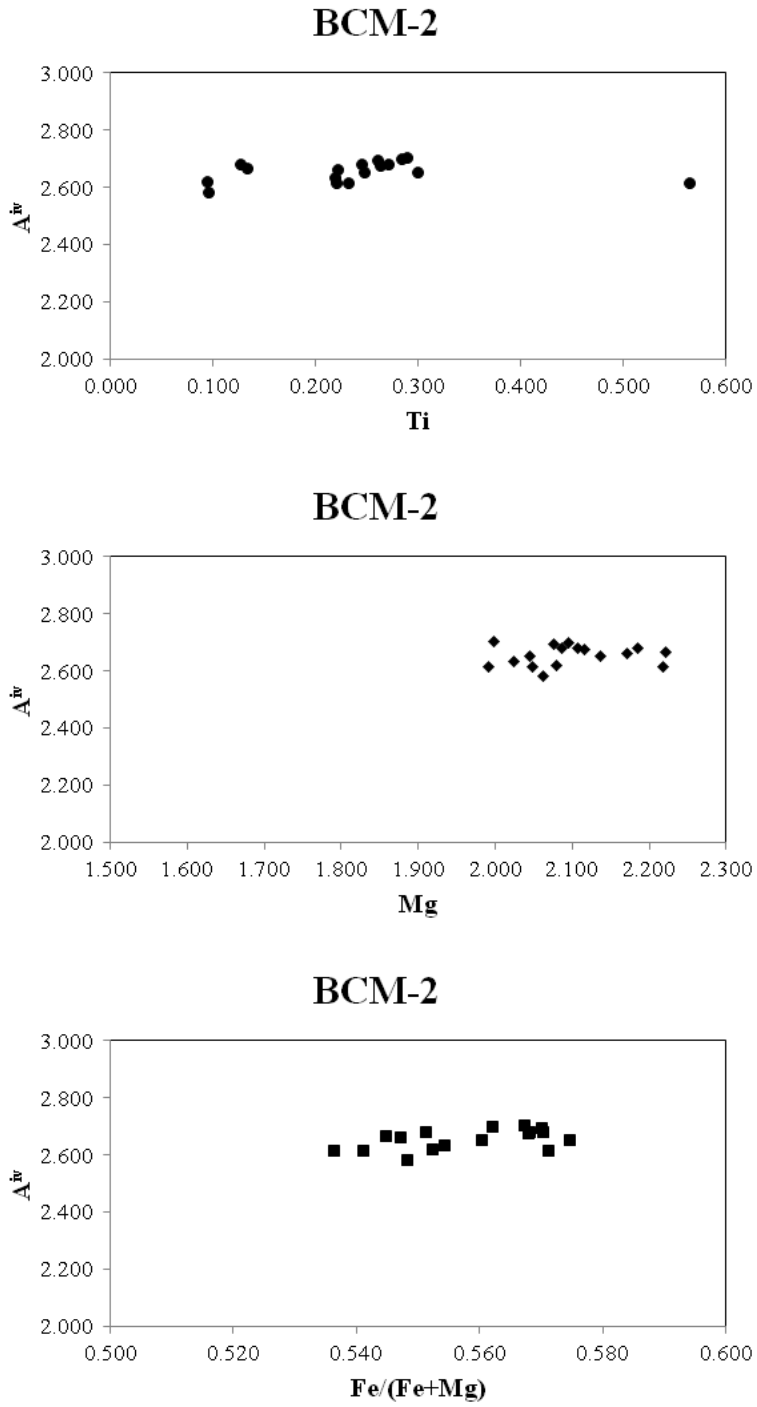

Figure 39. Compositions of biotites from BCM-2 (Beaucatcher Mountain) plotted on (A) Al^{iv} vs. Ti, (B) Al^{iv} vs. Mg, and (C) Al^{iv} vs. Fe/(Fe + Mg).

Other Minerals: Feldspar grain sizes range from 0.15 mm to 1.5 mm. The plagioclase crystals contained inclusions of quartz, ilmenite, monazite, and biotite. In some cases, the plagioclase is rimming garnet crystals separating it from biotite.

Feldspars from Beaucatcher mountain were characterized by albite rich plagioclases (X_{ab} = 0.63 - 0.69, X_{an} = 0.29 - 0.33; Table 22).

Table 22. Representative feldspar analyses for Beaucatcher Mountain

	bjhplag	bjhplag2	bjhplag3	bjhplag4	plag1-1	plag1-2	plag1-3	plag2-1	plag2-2	plag2-3	plag3-1	plag3-2	plag3-3	plag3-4
SiO2	60.00	60.45	59.81	60.79	61.66	61.17	59.86	60.79	61.19	60.30	61.22	59.70	60.21	59.55
TiO2	0.05	0.00	0.04	0.00	0.14	0.03	0.02	0.08	0.00	0.07	0.08	0.09	0.00	0.08
Al2O3	23.87	24.37	24.50	23.59	24.35	23.97	24.43	24.25	24.25	24.85	24.24	24.92	25.03	26.02
FeO	0.07	0.09	0.06	0.06	0.00	0.09	0.11	0.02	0.07	0.06	0.09	0.03	0.09	0.00
MgO	0.47	0.60	0.41	0.29	0.53	0.40	0.44	0.43	0.47	0.53	0.46	0.72	0.47	0.56
CaO	6.47	6.39	7.23	6.13	6.22	6.31	7.07	6.78	6.42	7.27	6.51	7.59	7.79	8.57
Na2O	7.53	7.65	7.31	7.79	8.21	7.82	7.30	7.75	7.86	7.46	7.79	7.11	7.41	7.06
K2O	0.03	0.17	0.21	0.19	0.19	0.26	0.20	0.19	0.14	0.16	0.06	0.21	0.21	0.10
Total	98.48	99.72	99.56	98.84	101.29	100.05	99.45	100.29	100.41	100.70	100.46	100.36	101.22	101.94
Si	2.71	2.70	2.68	2.73	2.71	2.72	2.68	2.70	2.71	2.67	2.71	2.66	2.66	2.62
Al	1.27	1.28	1.29	1.25	1.26	1.26	1.29	1.27	1.27	1.30	1.26	1.31	1.30	1.35
Ti	0.00	0.00	0.00	0.00	0.00	0.00	0.00	0.00	0.00	0.00	0.00	0.00	0.00	0.00
Fe	0.00	0.00	0.00	0.00	0.00	0.00	0.00	0.00	0.00	0.00	0.00	0.00	0.00	0.00
Mg	0.03	0.04	0.03	0.02	0.03	0.03	0.03	0.03	0.03	0.04	0.03	0.05	0.03	0.04
Ca	0.31	0.31	0.35	0.30	0.29	0.30	0.34	0.32	0.30	0.34	0.31	0.36	0.37	0.40
Na	0.66	0.66	0.64	0.68	0.70	0.67	0.63	0.67	0.68	0.64	0.67	0.61	0.63	0.60
K	0.00	0.01	0.01	0.01	0.01	0.01	0.01	0.01	0.01	0.01	0.00	0.01	0.01	0.01
X_{an}	0.32	0.31	0.35	0.30	0.29	0.30	0.34	0.32	0.31	0.35	0.31	0.37	0.36	0.40
X_{ab}	0.68	0.68	0.64	0.69	0.70	0.68	0.64	0.67	0.68	0.64	0.68	0.62	0.63	0.60
X_{or}	0.00	0.01	0.01	0.01	0.01	0.01	0.01	0.01	0.01	0.01	0.00	0.01	0.01	0.01

P-T CONDITIONS OF METAMORPHISM

Once the compositions of minerals had been determined, the exchange of Fe^{2+} and Mg^{2+} between garnet and biotite for thermometry was used (e.g. Spear, 1993 and references therein). This is typically temperature sensitive but not pressure sensitive. The barometers GASP (Gt + Als + Qz = Plg), GRIPS (Gt + Rt = Ilm + Als + Qz), and GRAIL (Gt + Rt = Ilm + Als) were used for samples containing these minerals. All of these are continuous net transfer barometers. The quantitative compositions were then run iteratively through GPT3, a spreadsheet program constructed by Reche and Martinez (1996) made for thermobarometric calculations in metapelitic rocks, until both P and T converged. Subroutine "average PT" of program Thermocalc 3.26 (Powell and Holland,

2002) was used to calculate an average P-T condition for each sample with appropriate error bars based on all possible reactions for a given mineral assemblage. Results from both programs are compiled in Table 23 and 24.

The average pressure calculated for Marble (GFT-7) is 5.5 to 6.5 kbars with both Thermocalc and GPT3 (Reche and Martinez, 1996) with temperatures of 532 ˚C to 543 ˚C (Thermocalc) and 549 ˚C to 564 ˚C (GPT3). P-T conditions calculated using Thermocalc for Little Pine Garnet Mine (LP-7) ranged from 11.0 to11.6 kbars and 894 ˚C to 900 ˚C. Calculations for the same sample using GPT3 yielded conditions of 5.4 to 7.1 kbars and 478 ˚C to 530 ˚C (Table 24, Fig. 40). The P-T conditions for the Savannah Church location (SVC-5) ranged from 7.7 to 9.3 kbars and 475 ˚C to 486 ˚C (using Thermocalc). Calculations for the same sample yielded 9.3 to 9.5 kbars and 661 ˚C to 663 ˚C using GPT3. The calculations for one Sylva sample (SV-4) averaged 13.3 to 13.5 kbars and 743 ˚C to 747 ˚C using Thermocalc and 17.5 to 18 kbars and 553 ˚C to 559 ˚C with GPT3. Another sample from Sylva (SV-7) yielded P-T conditions of 10.9 to 12 kbars and 723 ˚C to 729 ˚C using Thermocalc, and 12.8 to 21 kbars, 950 ˚C to 975 ˚C using GPT3. P-T conditions for Beaucatcher Mountain (BCM-2) using Thermocalc gave results of 7.0 to 7.7 kbars and 750 ˚C to 819 ˚C while GPT3 gave 5.8 to 7.2 kbars and 626 ˚C to 711 ˚C. All ThermoCalc results incorporated correlation of pressure with temperature, standard deviation, and sigfit (a parameter used to measure the reliability of the results). All results used had sigfits close to or slightly below the standard given in ThermoCalc. A small sigfit (equal to or below the automatic number given by ThermoCalc) means there is 95% confidence in the data. The sigfit will increase when

the number of independent reactions increases. Extents for ellipses in Fig. 40 are the PT ranges possible for each location.

Table 23. PT calculation results from Thermocalc.

ThermoCalc

Sample	Point	IR	P	SD	COR	SigFit	T	SD
GFT7	GT1C1	5	6.2	1.00	0.59	1.61	528	14
	GT1C2	5	6.5	0.90	0.57	1.43	533	12
	GT1C3	5	6.4	0.90	0.57	1.51	533	12
	GT2C1	5	6.5	0.70	0.55	1.23	531	10
	GT2C2	5	6.3	1.00	0.58	1.61	534	13
	GT2C3	5	7.1	0.60	0.53	0.96	532	8
	GT2C4	5	6.6	1.10	0.57	1.71	533	14
	AVERAGE	**5**	**6.5**	**0.89**	**0.57**	**1.44**	**532**	**12**
	GT1R1	5	6.4	0.90	0.57	1.51	533	12
	GT1R2	5	6.6	1.00	0.59	1.66	536	14
	GT1R3	5	6.5	1.10	0.58	1.78	536	15
	GT1R4	5	6.6	0.80	0.56	1.35	535	11
	GT2R1	5	6.4	1.00	0.59	1.69	535	14
	GT2R2	5	6.5	0.80	0.56	1.36	532	11
	GT2R3	5	7.2	0.80	0.64	0.82	606	32
	GT2R4	5	6.2	1.00	0.59	1.61	530	13
	AVERAGE	**5**	**6.6**	**0.93**	**0.58**	**1.47**	**543**	**15**
LP7	GT1C1	11	11.3	2.00	0.83	2.54	896	137
	GT1C2	11	11.1	1.40	0.83	1.83	887	98
	GT1C3	11	11.6	2.00	0.83	2.52	915	139
	GT1C4	11	11.3	1.80	0.83	2.39	887	126
	GT1C5	11	11.5	2.10	0.83	2.59	907	142
	GT1C6	11	10.9	1.90	0.83	2.51	877	133
	GT1C7	11	11.5	1.90	0.84	2.43	906	134
	GT1C8	11	11.1	2.20	0.84	2.75	885	151
	GT1C9	11	11.2	2.20	0.84	2.65	885	146
	AVERAGE	**11**	**11.3**	**1.94**	**0.83**	**2.47**	**894**	**134**
	GT1R1	11	11.1	2.00	0.83	2.50	897	137
	GT1R2	11	11.1	2.00	0.83	2.49	884	134
	GT1R3	11	11.3	2.10	0.83	2.63	896	143
	GT1R4	11	11.2	2.10	0.83	2.63	890	147
	GT1R5	11	11.7	1.50	0.84	1.86	917	103
	GT1R6	11	11.2	2.20	0.84	2.69	893	148
	GT1R7	11	11.6	1.70	0.85	2.08	912	119
	GT1R9	11	11.4	2.20	0.84	2.72	906	153
	GT1R10	11	11.2	2.30	0.85	2.77	895	158
	GT1R11	11	11.7	1.80	0.85	2.11	924	123
	GT1R12	11	11.3	2.60	0.85	3.04	907	176
	GT1R13	11	11.0	2.40	0.85	2.88	895	165
	GT1R14	11	10.9	2.10	0.84	2.70	870	144
	GT1R15	11	11.4	20.00	0.85	2.34	900	132
	GT1R16	11	11.0	2.10	0.84	2.92	880	162
	GT1R17	11	11.3	2.30	0.84	2.77	907	157
	GT1R18	11	11.4	2.40	0.85	2.90	908	167
	GT1R19	11	11.4	2.30	0.85	2.71	906	155
	GT1R20	11	11.6	1.90	0.85	2.26	919	133
	AVERAGE	**11**	**11.3**	**3.05**	**0.84**	**2.58**	**900**	**145**

Sample	Point	IR	P	SD	COR	SigFit	T	SD
SVC5	GT1C1	4	8.1	1.00	0.82	1.84	486	23
	GT1C2	4	8.1	0.90	0.82	1.82	486	22
	GT1C3	4	8.0	1.00	0.82	1.86	485	23
	GT2C1	4	8.3	0.80	0.69	2.03	494	18
	AVERAGE	**4**	**8.1**	**0.97**	**0.82**	**1.84**	**486**	**23**
	GT1R1	4	8.8	1.30	0.80	2.37	494	29
	GT1R2	4	8.1	1.20	0.79	2.28	447	27
	GT1R3	4	7.7	0.90	0.83	1.71	480	21
	GT1R4	4	7.6	0.90	0.82	1.83	477	22
	GT1R5	4	9.0	0.90	0.65	2.14	499	19
	GT1R6	4	9.3	0.50	0.63	0.12	521	11
	AVERAGE	**4**	**8.4**	**0.95**	**0.75**	**1.74**	**486**	**22**
SV4	GT1C2	8	14.1	1.70	0.94	2.42	757	52
	GT2C2	8	13.2	1.80	0.94	2.55	741	53
	GT4C1	8	13.2	1.80	0.93	2.63	742	54
	AVERAGE	**8**	**13.5**	**1.77**	**0.94**	**2.53**	**747**	**53**
	GT1R2	8	14.1	1.70	0.94	2.31	765	52
	GT1R5	8	13.9	1.80	0.94	2.55	765	55
	GT1R6	8	12.2	1.80	0.93	2.84	709	56
	GT2R4	8	13.8	1.70	0.94	2.40	749	52
	GT2R5	8	12.0	1.70	0.93	2.66	704	54
	GT2R6	8	14.1	1.80	0.94	2.43	767	53
	GT2R7	8	12.5	1.70	0.93	2.67	720	54
	GT4R2	8	14.0	1.70	0.94	2.29	761	50
	AVERAGE	**8**	**13.3**	**1.74**	**0.94**	**2.52**	**743**	**53**
SV7	GT1C1	9	11.9	1.60	0.90	2.07	724	60
	GT1C2	9	10.6	1.50	0.91	2.02	696	59
	GT1C3	9	12.0	1.60	0.90	2.10	736	62
	GT1C4	9	12.0	1.60	0.90	2.08	736	61
	AVERAGE	**9**	**11.6**	**1.58**	**0.90**	**2.07**	**723**	**61**
	GT1R1	9	12.6	1.40	0.96	1.18	766	53
	GT1R2	9	11.5	1.70	0.91	2.22	709	65
	GT1R3	9	12.1	1.90	0.90	2.46	748	72
	GT1R4	9	11.1	1.60	0.90	2.15	718	63
	GT1R5	9	11.7	1.70	0.91	2.31	720	67
	GT1R6	9	12.3	1.90	0.90	2.43	739	71
	GT1R7	9	10.9	1.70	0.91	2.23	703	66
	AVERAGE	**9**	**11.7**	**1.70**	**0.91**	**2.14**	**729**	**65**
GFT-23	GT1C1	7	11.8	6.50	0.98	3.53	714	234
	GT1C2	6	11.9	5.70	0.98	3.33	713	203
	AVERAGE	**6**	**11.8**	**6.10**	**0.98**	**3.43**	**714**	**219**
	GT1R1	7	13.2	6.90	0.98	3.67	754	244
	GT1R2	5	11.3	4.80	0.98	2.94	684	168
	GT1R3	6	6.0	3.20	0.98	2.31	474	117
	GT1R4	6	6.2	3.20	0.98	2.28	485	116
	GT1R5	6	6.2	3.20	0.98	2.30	481	118
	GT2R1	6	6.4	3.10	0.98	2.21	491	113
	GT2R2	6	6.5	3.30	0.98	2.37	494	122
	GT2R5	6	6.2	3.30	0.98	2.31	483	119
	Gt4R1	6	6.5	3.30	0.98	2.37	498	123
	AVERAGE	**6**	**6.4**	**3.20**	**0.98**	**2.53**	**487**	**138**

Sample	Point	IR	P	SD	COR	SigFit	T	SD
BCM-2	GT3C1	3	6.9	3.20	0.80	2.15	843	289
	GT4C1	3	6.3	2.00	0.83	1.50	725	168
	GT5C1	3	8.2	3.50	0.85	2.11	926	323
	GT6C1	3	7.5	1.40	0.83	0.72	673	100
	AVERAGE	**3**	**7.2**	**2.54**	**0.83**	**1.61**	**792**	**221**
	GT2R1	3	7.2	2.10	0.85	1.55	758	177
	GT2R2	3	8.1	2.40	0.86	1.63	840	210
	GT3R1	3	6.7	2.40	0.86	1.77	778	215
	GT3R2	3	6.5	3.00	0.82	2.19	798	275
	GT4R1	3	6.8	1.40	0.82	0.99	698	109
	GT4R2	3	6.9	1.50	0.82	1.06	702	116
	GT6R1	3	6.5	1.80	0.83	1.46	676	146
	AVERAGE	**3**	**7.0**	**2.09**	**0.84**	**1.52**	**750**	**178**

IR stands for number of independent reactions, P is pressure in kbar, T temperature in °C; SD is standard deviation, Cor: parameter for correlation of P with T; sigfit parameter indicating goodness of fit of results: the lower the value, the better the fit.

Table 24. PT calculation results from GPT3 (Reche and Martinez, 1996).

Reche/ Martinez PT Calc

Sample	Point	P	T
GFT7	GT1C1	6.7	562
	GT1C2	6.6	565
	GT1C3	6.8	582
	GT2C1	6.1	555
	GT2C2	6.7	564
	GT2C3	6.3	569
	GT2C4	6.5	552
	AVERAGE	**6.5**	**564**
	GT1R1	7.0	568
	GT1R2	6.3	551
	GT1R3	6.6	544
	GT1R4	6.4	529
	GT2R1	6.1	552
	GT2R2	7.4	557
	GT2R3	6.3	569
	GT2R4	5.5	523
	AVERAGE	**6.5**	**549**
LP7	GT1C1	6.9	545
	GT1C2	5.5	495
	GT1C3	7.4	582
	GT1C4	9.3	574
	GT1C5	7.2	549
	GT1C6	5.9	503
	GT1C7	9.0	569
	GT1C8	5.3	480
	GT1C9	7.1	476
	AVERAGE	**7.1**	**530**

Sample	Point	P	T
	GT1R1	5.6	504
	GT1R2	6.7	475
	GT1R3	7.1	543
	GT1R4	5.0	481
	GT1R5	6.9	567
	GT1R6	5.8	497
	GT1R7	6.0	509
	GT1R9	4.6	460
	GT1R10	6.2	456
	GT1R11	5.5	488
	GT1R12	5.0	455
	GT1R13	3.8	423
	GT1R14	4.9	444
	GT1R15	4.5	443
	GT1R16	5.0	441
	GT1R17	5.5	502
	GT1R18	3.9	450
	GT1R19	6.2	484
	GT1R20	4.8	466
	AVERAGE	**5.4**	**478**
SVC5	GT1C1	9.6	667
	GT1C2	9.2	670
	GT1C3	9.2	645
	AVERAGE	**9.3**	**661**
	GT1R1	8.9	615
	GT1R2	11.0	701
	GT1R3	9.0	656
	GT1R4	9.1	680
	AVERAGE	**9.5**	**663**
SV4	GT1C2	18.0	557
	GT2C2	18.0	568
	GT4C1	18.0	551
	AVERAGE	**18.0**	**559**
	GT1R2	19.0	562
	GT1R5	18.0	550
	GT1R6	17.5	
	GT2R4	18.0	523
	GT2R5	18.0	552
	GT2R6	18.0	588
	GT2R7	17.5	
	GT4R2	17.5	540
	AVERAGE	**17.9**	**553**

Sample	Point	P	T
SV7	GT1C1	18.2	968
	GT1C2	15.9	908
	GT1C3	19.9	1044
	GT1C4	18.4	982
	AVERAGE	**18.1**	**975**
	GT1R1	12.8	760
	GT1R2	17.2	925
	GT1R3	21.2	1099
	GT1R4	17.2	970
	GT1R5	18.5	983
	GT1R6	20.0	1040
	GT1R7	15.3	876
	AVERAGE	**17.5**	**950**
BCM-2	GT3C1	6.2	723
	GT4C1	5.8	645
	GT5C1	7.7	765
	GT6C1	7.5	605
	AVERAGE	**6.8**	**684**
	GT2R1	7.4	715
	GT2R2	8.5	767
	GT3R1	5.1	620
	GT3R2	3.9	579
	GT4R1	5.4	561
	GT4R2	4.3	531
	GT6R1	5.9	612
	AVERAGE	**5.8**	**626**

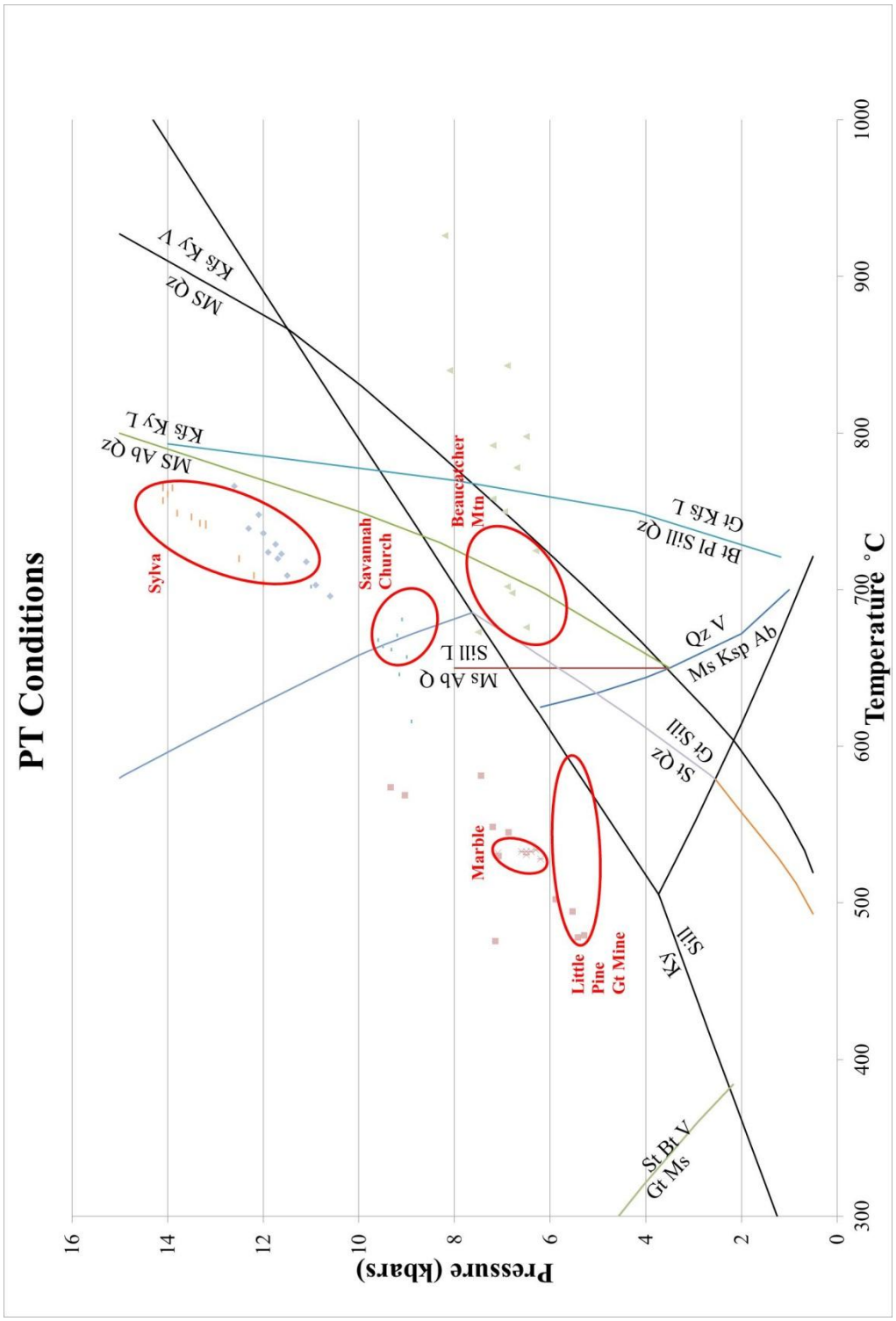

Figure 40. P-T conditions calculated for each location. Ellipses contain interpreted P-T conditions based on a combination of good thermobarometric results and phase relations. Marble ellipse represents sample GFT-7 (purple) results from ThermoCalc, Little Pine Garnet Mine uses sample LP-7 (pink) results from GPT3, Savannah Church uses sample SVC-5 results from GPT3 (navy), the Sylva ellipse encompasses results from SV-4 (blue) and SV-7 (orange) using ThermoCalc, and Beaucatcher Mtn uses BCM-2 (green)

results from ThermoCalc. Colored lines represent different reactions. Results used were chosen based on reliability and accuracy.

DISCUSSION

The P-T conditions calculated using Thermocalc (Powell and Holland, 2002) and the GPT3 spreadsheet (Reche and Martinez, 1996) are vastly different for several of the localities studied. For the Marble locality, P-T results from both programs were similar, placing them in the stability field of kyanite which has been recorded by Nesbitt and Essene (1982). P-T conditions recorded by Nesbitt and Essene (1982) for Marble were 4.5 ± 1 kbars and 540 ˚C ± 20 ˚C. Their pressure results are slightly below the 6.5 kbars calculated in this study, but their temperatures are almost identical to the 530 ˚C ± 30 ˚C value calculated here (Tables 23 & 24). These temperatures are also consistent with the high albite component of their plagioclase feldspars, and the stability limits of staurolite + muscovite (Figs. 40 & 41).

The P-T conditions calculated for Little Pine Garnet Mine using Thermocalc were extremely different from those obtained using GPT3. In the case of Little Pine Garnet Mine, the more realistic pressures and temperatures seem to be 5 to 6 kbars and 480 ˚C to 530 ˚C obtained using GPT3. Nevertheless, temperatures calculated from Little Pine Garnet Mine are most likely minima since most of the garnets were in contact with biotite in each sample analyzed from this locality, allowing for retrograde rim re-equilibration (resetting). The presence of staurolite crystals confirms that GPT3 results are more suitable because staurolite is unstable at T >600 ˚C at P < 5.5 kbars (Winter, 2001). Temperatures and pressures were only calculated using GPT3 for LP-12 but the temperatures calculated are most likely minima because the amount of biotite in this

sample is miniscule compared to the amount of garnet present, which would again allow for extensive resetting (e.g. Spear, 1993 and references therein). Using the GRAIL (Garnet (almandine) + rutile = aluminosilicate + ilmenite) and GRIPS (garnet + rutile = plagioclase + ilmenite + quartz) barometers, pressures were determined to be 5.5 to 6 kbars, temperature still being 500 ˚C to 550 ˚C based on the Gt - Bt thermometer. These conditions are consistent with the presence and stability of the inferred peak mineral assemblage (Spear, 1982; Robinson et al., 1982). Using textural relations and the chemographic projections shown above (Figs. 10, 11, and 12) for the garnet mine mineral assemblages, the reactions below seem reasonable:

$$\text{Ged} + \text{Bt} + \text{Gt} + \text{St} \leftrightarrow \text{Anth} + \text{Sill} + \text{Ms}$$

$$\text{Ged} + \text{Gt} \pm \text{Bt} \leftrightarrow \text{Chl} + \text{Ilm} \pm \text{Ms}$$

To have such vastly differing results for the same location warrants some explanation. Thermocalc does allow for the incorporation of two amphiboles in its average P-T calculation, but as cummingtonite (instead of anthophyllite) and gedrite. Thermocalc also allows for incorporating almost all of the minerals present (staurolite, sillimanite, etc.), and the average P-T conditions calculated are therefore based in the intersection of all possible reactions between these minerals, whereas GPT3 results are based on the intersection of one thermometer and one barometer, and does not account for the presence of the different amphiboles or other minerals that are not part of those specific geothermometers or geobarometers.

Temperatures calculated for Savannah Church using Thermocalc were ~ 200 ˚C less than those calculated using GPT3. The higher T of (~600 ˚C) seems more realistic

than the 400 ˚C from Thermocalc based on of the mineral assemblages of the area and the similarity to other locations like Sylva and Marble. However, unlike Marble, Savannah Church does not contain staurolite which would be consistent with a T >600 ˚C (Spear, 1993). These temperatures, however, are most likely minima since all of the garnets from Savannah Church were either in contact with or completely surrounded by biotite. The Savannah Church pressures calculated using GPT3 are maximum pressures since there were no aluminosilicates present, hence GASP can only yield a maximum pressure. Temperatures calculated using Thermocalc are incorrect because the thermodynamic data for amphiboles is less reliable and because Thermocalc uses a multiequilibrium approach as opposed to a simple intersection between the Gt - Bt thermometer and a barometer.

The pressures calculated using the two programs for Sylva are drastically different. All samples from Sylva yielded pressures of about 18 kbars in GPT3. This is abnormally high compared to all of the other results for the surrounding areas. Thermocalc results also produced high pressures of about 11 kbars in one sample and 14 kbars in another sample from Sylva. Results from both programs seem unrealistic and anomalous but the Thermocalc pressures seem less suspicious. The temperatures calculated using Thermocalc (740 ˚C) were also more reasonable than those calculated using GPT3. The 550 ˚C calculated from GPT3 is questionable since at these temperatures (along with the high pressures), mafic rocks would develop an eclogite facies mineral assemblage. This is not the case since the mineral assemblage described earlier for this area is typical of amphibolite facies. Moreover, the Sylva location exhibits evidence of partial melting which occurs at T of at least 630 ˚C depending on the presence of enough fluids and its bulk rock composition. Therefore, temperatures of 550

˚C are highly unlikely and the 740 ˚C seems more fitting. In addition, temperatures calculated from Sylva are most likely minima since the garnets were in contact or surrounded by biotite in each sample analyzed from this locality, which allows for retrograde resetting. Pressures calculated using GPT3 rely on the GASP barometer, and can only be considered maximum pressures given that no aluminosilicate was found in any of these rocks. Application of the GRIPS barometer to sample SV-4 resulted in an average of 12.5 to 13 kbars. The anorthite content of the plagioclase was highest in Sylva, which is also consistent with these rocks yielding some of the highest temperatures (~ 740 °C) for the study area.

Pressures calculated for Beaucatcher Mountain using Thermocalc were about 7 kbars, slightly higher than those calculated using GPT3 (5.8 to 6.8 kbars). Temperatures calculated for the same rocks using Thermocalc and GPT3 were 750 °C and 650 °C, respectively (Tables 23 & 24). Because there is partial melting at this location, the lower estimate would be more reliable with the stability of muscovite and quartz if the rock was infiltrated by water. Also, many of the garnets at Beaucatcher Mountain were in contact with some small amount of biotite therefore temperatures calculated for this locality should be considered as minima. The biotite analyses for this location also seemed to be more widespread therefore resulting in a wider temperature range obtained and making those results less reliable. Although Beaucatcher Mountain has stable muscovite + quartz, some of the P-T conditions lie outside the stability field of muscovite + quartz. This may be an indication that these rocks have undergone more than one metamorphic event, in which one event led to partial melting and was followed by a backreation between melt and rock to form retrograde muscovite. It is possible that during a second metamorphic

event, muscovite recrystallized in the foliation plane to appear as part of the peak assemblage and may contribute to the scatter in temperatures.

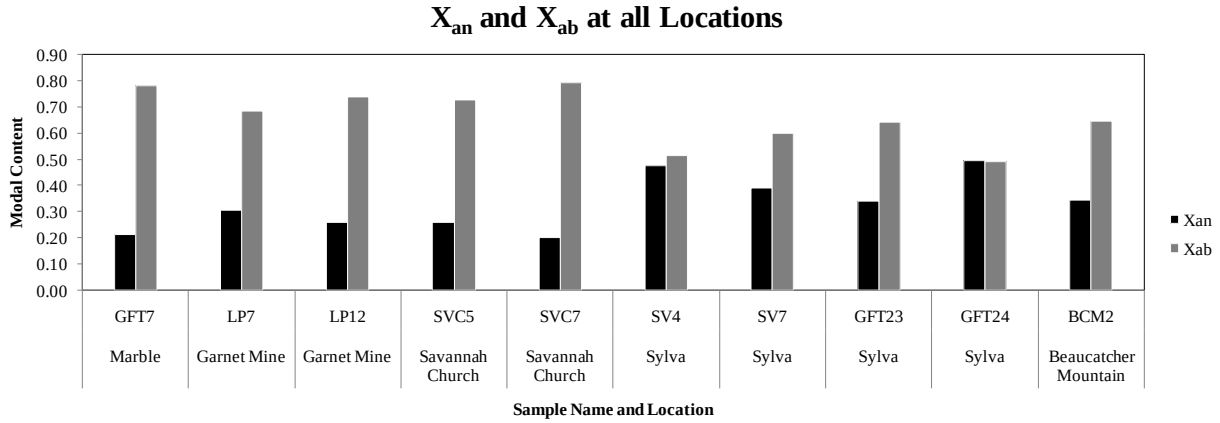

Figure 41. Graph displaying anorthite and albite contents of plagioclase per location. Note that Sylva has the highest X_{an} and Marble the lowest.

P-T PATHS

P-T paths can only be constructed for a few samples in this study in which the garnets are zoned, the amphiboles are zoned, or there are specific reactions that have obviously taken place. At the Marble location, the staurolite contains inclusions of garnet which indicates increasing temperature. The reaction for this is:

$$Gt + Ms \leftrightarrow St + Bt + V$$

This reaction indicates that the staurolite grew at the expense of garnet during a stage of increasing temperature. At the Little Pine Garnet Mine, anthophyllite + sillimanite formed after gedrite + biotite. This likely occurred during a stage of increasing temperature and decreasing pressure, suggesting a clockwise P-T path. The replacement of gedrite by anthophyllite also supports this conclusion as orthoamphiboles are stable at

lower pressures compared to clinoamphiboles (e.g. Robinson et al., 1982) assuming that the "gedrite" is really more of a clinoamphibole like grunerite, as supported by the extinction angles measured (Table 7). Savannah Church, Sylva, and Beaucatcher Mountain have garnet zoning where manganese increases towards the rims indicating that the garnets grew during a stage of decreasing temperature. The increase in Si and decrease in Al^{iv} from core to rim of amphiboles in Sylva is indicative of growth of these amphiboles under conditions of increasing pressure possibly accompanied by decreasing T (e.g. Robinson et al., 1982). This would be consistent with a counterclockwise P-T path for Sylva. Nonetheless, there is not enough evidence to suggest a clockwise/counter - clockwise P-T path for Sylva, Savannah Church, or Beaucatcher Mountain.

TECTONIC IMPLICATIONS

Simple stacking of all thrust sheets, as suggested by Hatcher et al (2005), would have the highest grade in the WBR, and the lowest in the EBR. The results from this study, as well as those of Eckert et al., (1989) Absher & McSween (1985), Moecher et al. (2004), and El-Shazly et al., (2011) clearly show that that was not the case. Marble clearly displays lower pressures and temperatures based on the results from this study and those of Nesbitt and Essene (1982). Little Pine Garnet Mine displays lower pressures compared to the rest of the CBR which suggests that it may actually be a part of the WBR. However, the abundance of mafic/ultramafic rocks at this locality indicates that it is part of the CBR according to Hatcher (2010). Based on the peak mineral assemblage for the garnet mine and the lack of that assemblage in surrounding rocks, this possibly

could have started as an ultramafic complex that started weathering with shale/mudstone deposited on top, both of which were subducted and metamorphosed. Comparing the pressure and temperature achieved for this area and the rest of the central Blue Ridge, the pressure and temperatures for the garnet mine are much lower. The lower conditions indicate that this location most likely is not part of the CBR but instead is part of the WBR since it was right along the edge of both.

In the CBR, P-T conditions for Savannah Church and Sylva are considerably higher than those recorded throughout the WBR. Both localities exhibit evidence of partial melting and migmatization, but it seems like Sylva (Cartoogechaye terrane thrust slice) was more deeply buried than Savannah Church (which belongs to the DGB) before they were both brought back to the surface, possibly during a later collisional/tectonic event.

The next problem to address is the relationship between the DGB and the Cartoogechaye terrane. Because there were not enough data to determine a P-T path for Savannah Church which is situated on the DGB, it is difficult to say whether the DBG was thrust on top of or below the Cartoogechaye terrane. According to El-Shazly et al. (2011), the CBR (Cartoogechaye terrane) was thrust under the WBR (Laurentia), followed by the Dahlonega gold belt being thrust beneath the CBR. These events were followed by the collision of the Tugaloo terrane, which was thrust on top of all three earlier terranes. According to El-Shazly et al. (2011), when the DGB was thrust underneath the CT, it caused the Cartoogechaye terrane to be first exhumed. When the Tugaloo terrane later docked into Laurentia, it caused the exhumed CT to be overthrust onto the Laurentian margin. This would explain the higher temperatures and pressures in

the CBR compared to the EBR (represented by the Tugaloo terrane), but would not explain the differences in the P-T conditions estimated for Sylva and Savannah Church.

The P-T conditions for the EBR are lower than those for the CBR. Despite the partial melting at BCM of the EBR (which is also recorded in SVC and SV), BCM records lower P-T conditions. These lower P-T conditions for the BCM (EBR) are consistent with the Tugaloo terrane being thrust on top of Laurentia, the Cartoogechaye terrane, and the DGB proposed by El-Shazly et al. (2011) and is consistent with the maps of Hatcher et al. (2005).

CONCLUSIONS

- Western Blue Ridge is characterized by the lowest P-T conditions which were recorded in Ducktown.
- Temperatures and pressures in the CBR are higher than the WBR and EBR.
- Sillimanite was found in the Garnet Mine location (Gt zone on Fig. 4), meaning the metamorphic zone for that area should be re - evaluated due to the discovery of mineral assemblages higher than what was mapped by Merschat et al. (in press).
- Little Pine Garnet Mine rocks represent some kind of a confined basin in which shales and greywackes were deposited on top of ultramafic and mafic rocks possibly related to continental rifting.
- The reason for very coarse grained garnets versus fine to medium grained garnets at Little Pine Garnet Mine is due to high growth rates and very few nucleation

sites. In the talc bearing rocks, the garnet is almost the only Fe and Mn bearing mineral, but in rocks with a mixed protolith, biotite and staurolite compete with garnet for Fe.

- Sylva may exhibit the highest pressures of the CBR, not the Winding Stair Gap as previously suggested by Carpenter (1970), Absher & McSween (1985), Eckert et al. (1989), and El-Shazly et al. (2011). It was possibly a thrust slice that was pushed back up from greater depths, not fitting in with the rest of the CBR, which would explain these higher pressures and intense mylonitization.
- Savannah Church is part of the Dahlonega Gold Belt and not the Cartoogechaye terrane, which would explain its metamorphism under lower P-T conditions. However, such conditions are inconsistent with the tectonic interpretations of Hatcher et al. (2005) and El-Shazly et al. (2011).

SUGGESTIONS FOR FUTURE WORK

These data are just the beginning for research on metamorphism in the Blue Ridge province. To aid in a better understanding of what has occurred in the different terranes, future research should include age dating of monazites and zircons, which would allow for the determination of which orogenic events were affecting each terrane. Included in the age dating might be the creation of P-T-t paths and the determination of whether metamorphism predates or post - dates movement along specific faults.

REFERENCES

Absher, B. S., & McSween, H. Y., Jr., 1985. Granulites at Winding Stair Gap, North Carolina: The thermal axis of Paleozoic metamorphism in the southern Appalachians, Geological Society of America Bulletin, 96, 588 - 599.

Bartholomew, M. J., and Lewis, S. E., 1988. Peregrination of Middle Proterozoic Massifs and Terranes within the Appalachian orogen, eastern USA: Trabajos de Geologia, University of Oviedo (Spain), v. 17, p. 155 - 165.

Butler, J. R., 1991. Metamorphism, *in* Horton, J. W., Jr., and Zullo, V. A., eds., The geology of the Carolinas:, Carolina Geological Society Fiftieth Anniversary Volume: Knoxville, University of Tennessee Press, p. 127 - 141.

Carpenter, R. H., 1970. Metamorphic history of the Blue Ridge Province of Tennessee and North Carolina: Geological Society of America Bulletin, v. 81, p. 749 - 762.

Eckert, J. O., Jr., Hatcher, Jr., R. D., & Mohr, D. W., 1989. The Wayah granulite facies metamorphic core, southwestern North Carolina: High - grade culmination of Taconic metamorphism in the southern Blue Ridge, Geological Society of America Bulletin, 101, 1434 - 1447.

El-Shazly A. K., Loehn, C., and Tracy, R. J., 2011. *P–T–t* evolution of granulite facies metamorphism and partial melting in the Winding Stair Gap, Central Blue Ridge, North Carolina, USA. Journal of Metamorphic Geology, 29: 753 – 780. DOI: 10.1111/j.1525 - 1314.2011.00940.x

Espenshade, G. H., Rankin, D. W., Shaw, K. W., and Neuman, R. B., 1975. Geologic map of the east half of the Winston - Salem quadrangle, North Carolina - Virginia: U.S. Geological Survey Map I - 709 - B, scale 1:250,000.

German, J. M., 1985, The geology of the northeastern portion of the Dahlonega gold belt: Georgia Geological Survey Bulletin 100, 41 p.

Goldsmith, R., Milton, D. J., and Horton, J. W., Jr., 1988. Geologic map of the Charlotte 1 - degree x 2 - degree quadrangle, North Carolina and South Carolina: U.S. Geological Survey Map I - 1251 - E, scale 1:250,000.Hadley, J. B., and Goldsmith, R., 1963. Geology of the eastern Great Smoky Mountains, North Carolina and Tennessee: U.S. Geol. Survey Prof. Paper 349 - B, 118 p.

Hadley, J. B., and Goldsmith, R., 1963. Geology of the eastern Great Smoky Mountains, North Carolina and Tennessee: U.S. Geological Survey Professional Paper 349 - B, 118 p.

Hadley, J.B., and Nelson, A.E., 1971. Geologic map of the Knoxville Quadrangle, North Carolina, Tennessee, and South Carolina: U.S. Geological Survey Miscellaneous Geologic Investigations Map I - 654, scale 1:250,000.

Hartley, M.E., III, 1973. Ultramafic and related rocks in the vicinity of Lake Chatuge: Georgia Geological Survey Bulletin 85, 61 p.

Hatcher, R. D., 1971. Geology of Rabun and Habersham Counties, Georgia - A reconnaissance study: Georgia Geological Survey Bulletin 83, 48 p.

Hatcher, R.D., 1973. Basement versus cover rocks in the Blue Ridge of northeast Georgia, northwestern South Carolina and adjacent North Carolina. American Journal of Science, 273, 671–685.

Hatcher, R. D., 1978. Tectonics of the western Piedmont and Blue Ridge, southern Appalachians: Review and speculations: Am. Jour. Sci, v. 278, p. 276 - 304.

Hatcher, R., 2010. Southeastern Tennessee - Western North Carolina Blue Ridge. Post - Goldschmidt Conference Field Trip.

Hatcher, R.D., Bream, B.R., Miller, C.F., Eckert, J.O., Fullagar Paul, D. & Carrigan, C.W., 2004. Paleozoic structure of internal basement massifs, southern Appalachian Blue Ridge, incorporating new geochronologic, Nd and Sr isotopic and geochemical data. Geological Society of America, Memoir, 197, 525–547.

Hatcher, R. D., Jr., Merschat, A. J., & Thigpen, J. R., 2005. Blue Ridge Primer. In Carolina Geological Society, Annual Field Trip, 1 - 24.

Hatcher, R. D., Jr., and Merschat, A. J., 2006. The Appalachian Inner Piedmont: An exhumed strike - parallel, tectonically forced orogenic channel, *in* Law, R. D., Searle, M., and Godin, L., eds., Channel flow, ductile extrusion and exhumation of lower - mid crust in continental collision zones: London, Geological Society of London Special Publication 268, p. 517 - 540.

Hatcher, R.D., Jr., and Goldberg, S.A., 1991. The Blue Ridge Geologic Province, *in* The Geology of the Carolinas: Carolina Geological Society 50th anniversary volume: Knoxville, University of Tennessee Press, p. 11 - 35.

Hatcher, R, and Merschat, A. J., 2005. Blue Ridge Geology Geotraverse East of the Great Smoky Mountains National Park, Western North Carolina. Carolina Geological Society Annual Field Trip. 1 - 144.

Hatcher, R. D., Jr., Bream, B. R., and Merschat, A. J., 2007. Tectonic map of the southern and central Appalachians: A tale of three orogens and a complete Wilson cycle, *in* Hatcher, R. D., Jr., Carlson, M. P., McBride, J. H., and Martínez Catalán, J. R., eds., 4 - D Framework of Continental Crust: Geological Society of America Memoir 200, p. 595 - 632.

Hibbard, J.P., van Staal, C.R., and Rankin, D.W., 2010. Comparative analysis of the post - Ordovician geological evolution of the northern and southern Appalachian orogen; in Tollo, R., Bartholomew, M., Hibbard, J., and Karabinos, P., From

Rodinia to Pangea; The Lithotectonic History of the Appalachian Region; Geological Society of America Memoir 206, p. 51 - 69.

Hibbard, J.P., van Staal, C.R., and Rankin, D.W., and Williams, H., 2006. Lithotectonic Map of the Appalachian Orogen, Canada - United States of America: Geological Survey of Canada Map 2096A, scale 1:1500,000.

Hibbard, J.P., van Staal, C.R., and Rankin, D.W., 2007. A comparative analysis of pre - Silurian crustal 'building blocks' of the northern and southern Appalachians, American Journal of Science, v. 307, p. 23 - 45.

Higgins, M. W., Crawford, T. J., Atkins, R. L., and Crawford, R. F., 2003. Geologic map of the Atlanta 30' x 60' quadrangle, Georgia: U.S. Geological Survey, Geologic Investigations Series Map I–2602, scale 1:100,000.

Holland, T.J.B. & Powell, R., 2005. AX: a program to calculate activities of mineral end members from chemical analyses. Available at: http://www.esc.cam.ac.uk/research/researchgroups/holland/ax (last accessed on 19 November 2010).

Hopson, J.L., Hatcher, R.D., and Stieve, A.L., 1989. Geology of the eastern Blue Ridge, northeastern Georgia and the adjacent Carolinas, *in* Fritz, W.J., Hatcher, R.D., and Hopson, J. L., editors, Geology of the eastern Blue Ridge, of northeast Georgia and the adjacent Carolinas: Georgia Geological Society Guidebook, v. 9, p. 1 - 40.

Force, E.R., 1991, Geology of titanium - mineral deposits: Boulder, Geological Society of America Special Paper 259, 113 p.

Leake, B.E., Woolley, A.R., Arps, C.E.S., Birch, W.D., Gilbert, M.C., Grice, J.D., Hawthorne, F.C., Kato, A., Kisch, H.J., Krivovichev, V.G., Linthout, K., Laird, J., Mandarino, J.A., Maresch, W.V., Nickel, E.H., Rock, N.M.S., Schumacher, J.C., Smith, D.C., Stephenson, N.C.N., Ungaretti, L., Whittaker, E.J.W., and Youzhi, G., 1997. Nomenclature of amphiboles: Report of the Subcommittee on Amphiboles of the International Mineralogical Association, Commission on New Minerals and Mineral Names. American Mineralogist, 82, 1019–1037.

McDowell, S. M.; Miller, C. F.; Fullagar, P. D.; Bream, B. R.; and Mapes, R. W. 2002. The Persimmon Creek Gneiss, eastern Blue Ridge, North Carolina–Georgia: evidence for the missing Taconic arc? Southeast. Geol.41:103–117.

Merschat, A. J., 2003. Inner Piedmont tectonics in the southwestern Brushy Mountains, North Carolina: Field and laboratory data revealing 3 - D crustal flow and sillimanite I and II metamorphism [M.S. thesis]: Knoxville, University of Tennessee, 198 p.

Merschat, A. J., 2009. Assembling the Blue Ridge and Inner Piedmont: Insights into the Nature and Timing of Terrane Accretion in the Southern Appalachian Orogen from Geologic Mapping, Stratigraphy, Kinematic Analysis, Petrology,

Geochemistry, and Modern Geochronology [Ph. D. thesis]: Knoxville, University of Tennessee, 455p.

Merschat, A. J., Hatcher, R. D., Jr., Bream, B. R., Miller, C. F., Byars, H. E., Gatewood, M. P., and Wooden, J. L., 2010, this volume, Detrital zircon geochronology and provenance of southern Appalachian Blue Ridge and Inner Piedmont crystalline terranes, in Tollo, R. P., Bartholomew, M. J., Hibbard, J. P., and Karabinos, P. M., eds., From Rodinia to Pangea: The Lithotectonic Record of the Appalachian Region: Geological Society of America Memoir 206, doi: 10.1130/2010.1206(26).

Merschat, C. E., and Wiener, L. S., 1988. Geology of the Sandymush and Canton Quadrangles, North Carolina: Raleigh, North Carolina Geological Survey Bulletin 90, 1:24,000 scale, 66 p.

Miller, C.F., Hatcher, R.D., Harrison, T.M., Coath, C.D. & Gorisch, E.B., 1998. Cryptic crustal events elucidated through zone imaging and ion microprobe studies of zircon, southern Appalachian Blue Ridge, North Carolina - Georgia. Geology, 26, 419–422.

Miller, C. F., Hatcher, R. D., Jr., Ayers, J. C., Coath, C. D., and Harrison, T. M., 2000. Age and Zircon inheritance of eastern Blue Ridge plutons, southwestern North Carolina and northeastern Georgia, with implications for magma history and evolution of the southern Appalachians orogen: American Journal of Science, v. 300, p. 142 - 172, doi: 10.2475/ajs.300.2.142.

Moecher D. P., Samson, S. D., & Miller, C. F., 2004. Precise time and conditions of peak Taconian Granulite facies metamorphism in the southern Appalachian Orogen, USA, with implications for zircon behavior during crustal melting events, Journal of Geology, 112, 289 - 304.

Nelson, A. E., Horton, J. W., and Clarke, J. W., 1998. Geologic map of the Greenville 1° x 2° quadrangle, Georgia, South Carolina, and North Carolina: U.S. Geological Survey Map I - 2175, scale 1:250,000.

Nesbitt, B. E., and Essene, E. J., 1982. Metamorphic thermometry and barometry of a portion of the southern Blue Ridge province: American Journal of Science, v. 282, p. 701 - 729.

Nesbitt, B. E., and Essene, E. J., 1983. Metamorphic volatile and equilibria in a portion of the southern Blue Ridge province: American Journal of Science, v. 283, p. 135 - 165. DOI: 10.2475/ajs.283.2.135

Powell, R., & Holland, T.J.B., 2002. Course Notes for "THERMOCALC Workshop 2002: Calculating Metamorphic Phase Equilibria" (Barcelona) on CD - ROM.

Quinn, M.J., 1991. Two lithotectonic boundaries in western North Carolina: Geologic interpretation of a region surrounding Sylva, Jackson County: Knoxville, University of Tennessee, M.S. thesis.

Quinn, M.J., and Wright, J.E., 1993. Extension of Middle Proterozoic (Grenville) basement into the eastern Blue Ridge of southwestern North Carolina: results from U/Pb geochronology: Geological Society of America, Abstracts with programs, v. 25, no. 6, p. A483.

Rankin, D. W., Espenshade, G. J., and Neuman, R. B., 1972. Geologic map of the west half of the Winston - Salem quadrangle, North Carolina, Virginia, and Tennessee: U.S. Geological Survey Map I - 709 - A, scale 1:250,000. 1252 - 1281.

Reche, J., and Martinez, F. J., 1996. GPT: an Excel spreadsheet for thermobarometric calculations in metapelitic rocks. Computers & Geosciences, 22, 775 – 784.

Robinson, P., Spear, F. S., Schumaker, J. C., Laird, J., Klein, C., Evans, B. W. and Doolan, B. L. (1982) Phase relations of metamorphic amphiboles: Natural occurrence and theory. In D. R. Veblen and P. H. Ribbe, Eds., Amphiboles: Petrology and Experimental Phase Relations, p. l - 227. Mineralogical Society of America, Reviews in Mineralogy, Volume 98.

Settles, D., 2002. Defining the Hayesville - Soque River and Allatoona faults and an Ordovician arc assemblage within the central Blue Ridge northwest of Dahlonega, Georgia, [M. S. Thesis]: Knoxville, University of Tennessee, 148 p.

Spear, F. S., 1982. Phase equilibria of amphibolites from the Post Pond Volcanics, Mt. Cube Quadrangle, Vermont. Journal of Petrology, 23, 383 - 426.

Spear, F. S., 1993. Metamorphic Phase Equilibria and Pressure – Temperature - time paths. Mineralogical Society of America, Washington D.C., 799 pp.

Stahr, D. W., Miller, C. F., Hatcher, R. D., Jr., Wooden, J., and Fisher, C. M., 2005, Evidence for high - temperature ductile Alleghanian deformation in the eastern Blue Ridge: Implications of new structural, petrologic, and geochronologic data from southwestern North Carolina: Geological Society of America Abstracts with Programs, v. 37, no. 7, p. 72.

Stewart, K., 1997. Paleozoic Structure, Metamorphism, and Tectonics of the Blue Ridge of Western North Carolina. Carolina Geological Society Field Trip. 1 - 87.

Tindle, A., 2000. MinFormula [online]: The Open University, Available from: http://www.open.ac.uk/earth - research/tindle/AGTWebPages/AGTSoft.html (accessed 16 March 2010).

Torres - Roldan R. L., Garcia - Casco, A., and Garcia - Sanchez, P.A., 1999. CSpace: an integrated workplace for the graphical and algebraic analysis of phase

assemblages on 32 - bit wintel platforms. Computers and Geosciences 26 (2000), p. 779 - 793.

Tull, J. F., and Holm, C. S., 2005. Structural evolution of a major Appalachian salient - recess junction: Consequences of oblique collisional convergence across a continental margin transform fault: Geological Society of America Bulletin, v. 117, p. 482 - 499.

Tull, J.F., Barineau, C.I., Mueller, P.A., and Wooden, J.L., 2007. Volcanic Arc Emplacement Onto The Southernmost Appalachian Laurentian Shelf: Characteristics and Constraints: Geological Society of America Bulletin, v. 119, p. 261-274.

Winter, John., 2001. Principles of Igneous and Metamorphic Petrology. 2nd ed. Pearson Prentice Hall. 446 - 702.